DISSERTATION

Submitted to the

Combined Faculties for the Natural Sciences and for Mathematics
of the Ruperto-Carola University of Heidelberg for the degree of
Doctor of Natural Sciences

presented by

Mgr. Biochemistry Anna Böhler

born in Kremennaja (Kremina), Ukraine

Date of oral examination:13.9.2024

Structure of the microtubule nucleation sites

Referees:

Prof. Dr. Elmar Schiebel

Dr. Stefan Pfeffer

Summary

Microtubules (MTs) are part of cytoskeleton responsible for cell cargo trafficking, cell shape and cell division. Nucleation of microtubules occurs at specific cellular organelle called microtubule organizing centrum (MTOCs). As the mayor microtubule nucleator is consider γ tubulin complexes (γTuC). In lower eukaryotes it is created via tetrameric complex created by GCP2, GCP3 and two copies of γ-tubulins, called γ tubulin small complex (γTuSC). In higher eukaryotes the complex is more intricate, formed with additional GCPs (GCP4-6). I have precipitated in discovery of the structure of vertebrates γTuRC (γ-tubulin ring complex). Surprisingly, vertebrates γTuRC is asymmetric to microtubule symmetry and deep inside of its structure is embedded actin molecule.

My PhD worked focused on understanding which conformational changes occurs in γTuRC upon microtubule nucleation and what is the fate of actin. Therefore, I established protocols for purification of γTuRC capped microtubule minus ends for purposes of the cryo EM analysis and the biochemical analysis.

From structure of *Xenopus leavis* γTuRC capped microtubule minus ends induced via RanGTP chromosomal pathway, I could observe the misalignment of MT protofilaments from spokes of γTuRC and as well as partial closure of γTuRC. These features may be recognised by MTs minus end binding proteins (-TIPs). I could demonstrate it with CAMSAP2, MT -TIPs proteins. CAMSAP2 specifically recognise the native or recombinantly prepared γTuRC capped microtubule minus ends. As well as I could demonstrate the increased MT nucleation in *Xenopus leavis* egg's extract with influence of CAMSAP2 and katanin p60.

With immunofluorescence analysis, I identified actin inside γTuRC. I could deny the possibility of actin filaments assembly from this position. I have purified the *Drosophila melanogaster* γTuRC, that resembled the conformation of vertebrates γTuRC and have densities corresponding to actin densities in vertebrates γTuRC. By omitting actin binding site, I could purify intact actin-deficient γTuRC from human cells and confirm that actin is not necessary for γTuRC assembly. By analysing the position of actin inside of γTuRC capped microtubule minus, I could observe the repositioning of actin densities, suggesting its involment into MT nucleation.

Mine work brought better insight into understanding of microtubule nucleation and its regulation.

Zusammenfassung

Mikrotubuli (MTs) sind Teil des Zytoskeletts und verantwortlich für den Zelltransport, die Zellform und die Zellteilung. Die Mikrotubuli-Nukleation erfolgt an bestimmten Zellorganellen, den sogenannten Mikrotubulus-Organiationszentrum (MTOC). Als wichtigste Mikrotubuli-Nukleator gelten yTubulin-Komplexe (yTuCs). In niederen Eukaryoten wird es über einen tetrameren Komplex erzeugt, der aus GCP2, GCP3 und zwei Kopien von y-Tubulinen besteht und als y-Tubulin-Kleinkomplex (y-TuSC) bezeichnet wird. Bei höheren Eukaryoten ist der Komplex komplexer und besteht aus zusätzlichen GCPs (GCP4-6). Ich war maßgeblich an der Entdeckung der Struktur des yTuRC (y-Tubulin-Ringkomplexes) von Wirbeltieren beteiligt. Überraschenderweise ist yTuRC bei Wirbeltieren asymmetrisch zur Mikrotubuli-Symmetrie und tief im Inneren seiner Struktur ist ein Aktinmolekül eingebettet.

Meine Doktorarbeit fokussierte sich auf das Verständnis, welche Konformationsänderungen in yTuRC bei der Mikrotubuli-Nukleation erscheinen und was das Schicksal von Aktin ist. Daher habe ich Protokolle erstellt für die Reinigung der mit yTuRC abgedeckten Mikrotubuli-Minusenden für die Zwecke der Kryo-EM-Analyse und der biochemischen Analyse. Anhand der Struktur der yTuRC bedeckten Mikrotubuli-Minusenden, die über den RanGTP-Chromosomenweg induziert werden, konnte ich die Fehlausrichtung der MT-Protofilamente von den Unterinheiten von yTuRC ebenso wie den partiellen Verschluss von yTuRC beobachten. Diese Merkmale können anhand der MTs Minusenden Endbindungsproteinen (-TIPs) erkannt werden. Ich konnte dies mit CAMSAP2, den MT-TIPs-Protein, demonstrieren. CAMSAP2 erkennt spezifisch die nativen oder rekombinant hergestellten yTuRC- bedeckten Mikrotubuli-Minusenden. Zudem konnte ich die erhöhte MT-Nukleation im Ei Extrakt des *Xenopus leavis* unter Einfluss von CAMSAP2 und Katanin p60 nachweisen.

Mit der Immunfluoreszenzanalyse konnte ich Aktin in yTuRC feststellen. Von dieser Stelle aus konnte ich die Möglichkeit einer Polymerisation von Aktinfilamenten ablehnen. Ich habe das *Drosophila melanogaster* yTuRC gereinigt, welches der Konformation von Wirbeltieren yTuRC ähnelt und Dichten aufweist, welche den Aktin-Dichten von Wirbeltieren yTuRC entsprechen. Durch das Weglassen der Aktin-Bindungsstelle konnte ich intaktes Aktin-defizientes yTuRC aus menschlichen Zellen reinigen und belegen, dass Aktin für den TuRC-Zusammenbau nicht notwendig ist. Mit der Analyse der Position von Aktin im yTuRC bedeckten Mikrotubuli-Minus, konnte ich die Neupositionierung der Aktin-dichten feststellen, welches darauf hindeutet, dass es an der MT-Nukleation beteiligt ist.

Meine Arbeit brachte einen besseren Einblick in das Verständnis der Keimbildung von Mikrotubuli und deren Regulierung.

Table of content

1. Introduction

1.1. Microtubules

Microtubules (MTs) are part of the cytoskeleton, which is responsible for cell's cargo trafficking, cell shape and its division. MTs are the biggest cytoskeletal elements with a diameter of 25 nm and relatively rigid structure. Depending on the cell cycle, MTs may fulfill different roles. In interphase cells or cells from differentiated tissue MTs create the tracks for cargo trafficking, such us signaling vesicles in axons of neurons and organelle transport or take part in cell's adhesion and its polarization. MTs play a fundamental role in segregating the chromosomes into two cells during the mitosis. For its crucial position in cell division, MTs are targeted in chemotherapeutic drug treatment of cancer.

1.1.1. Structure of microtubules and tubulin modifications

Structurally, MTs are hollow cylinders created by filaments of α- and β-tubulin dimers, called protofilaments. The assembly of protofilaments creates a polarized tubule with a fast growing plus end exposing β-tubulin as last subunit and a slowly growing minus end exposing α-tubulin (Fig 1-1a).

In most cells MTs are composed out of 13 protofilaments, with some exceptions on tissue specific manner (Fig. 1-1c). MT's function and structure are determined by the complexity of the tubulin, by its tissue specific isoform expression and by posttranslational modifications (Fig. 1-1b) [2]. For example, human cells express nine isoforms of α- and β-tubulin genes, from which *TUBA1A* and *TUBB* are expressed in all cell types while other isoforms are express tissue specify depending on MT function, such as motile function in the sperms and cargo trafficking in neurons[3,4]. Some isoforms may influence number of protofilaments in MTs, such as *mec-12* and *mec-7* coding for α- and β-tubulin in *Ceanorhabditis elegans* creating 15 protofilament MTs in mechano-sensory neurons (Fig.1-1c I) [5]. Additionally, 15 protofilaments were found in mechano-sensory cells in guinea pigs and mice (Fig. 1-1c III)[6,7]. Remarkably, some cells may change protofilament number from 13 to 15 protofilaments through biochemical signaling as it is in human blood platelets upon its activation (Fig. 1-1c IV) [8].

Cell's specific requirements may have the advantage to use 15 protofilament MTs as they are predicted to be more rigid then 13 protofilaments microtubules or may have advantage by forming microtubule bundles [9]. As well as, also in diameter smaller MT with 11 protofilaments were found in epidermal cells of grass lily *Ornithogalum umbellatum*[10] or 12 protofilaments as it is in lobsters in nerve cords (Fig. 1-1c II)[11].

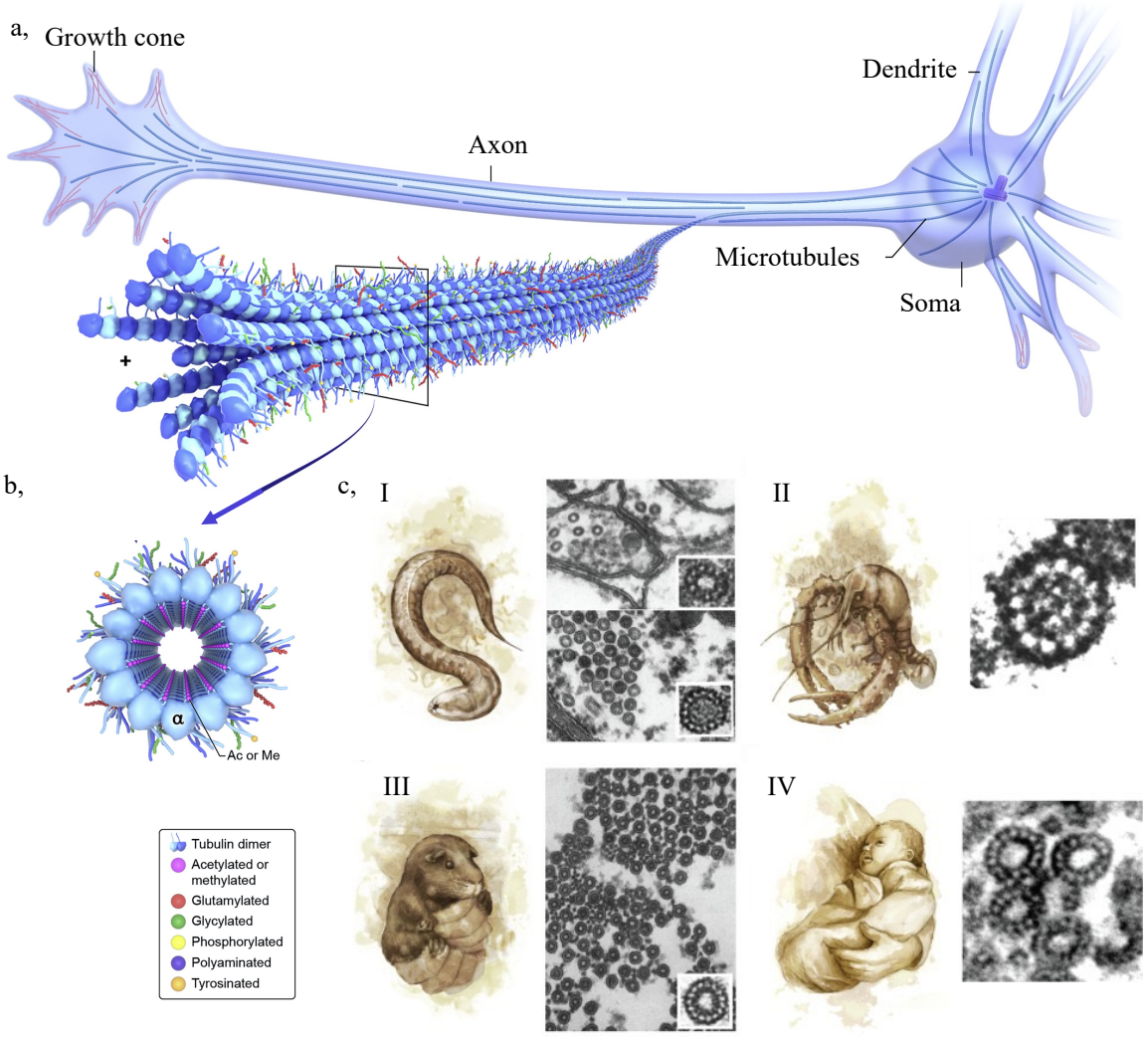

Fig. 1.1.: Tubulin code and posttranslational modification influencing function and structure of MT. a, b, MTs are crucial for neuronal development and function, it building blocks consisted of αβ-tubulin dimers undergo different posttranslational modifications. Picture is taken from[9]. c, examples of different protofilaments numbers in selected organisms. Taken from [9].

Further αβ-tubulins may differ by posttranslational modifications such us acetylation, phosphorylation, polyamination, glutamylation and glycylation of α- and β-tubulins or methylation, palmytoylation, detyrosination and removal of C-terminal glutamates in α tubulin

(Fig. 1-1a,b)[12]. Firstly, the posttranslational modification may as well influence protofilaments number, such it is by acetylation of α-tubulin by acetyltransferase which prompted formation of 15 protofilaments in vitro [13,14]. Secondly, various cargos determine their direction based on posttranslational modifications, for example lysosomes move between tyrosinated and acetylated MTs in direction to the cell's core [15].

MT's function is depended on its structured determined by tubulin code and posttranslational modification. Additionally, the structural arrangement in MT lattice alone, including GTP hydrolytic stage, can regulate the binding of the specific partners.

1.2. MT associated proteins (MAPs)

MTs are highly dynamic structures with defined polarity. Two ends of MTs differ in kinetic parameters such us speed of nucleation and occurrence of catastrophe. β-tubulin exposed plus end quickly polymerized, which is characterized with a more pronounced GTP cap and more structurally separated tubulin protofilaments. The plus-end is characterized by formation of MT mass and creation of interaction platforms with different subcellular structures, e.g. the kinetochore. Whereas the slowly polymerized minus end with the exposed α-tubulin subunit has a smaller GTP cap, is often capped and stabilized by the γTuRC and is anchored to the MT organizing centers (MTOC)[16–18]. MT associated proteins, shortly called MAPs, recognize the binding site of MTs based on differences in GTP stage and protofilament arrangement. Based on which end of the MT the MAP binds, we recognized plus and minus tracking proteins (+/- TIPs) [19–21] .

MAPs bind to MTs and fulfill different functions, from stabilization (such as CAMSAP protein family, CLASP, APC), anchoring of MT branches (augmin), facilitating of polymerization (γTuRC, ch-TOG, EB1), depolymerization (MCAK) to convoy transport processes (motor proteins kinesin and dynein).

1.2.1. MT plus end tracking proteins

MT plus end tracking proteins (+TIPs) have got structural and functional variations between its members. Fulfilling function in MT dynamics such us polymerisation or depolymerisation, stabilisation of MT seeds or supporting interaction with other structures.

+TIPs are classified based on their protein domain composition and function as EB proteins (EB1-3), CAP-Gly proteins (CLIP170, p150 ^{glued}), SxIP proteins (APC, MACF, STIM1), TOG proteins (ch-TOG, XMAP215, CLASP) or motor proteins (kinesin, dynein, myosin)[22].

The ability of the end-binding (EB) protein family to bind to the plus end of MTs was proposed based on recognised GTP stage of β-tubulin, which is more prolonged at the plus end of MTs [23], but later structural studies suggest that EB1 proteins recognised more disrupted lateral interactions of protofilaments at their plus end[24]. EB proteins are composed from the N-terminal calponin homology (CH) domain, which binds to the MTs. Closer to its C-terminus is a coil coiled domain responsible for dimerization[20] and the C-termini EB homology domain (EBH) [25]. Some EB proteins contain a C-terminal EEY/F motif[26]. Both EBH domain and EEY/F motives recruit other +TIPs to MTs[27] and serves as adaptor between MTs and other TIPs. A group of proteins which recognised EEY/F domain of EB proteins carry the cytoskeleton-associated protein glycine-rich (CAP-Gly) domain, such us CLIP proteins and the large subunit of dynactin complex p150^{glued}. A second group of proteins that bind to EB proteins share the small four residue motif Ser-x-Ile-Pro (SxIP motif)[28,29], where x is whatever amino acid [21,22,26]. Protein screens identified a large group of proteins containing the SxIP motif. These proteins consist of protein kinases, a small GTPases, centriole-, membrane-, and actin-associated proteins[30–32].

Another group of +TIPS are proteins contain TOG domains, named after discovery of colonic and hepatic tumour-overexpressed gene, called CKAP5. To this group includes human ch-TOG, its *Xenopus leavis* orthologue XMAP215, yeast Stu2 (suppressor of tubulin 2), and CLASPs proteins. ch-TOG together with XMAP215 consist of five ToG domains[22]. Yeast Stu2 contains only two TOG domains. The predisposition to binding to the plus end of MTs is based on TOG domains preferences to the curved conformation of the tubulin dimer and recognition of outwardly curved tubulin sheets or protofilaments[33,34]. XMAP215 consists of the C-terminal MT lattice-binding domain, a disordered basic region with affinity to the negatively charged MT lattice. ch-TOG has got plus end tracking behaviour comparable with EB proteins. Recent studies showing colocalization of ch-TOG together with γTuRC in spindle during mitosis and at Golgi apparatus during interphase. Recruitment of both, ch-TOG and γTuRC seems co-depended [35–38]. Where recently was shown that interaction with γTuRC is transient for facilitate MT nucleation from γTuRC and ch-TOG after that moved to the plus tip of growing MT[35]. ch-TOG is considered as MT nucleator, by its ability of binding tubulin dimers, binding to the pre-existing MT lattice or by brief binding to γTuRC and adding the tubulin dimers to growing

protofilament, where it increases the rate of MT assembly[33,39–42]. ch-TOG increases the speed of MT assembly by multiple folds [38,39,42].

Additional categories of TIPs are motor proteins tasked with cargo transport along MTs.

1.2.2. MTs minus end tracking proteins -TIPs

MAPs recognizing the specific composition of exposed α-tubulin at the MT minus end. Binding of MAPs to protofilaments or tubulin dimers based on their GTP status may have stabilization, depolymerization or nucleation function. These proteins are called minus tracking proteins (-TIPs).

1.2.2.1. γ-tubulin complexes γTuC

Microtubules nucleation depends on assembly of α- and β-tubulins into 13 protofilament's polymers. In 1990 researchers identified an additional form of tubulin named γ-tubulin[43]. Function of γ-tubulin was proposed to induce the α- and β-tubulin polymerization. γ-tubulin alone polymerizes to create filaments. Later, γ-tubulin was identified to bind to additional proteins, called γTuC component proteins - GCPs [44,45]. GCPs contain two domains, GRIP1 through which GCPs are laterally connected and GRIP2 that interacts with γ-tubulin (Fig. 1.2.a) [46].

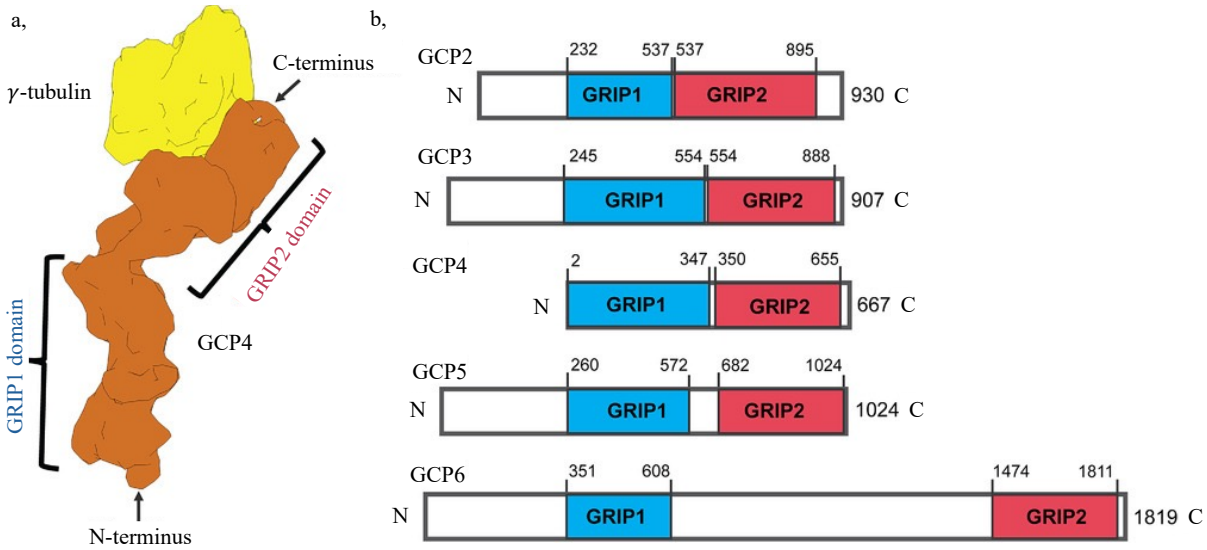

Fig. 1.2.: Domain characterization of GCPs, building blocks of γTuRC. a, Schematic of GCP4 with indicated N-terminus GRIP1 domain and C-terminus GRIP2 domain bound to γ-tubulin. b, Domain organization of *Homo sapiens* GCP2-6 aligned according GRIP1 domain. Adapter from[47] .

In *Saccharomyces cerevisiae*, two paralogues of GCPs, GCP2 and GCP3 with the bound γ-tubulin create a tetramer in V shape which is the basic model of the γ-tubulin small complex (γTuSC)[48]. Upon activation through the CM1 motive of the spindle pole body component Spc110, seven copies of γTuSC oligomerize into a left-handed, ring like structure that is symmetrical to MT [49,50]. Upon oligomerization, spoke 1 and spoke 14 overlap and create accessible only for 13 γ-tubulin molecules for nucleation [50].

Some other organisms such us *Schizosaccharomyces pombe*, *Aspergillus nidulans* or *Drosophila melanogaster* have got active not only γTuSC but also γTuCs with same comparable composition as the vertebrates system. The vertebrate γTuC system is more complex and therefore called γ-tubulin ring complex, γTuRC. Apart of having components of γTuSC, three additional GCPs are presented, GCP4, GCP5, GCP6 [51,52]. All GCPs contain GRIP1 and GRIP2 domains and differ in amino acids extensions of the N-terminus or C-terminus and the spacer region between the two GRIP domains (Fig.1.2.b) [47]. Apart from GCPs additional proteins are associated with γTuRC. Mitotic spindle organizing protein 1 and 2 (MZT1/2), together with NEDD1 (neural precursor cell expressed, developmentally down-regulated 1) and NME7 (nucleoside diphosphate kinase 7) were also identified as components of γTuRCs (Table 1) [53,54]. NEDD1 has functions in anchoring of γTuRC to MTOCs [55–57] and NME7 proposed function is in promoting of γTuRC nucleation activity [58].

Table 1.: Composition of γTuCs in chosen organism with indication of γTuSC and γTuRC building blocks. [47]

	Homo sapiens	Xenopus leavis	Drosophila melanogaster	Schizosaraccharomyces pombe	Aspargillus nidulans	Candida albicas	Saccharomyces cerevisea
yTUSC	GCP2	Xgrip110	Dgrip84	Alp4	GCPB	Spc97	Spc97
	GCP3	Xgrip109	Dgrip91	Alp6	GCPC	Spc98	Spc98
	y-Tubulin	Xtubg1	gammaTub 23C/37C	Tug1/Tubg1	mipA	Tub1	Tub4
yTURC	GCP4	Xgrip76	Dgrip75	Gfh1	GCPD	-	-
	GCP5	Xgrip133	Dgrip128	Mod21	GCPE	-	-
	GCP6	Xgrip210	Dgrip163	Alp16	GCPF	-	-
Other	Mzt1	Mzt1	Mzt1	Mzt1	MztA	Mzt1	
	Mzt2	Mzt2	-	-	-	-	-
	Actin	Actin	undetermind	undetermind	undetermind	-	-
	NME7	NME7	Nmdyn-D7	undetermind	undetermind	undetermind	-
	Nedd1	Nedd1	Dgp71WD	-	-	-	-

(-) = not abundant or not identified. Adapted from[47].

In 2020, three structural studies solved the architecture of γTuRC. revealing surprisingly conclusions. While γTuSC creates symmetrical rings very similar to MTs, γTuRC

is an asymmetrical structure. Comparable to the γTuSC, GCP2 and 3 together with γ tubulins create a tetramer and GCP4 creates tetramers with GCP5 and GCP6 (GCP4546). The positions of GCPs are from the first spoke GCP(2-3)4-GCP(4-5)-GCP(4-6)- GCP(2-3), with stoichiometry 5 (GCP2) : 5 (GCP3) : 2 (GCP4) : 1 (GCP5) : 1 (GCP6) [53,54,59].

MZT1 is important for the structural assembly of complex as well as an adapter that mediates anchoring and activation of γTuRC [60,61]. Consistent with two functions, MZT1 was found outside of the γTuRC but also in the lumen assisting the assembly of the γTuRC [62,63]. MZT1 creates modules with the N-termini of GCP3, GCP5 and GCP6 that decorate the exterior and the lumen of γTuRC (Fig.1.3.b,d) [63–65].

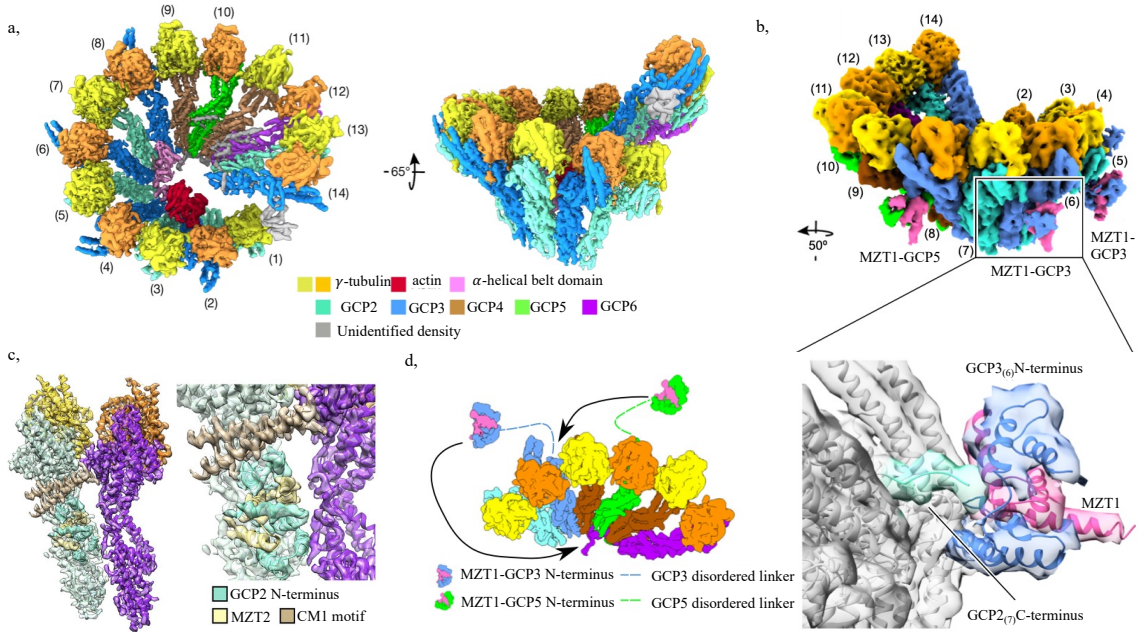

Fig. 1.3.: Architecture of vertebrates γTuRC. a, Cryo-EM reconstruction of *Xenopus leavis* γTuRC with colour identification of components. Picture adapted from [53]. b, Reconstruction of recombinantly prepared γTuRC with identification of additional densities belonging to modules of N-terminus of GCP3 and MZT1 at the outside of the ring complex. In the zoomed pictures the position of N-terminus of GCP2. Adapted from[62]. C, Position of CM1 motive at interphase of spokes 12 and 13 with close contact to N-terminus of GCP2. Adapted from[66]. d, MZT1-GCP5 module binds to outside of GCP3 at spoke 8, while the N-terminus of GCP3 (spoke 8) with the MZT1 module is in lumen of the γTuRC. Adapted from [62].

Additional protein associated with γTuRC is CEP215 (other names CDK5RAP2, Cnn in *Drosophila melanogaster* system). CEP215 contains the CM1 motif at its N-terminus that binds to γTuRC and promotes MT nucleation. The CM2 domain at the C-terminus promotes oligomerization of CEP215 via its leucine zipper domain [67,68]. Oligomerization occurs in

expanding PCM during mitotic entrance where CM1 motive is important for its centrosomal accumulation and recruitment of the γTuRC [69,70].

Wieczorek et al. using CM1 motif to purify γTuRC were able to identify the position of the CM1 motive of CD5RAP2 at spoke 12 and 13 (Fig.1.3.c)[59], further analysis of recombinant γTuRC revealed that this CM1 binding site contains MZT2 and the N-terminus of GCP2[62]. Compare to the yeast system it is possible, that similar interfaces for the CM1 binding site exists [71].

Position of NME7 and NEDD1 was still not resolved despite stoichiometrical composition as indicated by mass spectrometry of the purified γTuRC and high resolution analysis of the structure [53,54].

1.2.2.2. CAMSAP protein family and katanin collaboration

In mammalian cells the calmodulin-regulated spectrin-associated protein (CAMSAP) family is composed of four proteins, CAMSAP1-3 and ASPM. In *Drosophila melanogaster* only the homolog of CAMSAP3 called Patronin [72] exists that is involved in spindle assembly and maintenance of the MT network in interphase. Patronin also prevents depolymerization of MTs and protects the MT minus end [73].

Mammalian CAMSAP proteins differ in amino acid length but also in their expression during the cell cycle. While CAMSAP1 to 3 are expressed and are active in interphase. ASPM is active in mitosis during spindle assembly. CAMSAP2 and 3 co-localize to the minus end of non-centrosomal MTs in mammalian epithelial cells [74,75]. Using purified CAMSAP protein, it was observed that CAMSAP1 has MT minus end tracking properties comparable to EB proteins at the MT plus end (Fig. 1.4.a). CAMSAP2 and 3 decorate the lattice of the MT minus end. Tagged CAMSAP2 expressed in MRC5 cells colocalization with the γ-tubulin signal at centrosomes. Eventually, the CAMSAP2 signal migrate to the periphery of MT asters during mitotic spindle assembly[19].

The abnormal spindle like microcephaly associated (ASPM) protein participates in organising the mitotic spindle in cells (Fig.1.4.e,f) [76,77]. Defects in this protein are associated with microcephaly, neurodevelopmental disorder characterised by underdeveloped brain leading to retardation [78,79]. Like CAMSAP proteins, ASPM as well tracs MT minus ends and decorates the lattice [80].

CAMSAP proteins bind to MTs via their CKK domain. Analysis of the human CKK domain of CAMSAP1 shows that its recognition of MT minus end is based on the αβ-tubulin protofilament architecture, showing preferences to gently curved protofilaments that are caused by altered inter-protofilament interface. CKK recognises the enhanced lateral flattering of α-tubulin at the MT minus end (Fig.1.4.b). CKK binding causes the skew of protofilaments [81,82].

Interphase active CAMSAP2 and CAMSAP3 and mitotic ASPM have a conserved short helical motive which interacts with katanin and together they regulate the stabilisation and length of the MT minus end (Fig.1.4.c,d) [19,80,83].

Katanin together with spastin are part of MT severing proteins. Katanin is composed of two subunits, called p60 and p80. The p60 subunit has catalytical activity and belongs to the AAA family of ATPases [12]. Katanin is also involve in regulation of spindle assembly [84]. Even when its function is in severing of MTs, in this way it controls the MT mas: by increasing the MT seed number it promotes MT nucleation[85,86].

CAMSAP family proteins together with its counterpart katanin regulate spindle assembly as well as MTs from non-centrosomal MTOCs (Fig.1.4.c,d,f). Mutations inside of these proteins are associated with neurodegenerative disease supporting the importance of these proteins during development.

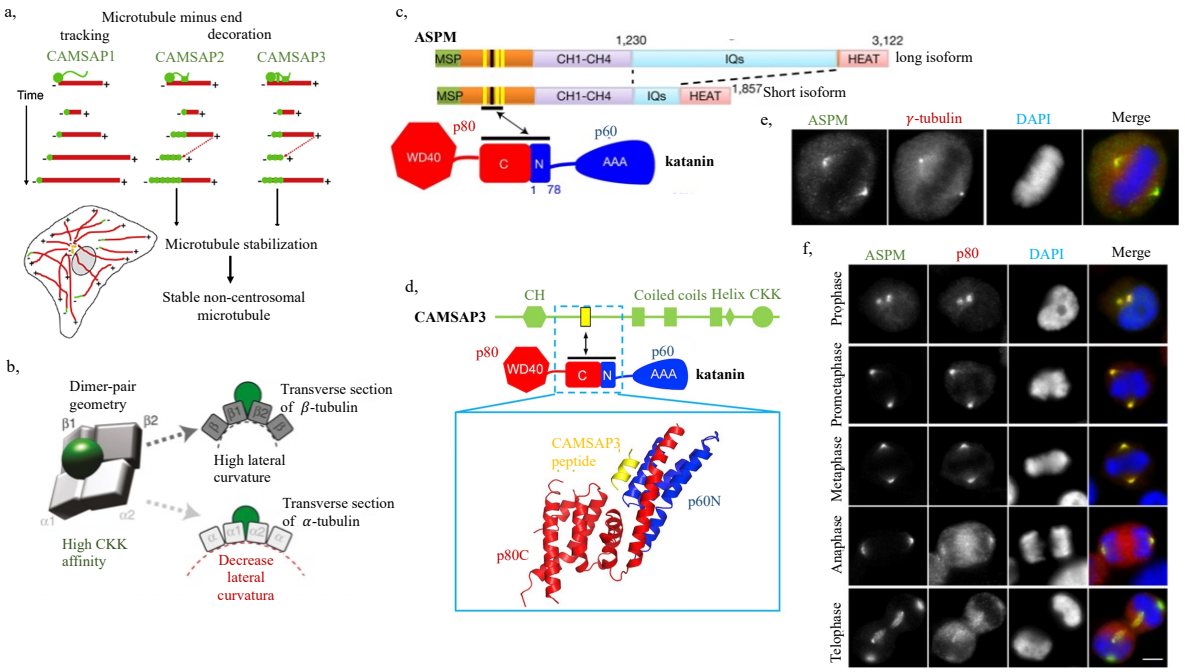

Fig. 1.4.: Characterisation of CAMSAP protein family and its interaction with katanin. a, Schematic characterisation of CAMSAP family proteins and its binding properties to the MT minus end. Adpated from [19] b, At the MT minus end α-tubulins are more flattered as at the MT plus end or middle part, this flattering compare

to angle of β-tubulin is proposed as conformational stage at which CKK domain of CMASAPs recognise binding sites. Adapted from [81]. c, domain composition of ASPM with identification of position of helical motive which interacts with the interface of p80 and p60 subunit of katanin. Adapted from[80]. d, Domain composition of CAMSAP3 with identification of the helical motif which interacts like ASPM with katanin. Adapted from [87]. e, colocalization of ASMP with γ tubulin at spindle poles during mitosis. f, Co-localisation and distribution of ASPM and p80 subunit of katanin in different phases of mitosis. e, and f, is adapter from [80].

1.3. MT organizing centers MTOC

MT nucleation occurs at specific positions in the cell, and it is correlated with the cell cycle and functional requirements. MT organization center (MTOC) is a cellular organelle from which all MTs are emerged. Cells can have multiple MTOCs, whereas MTOCs could be divided into centrosomal and non-centrosomal MTOCs. Each of these MTOCs have got their specific sets of proteins involved in MT nucleation [88,89]. Most prominent features of MTOCs are the presence of minus ends capping proteins, microtubule nucleator γTuCs or MT anchoring proteins. The second feature is its cell cycle regulated activity. Centrosomal MTOCs are activated during mitosis to fulfill assembly of the mitotic spindle. The exeption of non-centrosomal MTOCs, is the SPB in yeast and the chromatin that are involved in spindle assembly during cell division in cells lacking the centrosomes. Other non-centrosomal MTCOs fulfill its function in non-dividing cells in maintain cell needs in intracellular transport, cell motility and keeping cell architecture. The exeption of non-centrosomal MTOCs, is SPB of yeast and chromatin that are involved in spindle assembly during cell division.

1.3.1. Centrosomal MTOC (c-MTOCs)

Centrosomes are cytoplasmic organelles that are highly evolutionarily conserved and can be found in higher eukaryotes. Their main function is to act as the main MT organizing center (MTOC) and they also regulate actin organization [90]. Centrosomes are primarily studied during cell division in mitosis, where they serve as poles of the mitotic spindle that regulate chromosome segregation. During interphase, centrosomes organize the MT network, oversee cell motility and may form cilia [90–92].

Centrosomes are present in almost all eukaryotic cells, except for yeast, higher plants, and oocytes [93,94]. In *Xenopus leavis* egg extracts lacking centrosomes, spindle assembly is induced via the RanGTP chromosomal pathway with the help of motor proteins such as dynein

and kinesin, and the augmin complex mediates branching of MTs [95–97]. In yeast cells function of centrosome in assembly spindle poles fulfil SPB (Spindle pole body)[98].

Centrosomes are composed of two centrioles connected through linker proteins. Centrioles are cylindrical structures created by 9 -fold symmetrically arranged MTs triplets. Each A tubule of the MT triplets consist of 13 MT protofilaments. B and C tubes have got each 10 protofilaments. The centrioles are polarized structured, where at the proximal end inside of the lumen of the newly created centriole is localized the cartwheel structure. The cartwheel structure plays a crucial role in centriole formation and is typically retained even after centriole maturation in most species, but it is absent in human cells[99,100]. The main building block of cartwheel is SAS6 protein[101]. The MTs triplets at the proximal end of centrioles are connected by the A-C linker. The structural conservation between species of the centriole is evident, with differences in doublets or triplets of MTs. creating a nine-fold symmetrical cylinder on average. However, there are exceptions in certain organisms and cell types [90]. The size of the cylinder may vary from 100 nm in *C. elegans* to 4000 nm in *Trichonympha*, and some organisms lack a cartwheel [102].

After each cell division the cell contains two centrioles connected via linker proteins [18,90,91]. In the S phase, the new procentrioles assembles on the wall of the existing mother centrioles. The process starts with formation of spot consisting of oligomers of Polo- like Kinase 4 (PLK4). The recruitment of PLK4 is initiated via CEP152 and CEP192, that create scaffolds at the outer wall of centrioles [103,104]. While CEP192 is primarily situated near the inner regions of the PCM towards the centriole, CEP152 is positioned approximately 100 nm away [105,106]. These disproportions may be explained by interaction of CEP152 with another proteins CEP57 and CEP63, creating dimeric and trimeric complexes [107,108]. While CEP192 is always localized close to centrosomes, CEP152 has a cytoplasmic localization and upon trimerization with the above-mentioned proteins in late G1 phase. is recruited to the daughter centriole, which upon duplication will become the new mother centriole and will keep the CEP152 decoration[104,109]. CEP152 and CEP192 interact with CPB domain of PLK4 in a competitive manner *in vivo* [69], whereas CEP152 has got six-time stronger affinity to CPB compare to CEP192 [106]. This affinity and localization differences may define the further position and regulation of PLK4. CEP152 snaps the PLK4 bound to CEP192 and repositions it to the outer zone of the PCM. The loss of CPB binding ability in CEP152 results in centriole biogenesis defects, even in conditions of heightened cytoplasmic PLK4 concentration [69,105]. So this scaffold switching appears to be necessary for PLK4's function. In this stage PLK4 decorates the centrioles in ring like symmetry, which have to be positioned as single dot at the

future procentriole assembly site of the pro-centriole [110,111]. Lacking this reposition function leads to failure in SAS6 recruitment [111]. Notably this process may be important for activation of PLK4, which creates homodimers and trans-auto-phosphorylates itself [112].

Interestingly, the transition from a ring-like state to a dot-like state is not well understood, but two events may play a crucial role. PLK4 kinase is a self-destructive kinase, which upon phosphorylation of its degron motive at the N-terminus activates the E3 ligase βTrCP- mediated degradation [113,114]. A recent study showed that inactive PLK4 protects itself via phase separation through flexible linker region [110]. The autophosphorylation of the PC3 motive in the C-terminus CPB increases exposure of hydrophobic regions causing the clustering of PLK4 [111]. This suggests that autophosphorylation of CPB region promotes PLK4 ring to dot formation. A second key player is the protein STIL, called as well SAS5 or Ana2, which together with PLK4 recruits building blocks of cartwheel, protein SAS6 [115,116]. STIL is recruited to the PLK4 site where it becomes phosphorylated by PLK4. Studies suggest that STIL has a double influence on PLK4 [117–119]. Two discrete segments within STILL exert different influences on PLK4. Specifically, the coiled-coil region (721-746 aa) binds to and shields PLK4 from degradation, whereas the C-terminus region (1268-1287 aa) facilitates the autophosphorylation of the degron motif at the pericentriolar ring regions [118]. However, the regulation of this double function of STIL is still unknown.

The PLK4 -STIL complex regulates the localization of SAS6 protein. SAS6 is the building block of the central cartwheel at the proximal end of centrioles [115,116]. Structurally SAS6 is composed of N-terminal globular domain, the middle part is created by a coiled-coil domain and C-terminus is unstructured. The coiled coil domain is responsible for homodimerization of SAS6. 9 copies of SAS6 homodimers then interact via their N-terminal globular domain to from the ring–like structure of the central hub[120,121] SAS6 forms a central hub consisting of nine stalks. SAS6 occupies a central position within this hub and to theperiphery SAS6 interacts with CEP135 to create pinheads, which interacts with MT of A-tubules[116 122]. A-tubules consist of 13 protofilaments and are considered to be created by the γTuRC. Some data suggest even direct interaction between C-terminus of SAS6 and γTuRC[123]. The centriolar MTs assembles into triplets by mechanisms requiring δ- and e-tubulin within C-a B- tubulus[124,125] and MT elongation processes untill the end of S phase. Additional proteins, such as CEP120, SPICE1, CEP295, Centrobin, POC1 and POC5, etc. [126–131] are involved in this elongation. The process is stopped by recruitment of CP110 and CEP97 to the distal end of procentriole[132,133]. During the late G2 phase, the two mother centrioles undergo severing of

the centrosome link by NEK2 kinase. In addition, newly assembled centrioles are converted into centrosomes in G2. A further maturation step involves assembly of distal and subdistal appendages at the distal end of centrioles. Distal appendages are involved in docking of centrioles to the plasma membrane in case of cilia formation [134], subdistal appendages recruit factors involved in microtubule nucleation and anchoring [135].

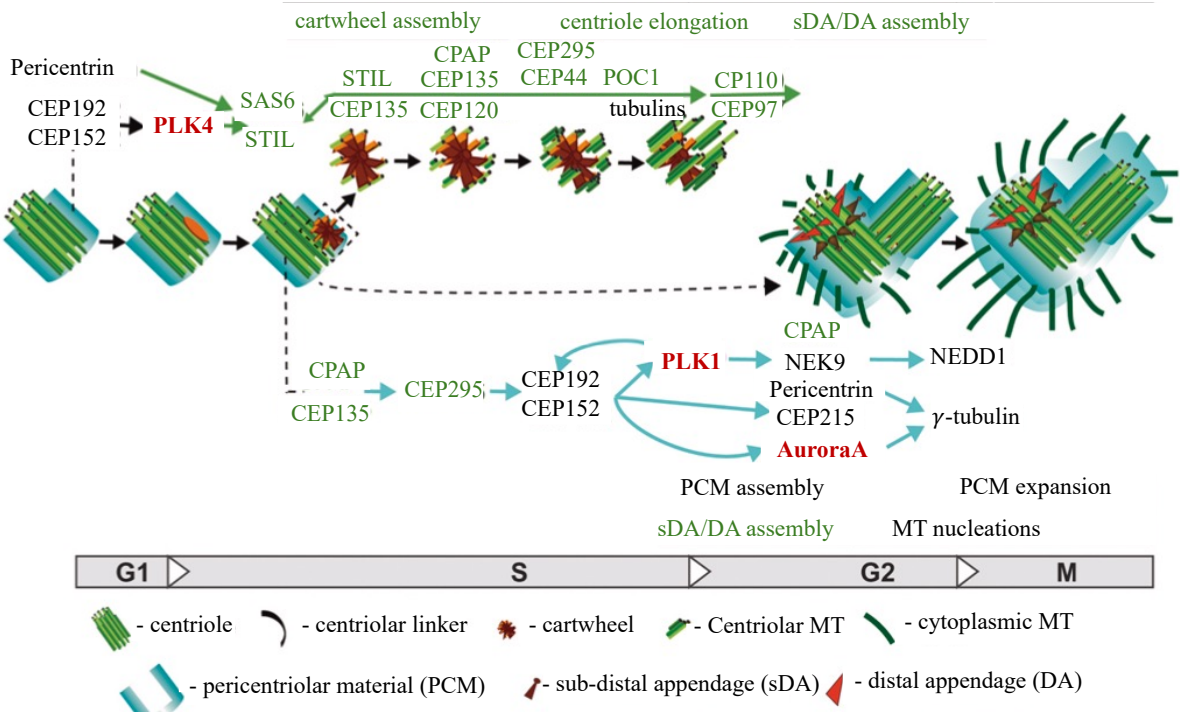

Fig. 1.5.: Model of centrosome assembly. Procentriole assembly is started with accumulation of kinases PLK4 to the wall of existing centriole via PCM components CEP192 and CEP152. PLK4 recruits the additional protein essential for procentriole assembly and elongation during the S phase. During G2 and M phase is activated the PCM assembly with activation of PLK1 kinase that recruits cytoplasmic proteins to the centrosomal site. During the M phase PCM is expanded and regulates MTs nucleation. Protein components of centrioles and PCM often collaborates and regulates each other. Taken from[90].

By entry into M phase, we refer to the older centrioles as a mother centriole with characteristic distal and sub-distal appendages, which are partially disassembled in mitosis, and the new centrioles as daughter centriole with the inner cartwheel[90]. Centrosomes are surrounded by an electron dense matrix called pericentriolar material (PCM)[136]. The PCM is the structure that harbors the gTuRC and is crucial for spindle assembly.

1.3.2. Non-centrosomal MTOCs (n-MTOCs)

Ciliary base and basal bodies are MT structured protrusions of cell surface that come in two types with different function. Motile cilia are responsible for movements of cell, whereas primary cilia are non-motile and are involved in transduction of sensory, homeostatic and developmental signaling pathways[137]**.** Upon cell differentiation, centrosomes frequently become inactive, and the mother centriole is used as basal body for cilia assembly. Keeping PCM components around basal body MT nucleation is dependent on γTuRC, CEP215, pericentrin[17]. MTs minus end stabilization protein CAMSA3 were identified as well as a component involved in cilia MTOC (Fig.1.6. a)[138,139].

Golgi complex and Golgi outposts (endosomes) play a crucial role in cell polarization and regulating cargo trafficking direction. MTs are anchored to the Golgi through the scaffolding protein AKAP450, which is bounded to the cis Golgi matrix component GM130 [70,140]. Subsequently, AKAP450 recruits CDK5RAP2 or its paralogue myomegalin. These two proteins interact with the major MT nucleator γTuRC. In the second approach AKAP450 interacts with CAMSAP2, which functions in stabilizing the minus end of MTs[17] . Additionally, *in vitro*, CAMSAP2 may induce MT assembly (Fig.1.6. b)[141]. Another pathway involves CLASP proteins, which contain TOG domains, and they are anchored to trans-Golgi via GCC185 protein[142]. This pathway is also involved in γTuRC dependent nucleation and in anchoring CAMSAP2 stabilized MT minus ends[17,22].

The **nuclear envelope (NE)** is another type of MTOC specific for plant cells, differentiated animal cells such us muscle cells, osteoclasts, and *D. melanogaster* adipocytes. The primary function of this MTOC is to guarantee the proper position of nucleus and maintain overall cell structure. Upon myoblast differentiation was observed the recruitment of PCM components to proximity to NE, such as pericentrin and γ-tubulin[143]. A key component in mammalian cells is a specific isoform of outer nuclear membrane protein Nesprin 1. Nesprin 1 is involved in the recruitment of PCM1 [144], kinesin 1 motors [145]. Nesprin 1α recruits AKAP450 to NE[146]. AKAP6 fulfils the function of an adaptor protein between Nesprin 1 and its targets AKAP450 (known as AKAP9) and pericentrin[140]. Both AKAP450 and pericentrin are involved in the recruitment of γTuRC. Whereas in the case of fly adipocytes MT nucleation occurs in

γTuRC independent manners and key components are orthologues of Nesprin-spektraplaktin, XMAP215 and microtubules minus end stabilization proteins CAMSAP (Fig.1.6. c)[147].

The cell cortex plays a critical role in cell structure organization with its dense cytoskeletal composition. MTs as the most rigid part of the cytoskeleton bind to cell cortex with their minus end and the growing plus end is directed towards the inside of the cell body to ensure correct transport of structural and signaling components. This orientation is typical for plant cells and animal's epithelial cells[17,22,148]. Two pathways are involved, one γTuRC depended and one CAMSAP dependent, that anchor and stabilize the MT minus end. Apical cortex MTOCs are dependent on polarity regulators proteins, such as PAR3, PAR6, and aPKC [149,150]. PAR6 in *C. elegans* epidermis cells binds to the ninein orthologue NOCA1 [151], which interacts with γTuRC but also with the fly CAMSAP orthologue Patronin (Fig.1.6. d) [150]. The composition of the mammalian and fly apical cortex MTOC is similar to worms, where we find CAMSAP3, ninein and γTuRC [152,153]. Binding of CAMSAP3 that stabilizes MT minus ends is mediated by spectraplakin [154]. Interestingly, in fly salivary gland, CAMSAP stabilized MTs are released from centrosome via action of katanin and bound to the cortex via spectraplakin [155]. CAMSAP3 is involve in binding to adherens junctions [156], whereas ninein binds to desmosomes via desmoplaktin [157].

Chromatin and kinetochores fulfil the function of an MTOC in mitosis in cells lacking centrosomes, such us oocytes or plant cells [93,94]. The molecular pathway involved in MT nucleation depends on RanGTP and is later further discussed. Apart from the activation of the RanGTP chromosomal MT nucleation pathway, molecular key players are TPX2, Aurora A, γTuRC anchoring protein NEDD1 and augmin [17,158,159].

MT walls suits as for anchoring of augmin complex which binds γTuRC and promotes γTuRC depended microtubule nucleation[160]. Augmin is localized to the sites where branching of microtubules occurs[161], such us mitotic spindles in centrosomal or chromosomal spindle assembly[159,162], or in intherphase by plants or neurons[163–165]. Apart from γTuRC, additional key pleayers are TPX2, NEDD1 and Aurora A (Fig.1.6. e)[158,159,166].

Mitochondria in *D. melanogaster* spermatids have an interesting function in elongation of sperm cells via MT grow. MTs are organized at sites of one expanded

mitochondria that contains the testes specific isoform of CEP215, *Drosophila melanogaster* testes variant CnnT, that recruits γTURC. This system represents the basic system for MTOC generation (Fig.1.6. f)[167].

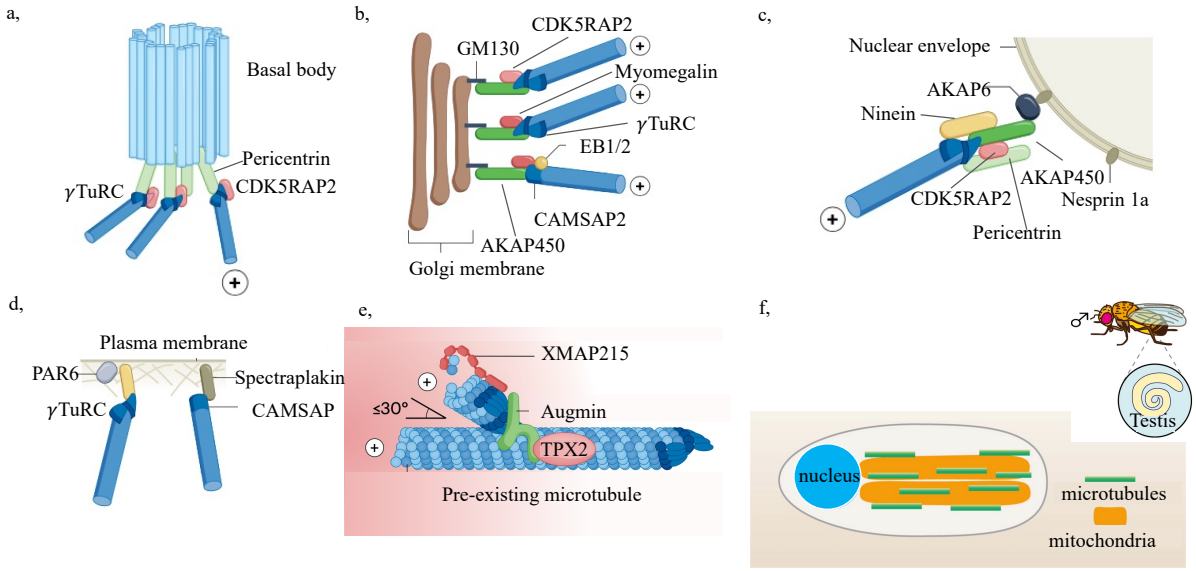

Fig. 1.6. : Non-centrosomal MTOCs. a, Ciliary basal body is created with mother centriole which carries with itself pericentriolar material containing pericentrin, CDK5RAP2 with γTuRC as basis for MT nucleation. b, The Golgi apparatus anchors MTs via G130 and AKAP450 proteins. CDK5RAP2 together with myomegalin binds γTuRC capped MTs. The second pathway is promoted by myomegalin bound to CAMSAP2 stabilized MT minus ends. c, AKAP6 as a part of nuclear envelope binds to AKAP450 which recruits pericentrin and ninein. Pericentrin binds to CDK5RAP2 activated γTuRC. d, The cell cortex contains cytoskeletal components, where MTs are bound via PAR6 - γTuRC interaction or via suggested binding of spectraplakin to the CAMSAP stabilized MT minus ends. Images a-d were adapted from [148]. e, Augmin as main component in the branched MT pathway is activated via TPX2 and the bounds to γTuRC. XMAP215 promotes grow of MTs via adding ab-tubulin subunit to its plus end. Picture is taken from[168]. f, The sperm in *Drosophila melanogaster* is elongated through interaction of giant mitochondria with MTs, where mitochondria anchor the MTs and organize them in prolonged manner. Pictures a,-d, are taken from[169]. Picture e, is taken from [168], picture f, is taken from [167].

1.4. MT nucleation

MT nucleation is a dynamic process in cells but also shows high dynamicity in the *in vitro* situation. We distinguish *de novo* assembly of MTs in *in vitro* conditions based on αβ-tubulin properties. MT nucleation in cells is highly regulated to ensure proper localization and functionality of MTs. In cells MT nucleation is regulated by multiple MAPs, where mayor influence on speed and efficiency have the γTuC complex and ch-TOG. As ch-TOG is out of

scope of my thesis, more information is available in[33,38]. During cell division, it is necessary to assemble spindle poles with sufficient numbers of MTs for chromosome segregation. Based on cell types two pathways exist that ensure spindle assembly: centrosomal and chromosomal MT nucleation pathways.

1.4.1. αβ tubulin dimer assembly into MTs – de novo nucleation

Kinetics measurements of MT nucleation resulted in a sigmoidal curve, with an initial lag phase that is characteristics with the formation of a stable core of αβ-tubulins dimers. At optimal αβ-tubulin concentrations the elongation of the MT seed continues spontaneously till it reaches a plateau phase where the concentration of polymerized and free αβ-tubulins is in balance (Fig. 1.7. a, b). One of the factor which influenced the stability of MTs is the balance between polymerized and free αβ-tubulin. When the balance is disturbed, MTs will disassembly to increase concentration of free subunit αβ-tubulin [170]. The major factor influencing polymerization rate is the critical αβ-tubulin concentration Critical αβ-tubulin concentration is concentration of the αβ-tubulin dimers that allows the assembly of microtubules. That concertation is defined in solutions in *in vitro* conditions and can differ between organisms and isoforms. In cells the local concentration of tubulin is regulated with MAPs. Other factors that determine the polymerization rate are the temperature characteristic to the body temperature of the αβ-tubulin source, accessibility to GTP, viscosity of the solution – which is modulated by glycerol in *in vitro* experiments - and by adding MT bindings proteins.

MTs are highly dynamic structures, which undergo repeatedly cycles of assembly and disassembly. This process is called dynamic instability. Driving force of this process is hydrolysis of GTP. Both, α- and β-tubulins bind to GTP upon polymerization, but only GTP bound to β-tubulin undergoes hydrolysis to GDP and Pi [171]. The speed of the hydrolytic reaction leads to creation of a GDP αβ-tubulins lattice in the middle part of microtubules and a GTP αβ-tubulins cap at the ends of the MT. Interestingly, at the GTP stage MTs are more stable whereas GDP hydrolysis induces the conformational change inside of ab-tubulin dimers leading to lower stability of the MT lattice. In this way, the GTP cap creates a protection barrier from depolymerization and triggers further MT grow[172]. Loosing of GTP cap leads to uncovering of GDP lattice and will lead into quick depolymerization causing the shortening of

MTs. The event is called catastrophe[173]. After that the MT may depolymerize completely or may be rescued by regrowing αβ-tubulin protofilaments creating a new GTP cap[174,175].

One question which is still not well understood is how the MTs are assembled. Protective function of the GTP cap is the most prominent hypothesis of stabilization of the MT seed. Whereas the GTP cap assembly may have three different views [176]. First, MTs grow from straight protofilaments by addition of αβ-tubulin subunits to the protofilaments, whereas GTP tubulin is straight and upon hydrolysis αβ-tubulin becomes curved (Fig.1.7. c I.)[177]. Second, MT grow in sheet like structures, which later on roll up to create the MT cylinder. This model is supported by *in vitro* nucleation studies (Fig.1.7. c II.)[178–180]. The 3rd model based on cryo electron tomography of cells of six species suggests that protofilaments assemble to MTs through stages of curvature of the growing end which is caused by adding curved GTP ab-tubulin subunits to curved protofilaments. Then the thermal fluctuation straightens the curved protofilaments to form lateral bonds between protofilaments that lead into stabilization of the MT seed (Fig.1.7. c III.)[181]. Interestingly, depolymerization also leads to curved protofilaments at the tip, suggesting that lateral interactions will weaken as first [177,181].

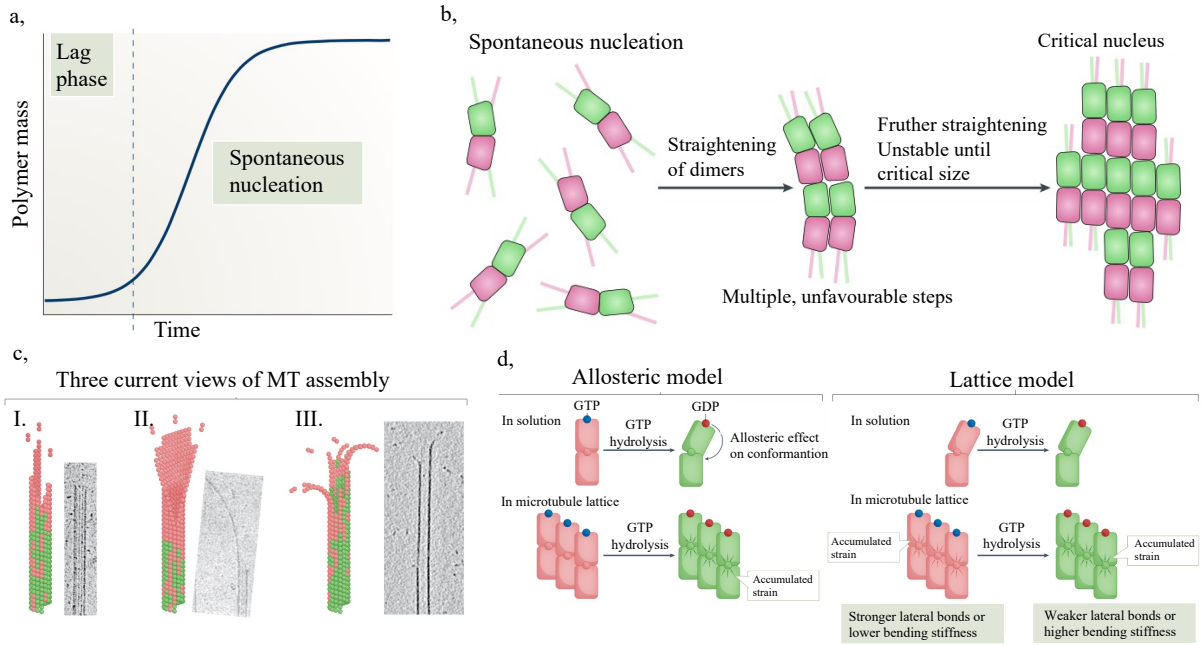

Fig. 1.7.: Spontaneous MT nucleation. a, characteristic sigmoidal curve of *in vitro* MT nucleation. Lag phase is characteristic by rapid MT instability [170]. b, Spontaneous nucleation involves multiple disadvantageous steps. Ab-tubulin dimers are curved and upon binding to longitudinal and lateral interactions need to be straighten. Addition of ab-tubulin buildings blocks created a critical nucleus which is necessary to overcome the initial instability in lag phase and nucleation from that point is linear [182] c, Models of MT growth with straight protofilaments (I.),

open sheet (II.), curved filaments at the tip (III.) with corresponding electron microscopic images. d, Allosteric and lattice model of GTP cap. Pictures a, is adapted from [170], b, is taken from [182] d, and c, are adapted from[176].

It is still questionable why GTP αβ-tubulin creates a more stable lattice as GDP αβ-tubulin. Two models try to explain this phenomena (Fig.1.7. d) [176]. The allosteric model suggests that hydrolysis of GTP causes a more bend conformational position inside of αβ-tubulins. Therefore, straight GTP αβ-tubulins create more stable lateral interaction, and GDP αβ-tubulin creates tension between protofilaments and cause instability. The second hypothesis is the lattice model, where both GTP and GDP αβ-tubulins are curved, and lateral interaction forces between them lead to the straightening. In this model GTP αβ-tubulin hypothetically is more flexible to the straitening or creates more stable interactions with αβ-tubulins in lateral protofilaments. By GTP hydrolysis, this interaction is weakened. Both models are still openly discussed, where more recent studies support the lattice model[179,182–188].

1.4.2. γTuC - dependent MT nucleation

MTs can assemble spontaneously under optimal conditions, at optimal αβ-tubulin concentration, GTP presence, body temperature of αβ-tubulin source and higher viscosity in *in vitro* conditions. In cells this process is tightly regulated below the critical αβ-tubulin concentration by MAPs and MT nucleators, such is the γTuCs and ch-TOG.

Key component of MT nucleation is γ-tubulin. γ-tubulin belongs to the tubulin protein family and on the structural and amino acids sequence level resemble to β-tubulin. Similar to β-tubulin, upon binding to the α-tubulin subunit of the tubulin dimer, γ-tubulin together with α-tubulin creates GTP hydrolysable captivity [189,190]. It was observed that γ-tubulin can oligomerize and polymerized [190–192] and *in vitro* creates double stranded filament and fibrillar network [189]. However, the *in vivo* relevance of oligomerization property of γ-tubulin is unclear.

γ-tubulin inside of cells is mostly bound with GCPs and creates γTuC. γTuSC is in its subcomplex arrangement in cells. Only upon requirement to fulfil γTuSC dependent MT nucleation, it is oligomerized into ring like structure. While vertebrates γ TuRC exists as already assembled in cells[46,52,67].

Kollaman at all. performed three structural studies of the γTuSC and oligomerisation, where γTuSC creates left handle spirals based on lateral interactions of γ-tubulin in *in vitro*

conditions [46]. These spirals undergo conformational changes from "open" to "closed" conformation. The open conformation of the spiral is not compatible with the structure the MT, while upon crosslinking the γTuSC spiral assumes a "closed" conformation which resembles the MT cylinder and has higher MT nucleation activity than the open conformation (Fig.1.8. c)[50]. Elongation of N-Spc110$_{1-220}$ to Spc110$_{1-401}$ stops the spiralisation of the γTuSC and leds to creation of seven copies of γTuSC ring like structure (Fig.1.8. d). Using the tomography of yeast spindle pole body, they were able for the first time to show 3D structure of the MT minus at resolution of 120 Å (Fig.1.8. a,b). Resolution limits the further analysis, but it was shown that yeast MT minus end capped with the γTuSC ring has a symmetrical arrangement to its MT counterpart [50].

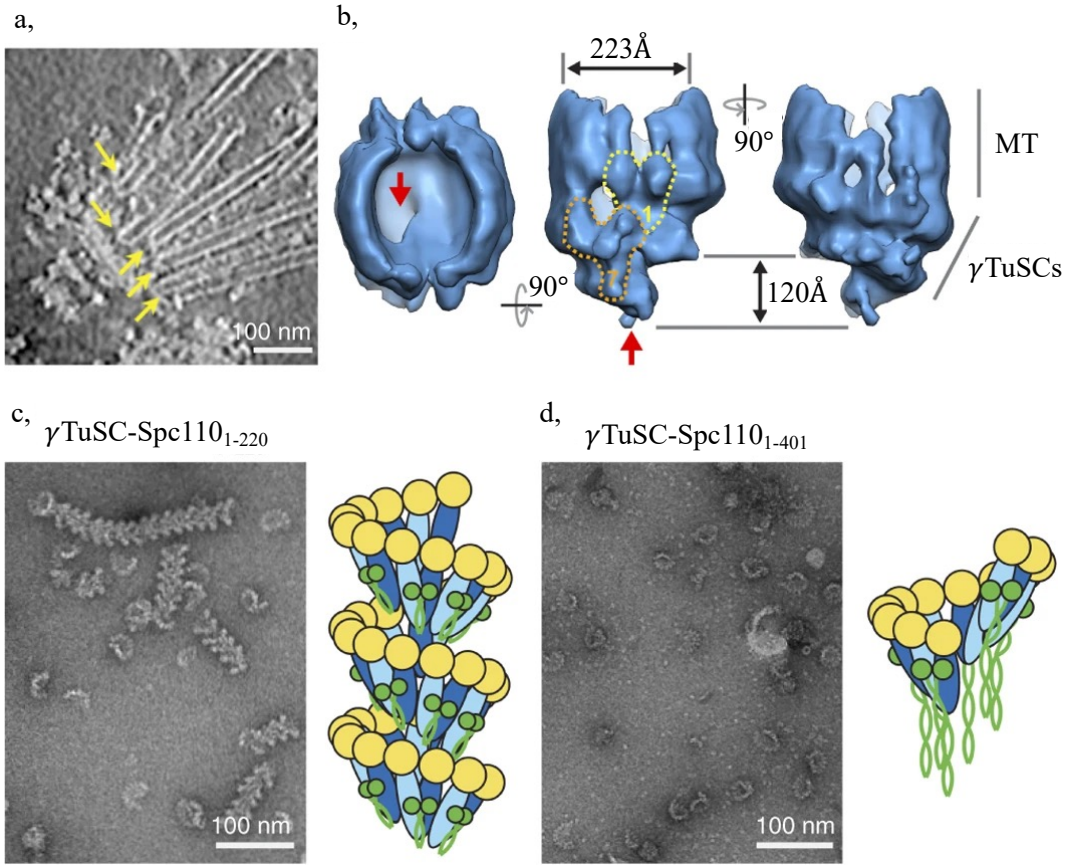

Fig. 1.8.: The yeast γTuSC ring is limited in its size to seven copies of the γTuSC by Spc110. A, Image of tomograph of yeast spindle pole body showing γTuSC ring-capped minus ends. b, 120 Å 3D average of tomographs of spindle pole bodies MT minus ends showing overlap between first and fourteenth spokes of γTuSC ring. c, Spc100$_{1-220}$ promotes the spiralization of γTuSCs, whereas d, Spc110$_{1-401}$ containing prolonged region of coiled coil domain stabilise the number of incorporated γTuSC to seven copies in a left handled ring like structure. Image is taken from [50].

Structural analysis of isolated vertebrate γTuRC not attached to MTs revealed surprisingly controversial conclusions. While the oligomerized γTuSC creates symmetrical rings as in MTs, the γTuRC structure is asymmetric (Fig. 1.9.)[53,54,59]. γ-tubulin arrangement does not reflect the arrangement of α-tubulins in MTs with 13 protofilaments (Fig. 1.9. a,b,c). This suggests that the γTuRC needs to undergo conformational change to accommodate the symmetry of MTs.

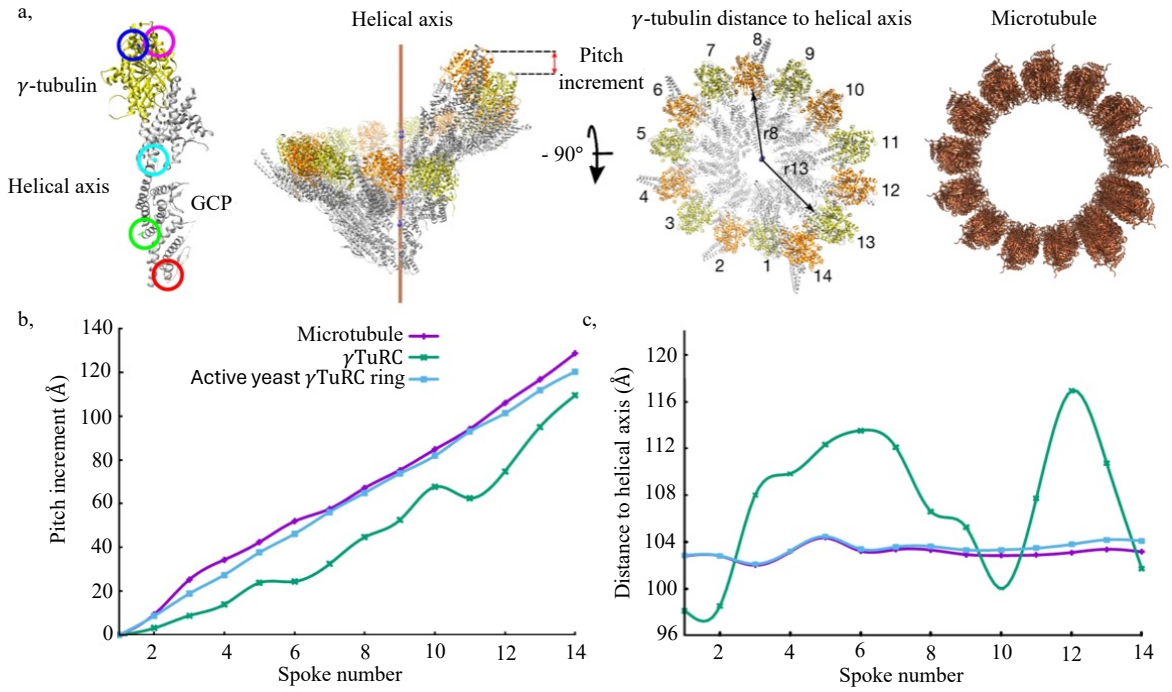

Fig. 1.9.: Geometrical and conformational analysis of vertebrates γTuRC compared to closed yeast γTuSC rings and 13 protofilament MTs. a, Shown are the residues of GCPs (coloured) used for definition of the position of the helical axis (brown). b, pitch increment of γ-tubulin and c, distance of γ-tubulin to helical axis compared to γTuSC spirals (PDB code 5FLZ) and a 13-spoked MT (PDB code 6EW0). Adapted from [53].

The symmetry of first 8 spokes of the γTuRC exhibits only slightly difference to the MTs. From spoke 10 to 14 starts the deviations from helical axis in both γ-tubulin pitch and diameter of the γTuRC (Fig. 1.10.a). These deviations are accompanied by mismatch between γ- and α-tubulin (Fig.1.10.b).

Assembled vertebrate γTuRC may be in an inactive form. Recruitment to the MTOC by for example CDK5RAP2 could activate the γTuRC by introducing a change towards the closed conformation. The CM1 motive of CDK5RAP2 binds to spokes 12 and 13 of the γTuRC [59]. Studies confirm the increases in MT nucleation activity of the γTuRC by binding of CM1

in vitro and *in vivo* [53,67,193,194], but structural analysis by negative stain analysis did not observe conformational changes in γTuRC asymmetry[53,59]. In *Xenopus leavis* extract CM1 together with RanGTP but not CM1 alone led to significant increase in MT asters formations[53,195], suggesting that additional factors are required. This could be the dimerization of the CM1 motive which increases its activation capacity[195].

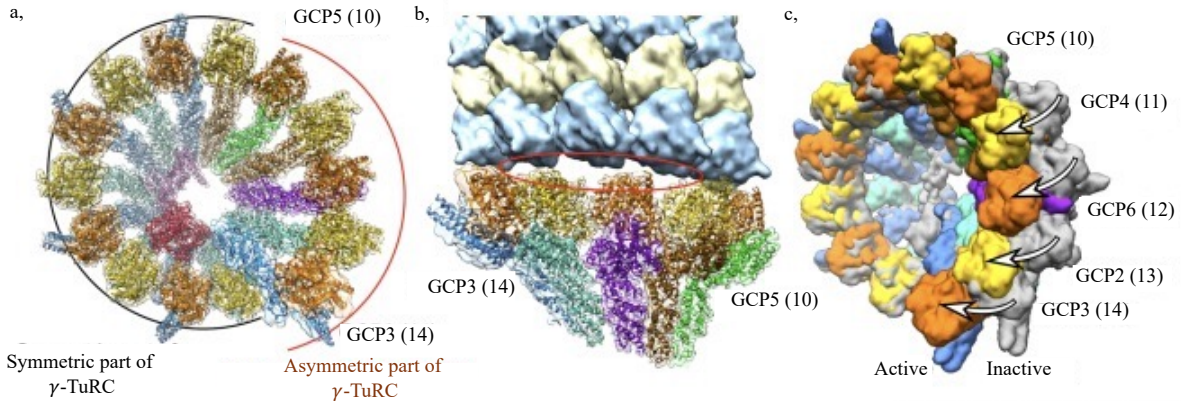

Fig. 1.10.: γTuRC needs to undergo conformational change to accommodate MT symmetry. a, structure of γTuRC showing that spoke 1 to 8 are in symmetrical position to the MT lattice in MTs with 13 protofilaments, while spokes 9 to 14 exhibit detachment from symmetry. b, The helical pitch of γTuRC is deviated from α-tubulin lateral symmetry creating the gap between α-tubulins and γ-tubulins from spoke 10 to spoke 14. c, Indication of movement which the γTuRC should undergo at spokes 10 to 14 to accommodate the "closed" γTuRC ring like structure. Adapted from [66].

XMAP215 seems to have transient binding to γTuRC and as well facilitate γTuRC nucleation activity[35]. Another key component in γTuRC re-arrangement could be binding of the αβ-tubulins dimers, which may promote with its longitudinal and lateral interactions movement of γTuRC spokes 10 to 14 towards protofilament conformation[37,194] .

1.4.3. Centrosomal MT nucleation pathway

The PCM creates a higher-ordered protein matrix around centrioles. Structurally, defining it proves challenging due to the low electron density and the intricate complexity of the proteins involved. The molecular architecture of the PCM changes depending on the cell cycle. Whereas in interphase the PCM decorates only mother centrioles and upon entrance into mitosis the PCM is expanded and covers the entire centrosome. In interphase, the PCM layer attached to centrioles is highly ordered and with a ring-like decoration around centrioles with

a diameter from 250 nm to 500 nm. The layer may be divided into two zones depending on protein composition. CEP57, CEP63 and CEP295 localized in zone I near the MT wall of thecentriole[196–200]. More distantly is zone II composed of pericentrin, CEP152, CEP192, CEP215 and γ-tubulin. Pericentrin and CEP152 form clusters with 9-fold symmetry organized in an intertwined form. Other proteins from zone II (CEP192, CEP215 and γ-tubulin) do not display any polarity preferences [162,201]. During M phase, the PCM starts to expand to cover the whole centrosome. Proteins from the distal layer, such as pericentrin, CEP215 and CEP192 move to distal parts creating a gel-like phase-separated condensate[90]. Crucial point in centrosomal maturation and formation of mitotic PCM is the docking of active PLK1 kinase to the centrosomes[202]. Docking is probably promoted by Cep192 [203,204].

Another interesting aspect is the formation of a gradient of PLK1 kinase with higher concentration around centrioles and lower in the periphery of the PCM. PLK1 phosphorylates PCM components, such as CEP192, CEP215, and pericentrin promoting their oligomerization [205]. All three proteins are involved in recruitment and anchoring of γTuRC to the centrosome [202,206–208].

In hierarchy of influencing the spindle assembly, CEP192 may play upstream role to CEP215 or pericentrin. Upon depletion of CEP192, spindle assembly is perturbated by reduced recruitment of pericentrin and CEP215 [209]. Conversely, simultaneous depletion of CEP215 and pericentrin revealed that the remaining thin layer of CEP192 on the mother centriolar wall was sufficient to sustain a proper bipolar spindle[209–211]. The absence of CEP192 led into reduction of centrosomal γTuRC[209] and misplacement of Aurora A at centrosomes[202]. Removal of pericentrin and CEP215 had less harmful consequences leading into still preserved functional spindle poles. Depletion of Cep1215 led into loss of astral MTs[211] and pericentrin reduction causing the shortening of mitotic spindles and mitotic errors [212,213].

PLK1 together with Aurora A facilitate centrosome maturation and recruitment of γTuRC[202,214]. PLK1 directly or indirectly through NEK9 phosphorylates NEDD1, which targets γTuRC to PCM[55,215]. Another target of PLK1 is the SAS4 protein, and its phosphorylation at the TT211 site is crucial for the recruitment of Cnn (*Drosophila melanogaster* homolog of human CEP215), which binds to γTuRC [216].

The mitotic centrosomal MT nucleation pathway is based on the phosphorylation function of PLK1 to create a gradient that recruits PCM components and scaffold proteins involved in MT assembly and regulation (Fig.1.11.).

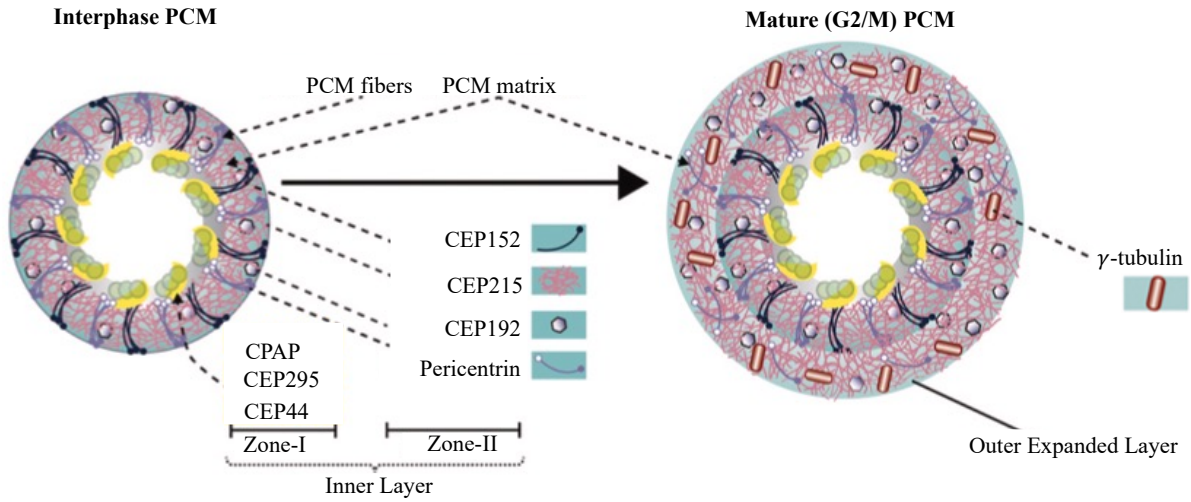

Fig. 1.11.: Model of PCM expansion upon mitotic entrance. Upon PCM maturation, components as CEP152, CEP215, CEP192 and pericentrin expand to the periphery of centrosome and recruits γ-tubulin complexes. Figure adapter from [90].

1.4.4. RanGTP chromosomal MT nucleation pathway

Interestingly, many proteins involved in regulation of nuclear pore transport and DNA regulation are as well involved in spindle assembly. One of them is RanGTP. RanGTP protein acts like a moonlight protein with different functions depending on cellular requirement.

The most studied function of the GTPase Ran is in nuclei-cytoplasmic transport. Whereas the transport into the nucleus is promoted by nuclear pores complexes (NPCs), and small cargos with size about 40 kDa can diffuse through NPCs without the assistance of Ran, bigger cargos need active transport with the involvement of soluble nuclear transport receptors (NTRs) from the karyopherin-β protein family. NTRs facilitating transport into nucleus are called importins and they recognize their cargo via a signaling sequence rich in basic amino acids, called nuclear localization signal (NLS). The export of macromolecules out of the nucleus is facilitated by exportins that carry a nuclear export signal (NES) rich in hydrophobic amino acid residues. In its GTP bound form Ran (RanGTP) has higher affinity to NTRs. RanGTP formation is promoted by the RanGEF (guanine nucleotide exchange factor) RCC1 which associates with chromatin. In contrast, RanGAP (GTPase activating protein) is in the cytoplasm, leading to the higher accumulation of RanGTP in the nucleus and RanGDP in the cytoplasm. RanGTP stabilizes exportin-cargo interactions and destabilize importin-cargo interactions. Importins localized in the cytoplasm where they bind to NLS-cargos followed by the transport into the nucleoplasm by diffusion through the NPC. Upon binding of RanGTP,

the cargo is released from the importin into the nucleoplasm. RanGTP facilitats the transport of exportins with bound cargo into cytoplasm. On the cytoplasmic site of the NPC, the RanGAP is part of the cytoplasmic filaments of the NPC. GTP hydrolysis then causes the release of exportin from the cargo into the cytoplasm.

Upon cell division nuclear envelope is breaking down and it is no longer necessary to regulate the transport. Spindle assembly factors (SAFs) bound to importins become exposed to RanGTP still bound to chromatin upon nuclear envelope breakdown. The liberated spindle assembly factors then promote spindle assembly. Recently is identified about 22 candidates for SAF [95,97,217,218].

The most prominent SAF is TPX2. TPX2 is inhibited via its interaction with importins and RanGTP release of them[218,219]. N-terminus of TPX2 after that binds to the catalytic domain of Aurora A and in this way protects it from phosphatase. TPX locks Aurora A in an active stage[220,221]. For the activity of Aurora A, the phosphorylation at Thr288 is crucial. This is induced by autophosphorylation after binding to proteins such us TPX2, Ajuba, Cep192, nucleophosmin, Bora, protein phosphatase inhibitor-2 and PAK[220–227] or PKA phosphorylation [228]. Each autophosphorylation induced by a specific protein leads to a define output because of the distinct localization of the activator. For example, Bora induced autophosphorylation in G2 phase promotes mitotic entry[223,229,230]. Cep192 induces the dimerization of Aurora A, leading to subsequent trans-autophosphorylation of Aurora A. This process, in turn, prompts centrosomal maturation [224,231]. TPX2 triggers spindle assembly. More specifically, TPX2-binding induces conformation change in Aurora A catalytic domain causing movement of Thr288 deeper into protein fold, thus prevents its access to phosphatases[220]. Aurora A subsequently phosphorylates NEDD1 on S405 site, which is required for the chromosomal pathway and the centrosomal spindle assembly[232 233]. Another component of this pathway is XRHAMM which coprecipitates with the γTuRC complex and with NEDD1 in *Xenopus leaves egg* extracts [97].This indicates the formation of a stable complex of XRHAMM-NEDD1-γTuRC at least under meiotic II conditions. Interestingly this pathway fulfils its function in a centrosome independent way, which is demonstrated by an experiment with adding purified centrosomes into an egg extract with depletion of XHRAMM and TPX2. Centrosomes nucleation still occurs [97].

An addition interaction partner of TPX2 is XPMAP215[217,234]. TPX2 also stimulates augmin induced branching in spindle formation[159].

Chromosomal nucleation pathway is based on RanGTP release of SAFs from its inhibitory connection to importins accumulating in chromosomal proximity based on RanGTP

gradient (Fig.1.12.). Chromosomal pathway is active in specific cell types lacking centrosomes, such us oocytes.

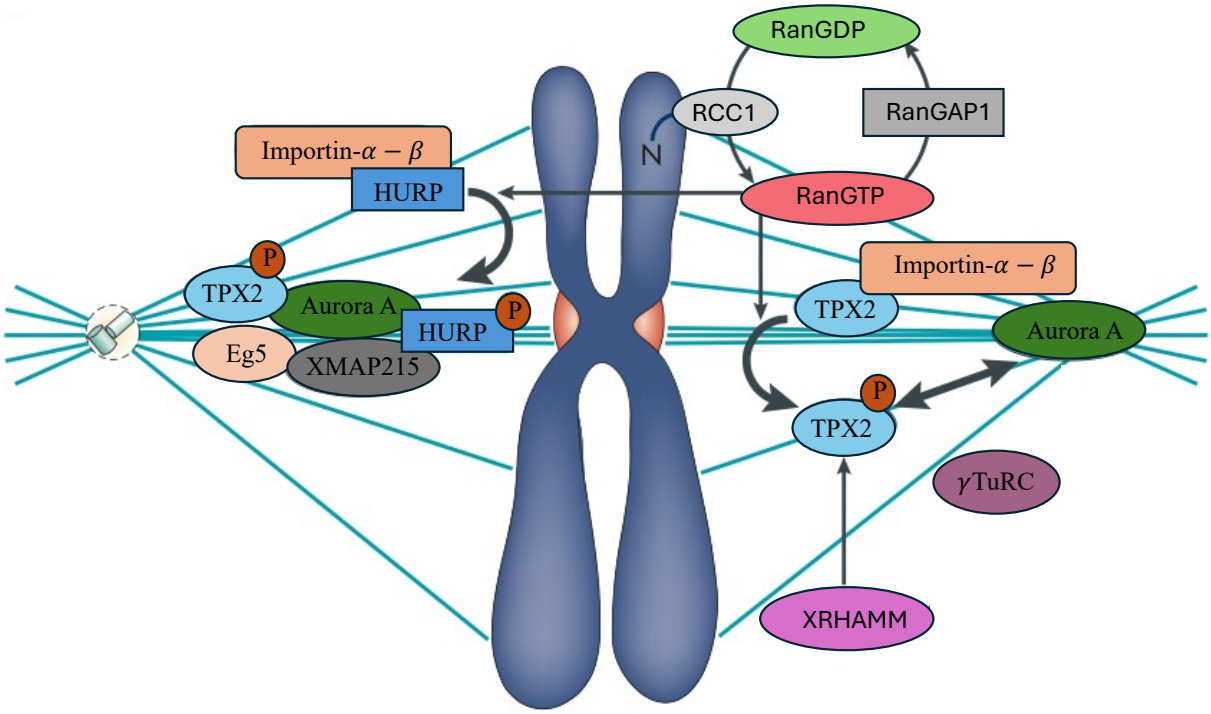

Fig. 1.12.: Model of RanGTP chromosomal nucleation pathway. Upon binding of RanGTP to the imporitin - α-β, SAFs are released from its inhibitory binding with importins, such as TPX2. TPX2 upon phosphorylation creates interaction with Aurora A and regulates the function γTuRC and other MAPs. Adapted from[217]

1.5. Aim of the thesis

I have participated on the discovery of the structure of the vertebrate γTuRC. As this structure is asymmetric compared to MTs, a more prominent questions was how this super-complex nucleates MTs and how this process is regulated.

The most prominent questions, that triggered my project, were:

- Knowing that most of the eukaryotic cells have 13 protofilament MTs [9], how the γTuRC accommodates the structural rearrangement to achieve a MT compatible conformation?
- What are the consequences of this rearrangement, and how might it impact the behavior of MTs?
- What characteristic changes occur at the MT nucleation site, such as the surfaces of γTuRC and the MT minus end?
- What is the fate and function of actin inside the γTuRC during MT nucleation?

I was aiming to address these questions using protein biochemistry, microtubule nucleation essays, fluoresce microscopy analysis and structural biology.

2. Results

2.1. Strategies of acquiring γTuRC-capped MT minus ends

At the beginning of my PhD, I was participating in a study of the structure of γTuRC. During this study, Peng Liu purified γTuRC from *Xenopus leavis* egg's extracts and Erik Zupa performed a cryo-EM analysis of the complex. Where I performed the biochemical analyses mentioned later on, specifically on the investigation of the presence and function of actin and an Insersion domain (IDo) of GCP6 as a potential component of the luminal bridge. γTuRC is created from 14 spokes composited from one GCP and one molecule of γ-tubulin, from which GCP2 and GCP3 with corresponding γ-tubulin create γTuSC structure. These 14 spokes created a left-handed spiral ring with composition from the first spoke GCP(2-3)$_4$-GCP(4-5)-GCP(4-6)-GCP(2-3), with stoichiometry 5x (GCP2): 5x (GCP3): 2x (GCP4): 1x (GCP5): 1x (GCP6). As well as the architecture of γTuRC is asymmetric to the regular ring-like structure of microtubules[53,54,59].

To answer the questions defined in the aim of the study, I first started microtubule nucleation experiments using purified γTuRC from *Xenopus leavis* and pig brain tubulin. γTuRC facilitated MT nucleation as judged by the increased number of MT seeds. However, identification of γTuRCs in this complex network of MTs was challenging. Nevertheless, together with Erika Župa and Annett Neuner, we performed cryo-EM freezing of in vitro nucleated *Xenopus leavis* MT asters for cryo-EM tomography purposes. Manually we analyzed about 80 tomographs. Unfortunately, during the acquisition of the tomographs, it was not possible to visualize the samples from all directions (360° angle) due to technical limitations of tilting of the grids. Due to the irregular protein composition of γTuRC, the low number of identified γTuRC-capped MT minus ends, and the inability to cover 360° degree, we decided to modify the approach and go back to cryo-EM single particles analysis, where the 3D structure is created by the averaging of many particles from different views.

For this purpose, I focused on the preparation of a sample with defined properties:

- high concentration of γTuRC capped MT minus ends
- less contaminated with empty MT seeds
- MT length should be rather short (2-3 μm), so the MTs will not lay on each other and create electron-dense accumulations on the grid.

During this study, I developed multiple strategies how to achieve this goal. At the beginning of the study, only native isolated γTuRC from *Xenopus leavis* was available as input material. First, I optimize the MT nucleation reaction to get a preparation with more concentrated γTuRC capped MT minus ends.

For this, I influenced the parameters of MT nucleation. I lowered the αß-tubulin concertation in the presence of *X. laevis* γTuRC, in an attempt to increase the specificity of the reaction. This led to a lower number of MT seeds. The number of nucleated MTs that were obtained was not suitable for cryo-EM grid preparation that requires a 10-fold higher concentration compared to negative stain EM analysis. Second, I used MT stabilizing agents to increase the stability of the MT seeds in the initial phase of MT nucleation. GMPCPP variant of GTP slows down the MT polymerization reaction and makes MT nucleation curvature almost linear. In addition, GMPCPP stabilized the bonds between tubulin molecules. However, the result of the GMPCPP strategy was not satisfactory. MTs were shorter but also the number of the seeds was low. As an alternative, I used the drug taxol that binds to ß-tubulin in the αß-tubulin heterodimer and stabilizes microtubules. In in vitro conditions taxol speeds up nucleation reaction leading into high amount of MT seeds. But, I struggled with the identification of γTuRC capped MT minus ends by immunofluorescence and with negative stain EM.

Published data showed that the γTuRC is a poor nucleator in vitro, where only 0.5-2% of γTuRC molecules are able to nucleate[38,54,59,194]. Therefore, I explored the possibility to concentrate γTuRC-capped MTs by affinity purification of the γTuRC. I explored three different ways how to enrich γTuRC-capped MT minus ends as outlined in the next section 3.2.

2.1.1. Recombinantly prepared γTuRC-capped MT minus ends

A breakthrough in the development of the in vitro protocol was the development of recombinantly expressed human γTuRC by Martin Würtz in our laboratory [62,65].

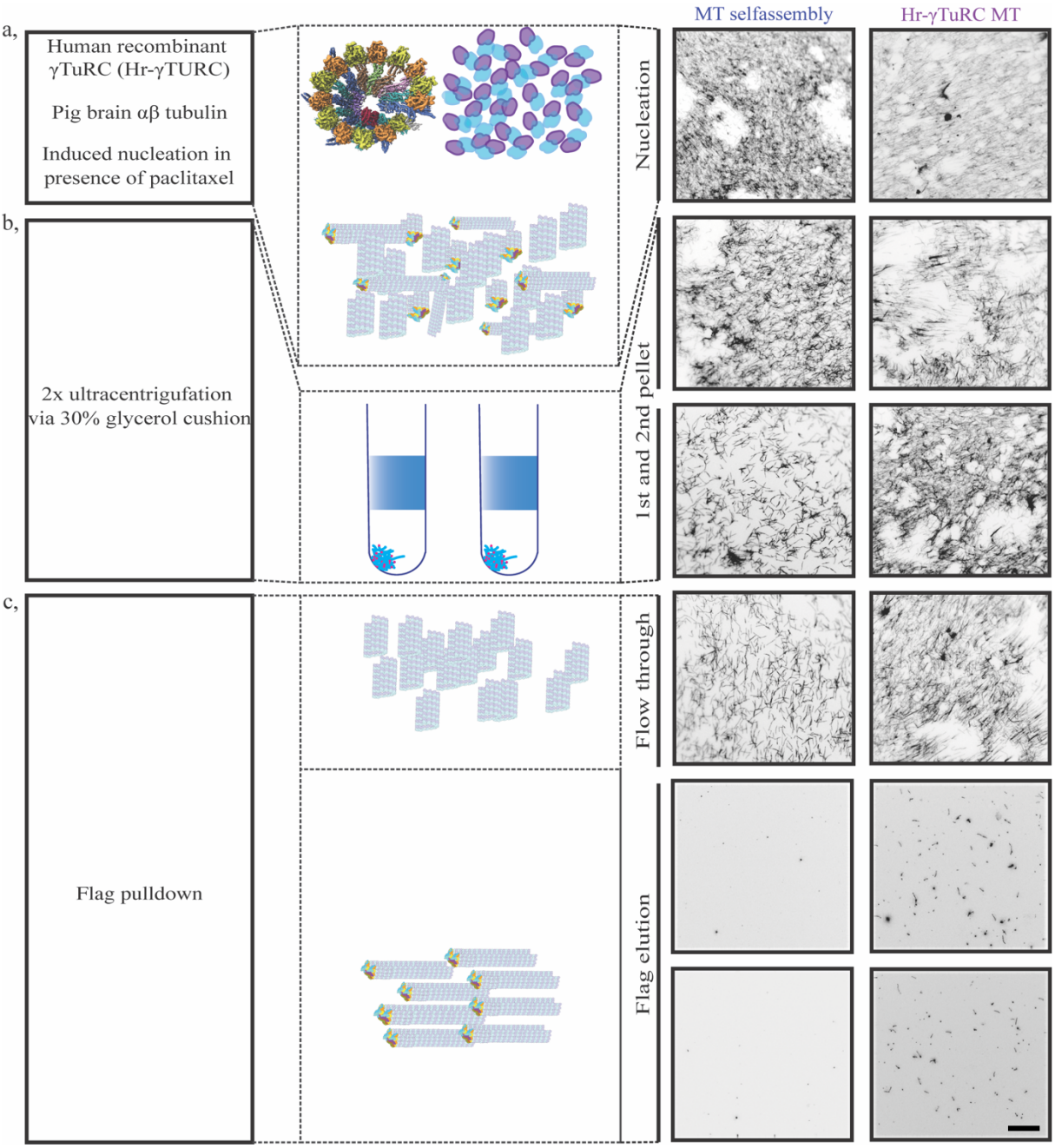

Fig. 3.1.: Purification of recombinantly prepared γTuRC capped microtubules minus ends. a, The nucleation assay was composed of 30 µM purified pig brain tubulin with human recombinant γTuRC. After 5 minutes of initial nucleation was added 10 µM paclitaxel and further incubated for additional 5 minutes. b, The nucleation mix was two-times pleeted through 30% glycerol cushion in attemt to remove free αβ- tubulin dimers and components that are not associated with MTs. Pelleted MTs were after that resuspended in the 1xBRB80 buffer suplemented with 100 mM KCl. c, γTuRC capped MTs minus ends were pulled down via Flag affinity purification. Samples from each step of preparation were taken, crosslinked and used for flourescncence analysis. . Scale bar 10µm.

Recombinant expression enabled us to get a higher concentration of the γTuRC compared to the natively purified γTuRC purfied from *Xenopus leavis* egg extract.

Additionally, it allow us to use differently tagged γTuRC subunits. The γTuRC's protein GCP5 was modified by adding 2xFlag tags at its N-terminus using a recombinant expression system in insect cells. GCP5 protein was incorporated into the γTuRC complex upon assembly and then the whole complex was purified using an affinity-based pull-down with a Flag tag and later eluted with the 3xFlag peptide [62,235].

The recombinant γTuRC showed normal nucleation activity compared to isolated and native *X. laevis* γTuRC (Fig. 3.2.c,). Upon nucleation, where γTuRC is bound to MT minus ends, the molecular weight of the γTuRC-capped MT minus end super complex was significantly higher compared to the isolated γTuRC or αβ-tubulin. This enabled me to separate unincorporated components from the super complex by ultracentrifugation(Fig. 3.1.a,). Ultracentrifugation through a 30% sucrose cushion led to pelleting of MTs while smaller components were retained in the cushion, such as isolated γTuRC, αβ-tubulin dimers and 3xFlag peptide (Figure 3-1b, middle part). That way I was able to again rebind the Flag-GCP5-γTuRC from the pelleted MTs to beads with anti-Flag antibodies. That step led into enrichment and concentrating the MT minus ends capped with γTuRC (Fig. 3.1.c,).

As it is demonstrated by fluorescence images (Fig. 3.1., right side), activation of MT nucleation by Ran-GTP led to a huge amount of MT seeds where it was challenging to find and identify the γTuRC capped MT minus ends. Therefore, the concertation step based on affinity purification of γTuRC was a crucial step to visualize the capped MT minus ends (Fig. 3.2.a, b,). Comparing the number of MT seeds from nucleation (Fig. 3.1.a,) with the affinity purified fraction (Fig. 3.1.c,), showed that only a small portion of MTs were capped with γTuRC. This result agrees with the published TIRF microscopy measurements, according to which only 2% of γTuRCs are active for MT nucleation [54,194]. Our main perspective was to achieve a concentration suitable for cryo-EM analysis, therefore we considered adding additional factors, which may increase the amount of γTuRC-capped MT minus ends.

CDK5RAP2 is considered as a γTuRC activation protein, which binds to γTuRC between positions 12 and 13[59]. But neither the addition of its CM1 motif nor the entire protein led to an increase in MT nucleation activity or a significant conformational change of the γTuRC [53,236]. Significant changes in nucleation upon the addition of this factor are visible in systems, which mimic the in vivo situation, such as Xenopus leavis egg's extract (Fig. 3.3.)[53]. This led to the hypothesis that this activation mechanism involves additional protein interactions that occur in cells extracts but not in the purified system because of the absence of the CDK5RAP2 cooperating protein.

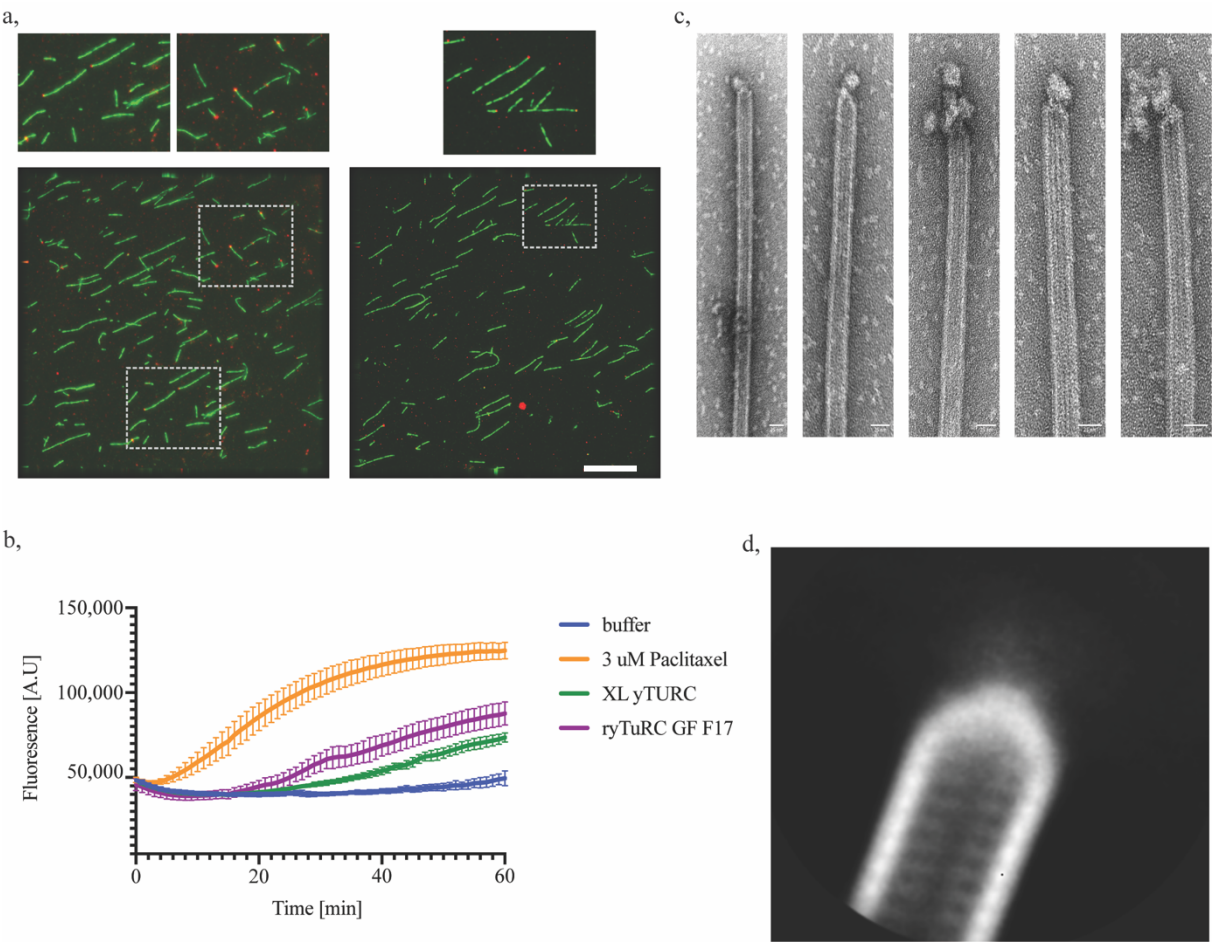

Fig. 3.2.: Analysis of recombinantly prepared γTuRC capped microtubules minus ends. a, γ-tubulin signal of recombinantly prepared γTuRC is presented at the one of the MT ends, indicating the position of MT mins end Scale bar 10 µm. b, The recombinant γTuRC exhibits the same nucleation activity as the native purified *X.laevis* γTuRC (green). Published in[235]. c, NS EM images showing a cap-like structure at MT end corresponding to the γTuRC. Scale bar 25 nm. Published in[235]. Negative Stain EM (NS EM) performed by Annett Neuner d, 2D image of recombinant γTuRC-capped microtubules minus ends prepared with cryo EM analysis, showing low representation of γTuRC densities. Cryo EM analysis performed Bram Vermeulen.

Tovey et al. showed that the *Drosophila melanogaster* homolog of CDK5RAP2, called Cnn, carries an auto-inhibitory domain behind the CM1 that binds to the γTuRC[237]. This may explain the lack of activity of the human CM1 in vitro [53,194]. Therefore, I tested the effect of human CM1 without the auto-inhibitory domain (CM1 1-100 aa) in the presence of Ran-GTP on the nucleation activity of the γTuRC in *Xenopus leavis* extract (Fig. 3.3.). Compared to the activation by full length CM1 (1-220 aa), I could not observe enhanced nucleation by Ran GTP activation in the case of CM1 1-100 aa. In addition, formation of asters was only moderately increased by CM1 1-100 aa (Figure 3-3b). One of the reasons may be that the CM1 1-100 aa part has no described function in the human CDK5RAP2, or the purified protein does not create a proper fold to bind to γTuRC. In any case, if we cannot observe the activation mechanism in

cell extracts, the chances are low to observe an effect of the CM1 motif in the purified system[53,236].

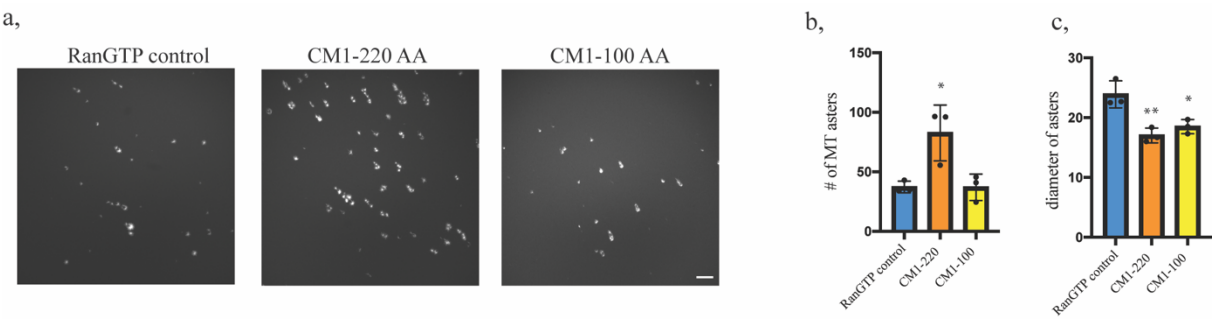

Fig. 3.3.: Effect of CM1 motif of CDK5RAP2 on MT aster formation in *Xenopus leavis* egg's extract. A, A representative fluorescence image of MT asters induced with RanGTP in presence of different lenghts of CM1 motive of CDK5RAP2. Scale bar 100 µm. b, the amount of asters per image is increased in the case of $CM1^{220}$, but not in the case $CM1^{100}$. c, a diameter of the asters (in µm) is decreased in case of $CM1^{220}$.

Nevertheless, we performed the cryo-EM analysis of *in vitro* prepared γTuRC-capped minus ends from up-scaled concentrations. The distribution of MT seeds was not optimal, and γTuRC-capped MT seeds numbers were low. We could complete the analysis only by 2D classification (Fig. 3.2.d,), where I could observe that γTuRC has got low resolution or is poorly defined. That would not able the correct spoke arragment of γTuRC. Continuum of the analysis with this type of γTuRC-capped minus ends would require an increased amount of input material, increased time and effort for data acquisition and as well as for manual collection of the particles.

In spite of these limitations, this *in vitro* γTuRC-capped minus ends sample is still suitable for biochemical and lower-resolution microscopy analysis, where the requirement of the number of particles is not demanding.

2.1.2. γTuRC -capped MT minus end purified from HEKT293 cells

The second approach was to prepare the γTuRC-capped MT minus end from the HEKT293 cell. With the help of Enrico Antorini, who prepared the HEKT293 cell line with endogenous expression of FLAG-tagged GCP6 variant upon doxycycline activation, I was able to extract MTs from the human cell line [62].

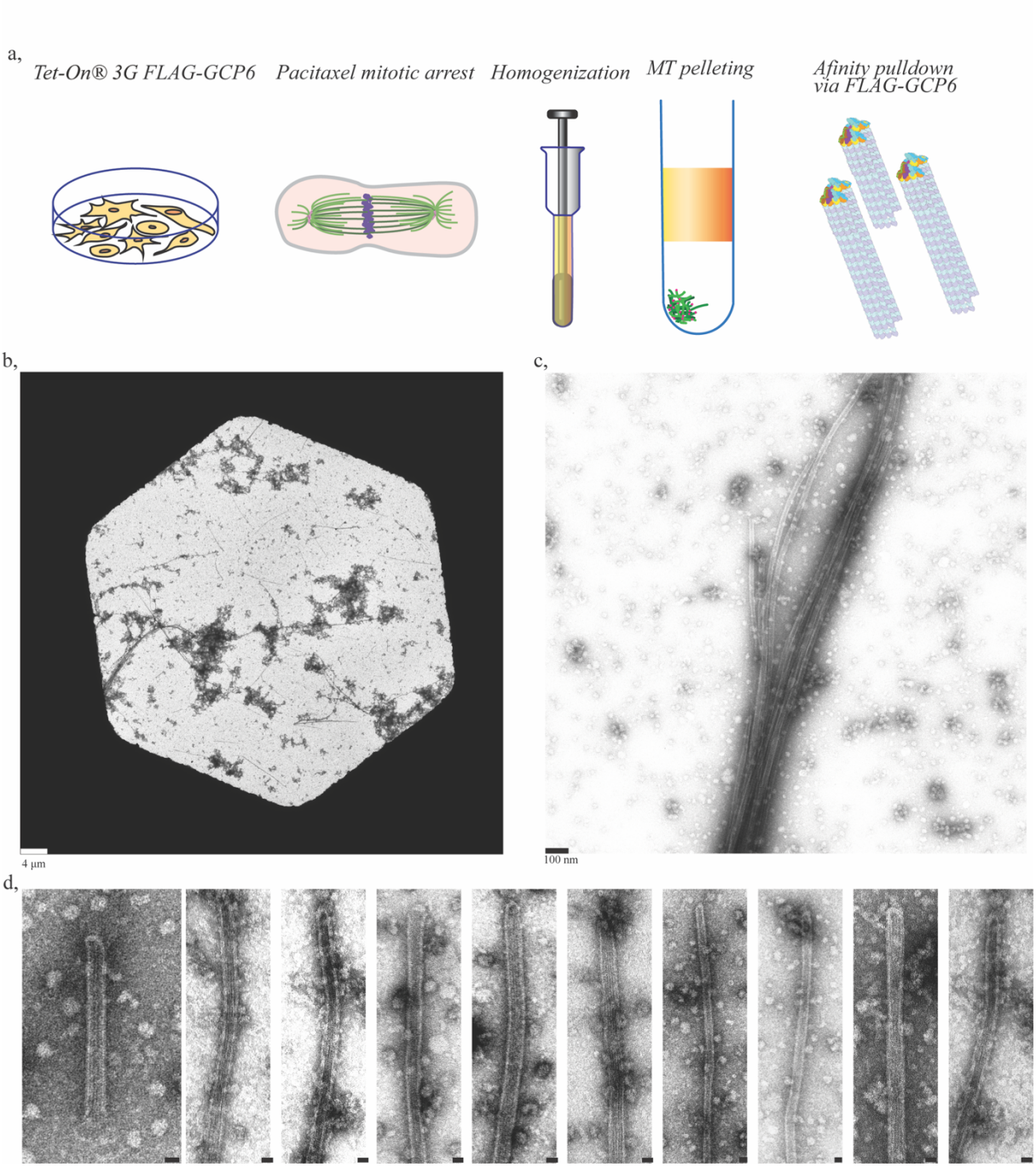

Fig. 3.4.: Purificatio of the native MTs minus ends from HEKT293 cells utilizing FLAG-GCP6 overexpression a, The HEKT293 cell line with genome-integrated *TUBGCP6-FLAG* was created using Retro-X™ Tet-On® 3G Inducible Expression System by Enrico Atorino. FLAG-GCP6 expression was induced with doxycycline and cells were arrested in mitosis with paclitaxel. Harvested cells were homogenized and microtubules were pelleted through a 30% glycerol cushion. The γTuRC capped MTs were purified via FLAG afinity purification. b, Representative images of the NS EM mesh of the purified native human γTuRC capped MT minus ends. Scale bar 4 µm. c, Zoomed NS EM images of purified native human MTs showing created MT bundles. Scale bar 100 nm. d, Selected NS EM image showing MT with a cap-like structure on one of MT ends indicating the presence of γTuRC. Scale bar 20 nm. NS EM performed by Dr. Annett Neuner.

I upscaled the cells to higher amount and with low concertation of doxycycline-induced *FLAG-GCP6* expression. The C-GCP6-Flag incorporates into γTuRC, as it is demonstrated later in results (Fig.3.21.a,). 24 h after induction of *FLAG-GCP6* expression cells were arrested in mitosis with paclitaxel. Paclitaxel incorporates into tubulin dimers and inhibits MT depolymerization. Therefore, MTs cannot separate chromosomes leading to mitotic checkpoint activation and cell cyclus is arrested in prometaphase. After 16 h most of the cells were in mitosis with stabilized MTs. I harvest the cells and resuspended them in a low volume of lysis buffer suitable for MT purification. Homogenization increased the efficiency of cell lysis. After I pelleted the MTs through a 30% glycerol cushion to remove inactive γTuRC, which may lead to its saturation on the beads and therefore lead into the decrease in the amount of γTuRC-capped MTs. After that, γTuRC-capped MTs were affinity purified via FLAG beads and eluted with 3xFlag peptide (Fig.3.4.a,).

With this approach, I was able to receive relatively long MTs (Fig. 3.4.b,). The MT density was releatively low. Upon closer examination, me and Annett Neuner identified a cap-like structure on one end of the MT ends (Fig. 3.4.d,), which is an indication for the presence of the γTuRC.

As it is demonstrated in Fig. 3.4.b,c, we received relatively long MTs , which is a disadvantage for the cryo-EM analysis. It will create high-density “rail way” structures on grids leading to difficulties in the identification of cap-like structures and their analysis. On top of it, longer MTs show higher clustering tendencies (Fig. 3.4.c,). In addition, the contamination of the sample with unknown particles, which was visible on NS EM grids (Fig. 3.4.b,), may interfere with the preparation of ice on the cryo-EM grid. Because of the MT length, the contamination with other particles and the low MT density, this sample preparation was not suitable for cryo-EM analysis.

I considered some modifications of the protocol, but this will lead to technical challenges. First, it is necessary to upscale. This purification was prepared from 100 ml of the cells. Upscaling will lead to a higher volume of cells, which is necessary to resuspend with the higher volume of lysis buffer to homogenize it. The higher volume will dilute the protein and consequentially lead to the dilution of tubulin concentration below the critical concentration for polymerization. In the lab, we observed that the influence of the taxol will not be sufficient to stabilise microtubules in condition of low tubulin concentration and that will cause depolymerization of microtubules. As I can observe lower yeald already, I can assume that the process of concentration dependent depolymerisation is occuring in this protocol. Therefore,

this sample is considered to be used for biochemical analysis and microscopy techniques with low concentration demands.

2.1.3. Purification γTuRC-capped MT minus ends from *Xenopus leavis* egg's extract

Parallel to other purification approaches, I have worked on extracting the γTuRC-capped MT minus ends from *the Xenopus leavis* egg extract. *Xenopus leavis* egg's extract offers advantages compared to the other systems. Namely, egg's extracts are prepared in a way that keep endogenous proteins as concentrated as possible[238]. This is why the tubulin is above the critical concentration and allows us diluting the sample to 10% of the original volume without losing MT nucleation activity. Additionally, within this system, the influence of RanGTP is established, acting as an upstream activator for the chromosomal microtubule nucleation pathway.

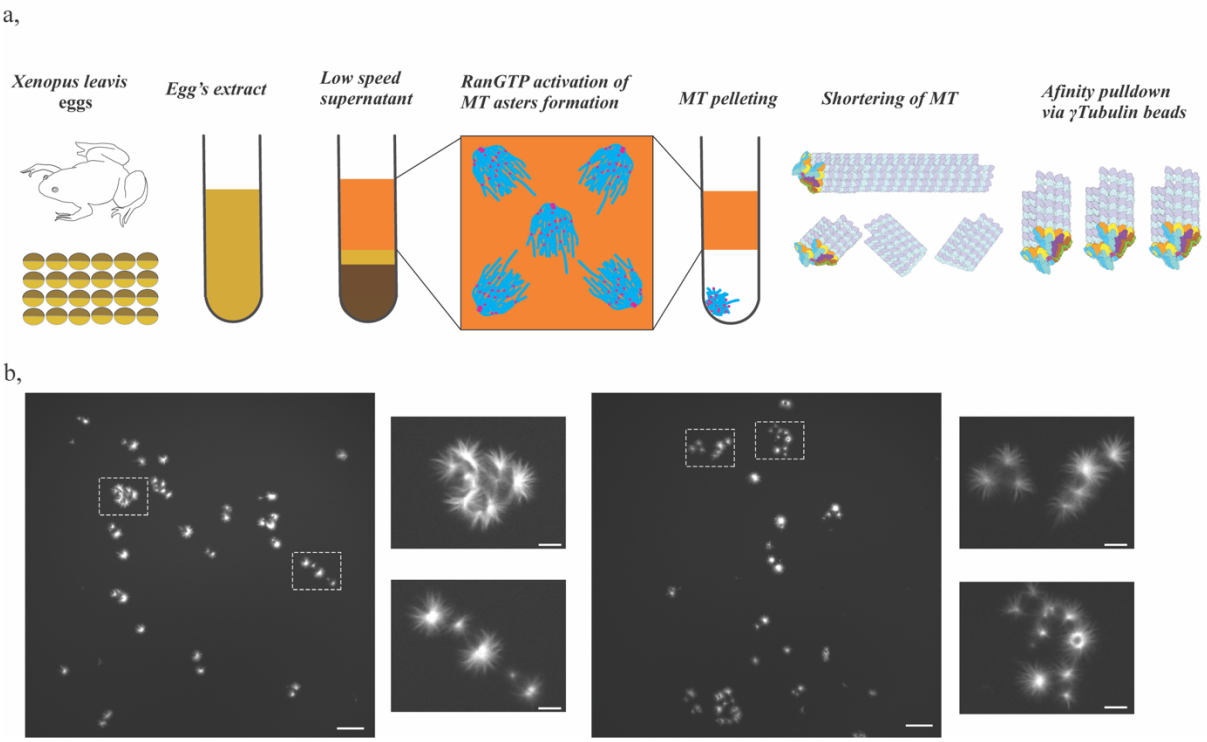

Fig. 3.5.: Purification of the native *Xenopus leavis* γTuRC capped microtubules minus ends. a, A schematic of the strategy of purification of the *Xenopus leavis* γTuRC capped MT minus ends. *X. laevis* CSF arrested eggs in meiosis was used for extracts preparation. By ultracentrifugation was obtained low- speed supernatant (LSS) in which was activated the Ran GTP chromosomal MT nucleation pathway with modified Ran(Q69L). MT asters, were pelleted through a 30% glycerol cushion. MT shortening protocol adjusted from[239] lead into mechanical fragmentation of MT asters. The γTuRC capped MT minus ends are affinity purified via γ-tublin affinity

purification. b, Representative flourescence pictures of MTs asters in LSS activated via Ran (Q69L). The scale bar is 100 μm and in the zoomed pictures is 25 μm. Published in [240].

Xenopus leavis egg's extract is prepared by Prof. Oliver Gruss, whose team maintain the frogs. During the development of the protocol, I switched to the low-speed supernatant of the extract (LSS), which was later on also prepared by Prof. Oliver Gruss. LSS allow clarifying extract of high molecular compartments and fat components, leaving behind pure cytosolic fraction with high protein concentration. LSS is prepared by ultracentrifugation of extract and only the upper phase without the fat layer is collected (Fig. 3.5.a,). The addition of RanGTP activates the upstream pathway[96,97,217,219,241], which induces MT assembly in the form of aster formation (Fig. 3.5.b,)[96,218]. This reaction is induced in the environment mimicking the body temperature of the frogs. After initial aster induction with RanGTP, taxol is added to stabilize the MTs. Finally, I pelleted the asters through a 30% cushion by ultracentrifugation with the purpose to remove components as free γTuRC.

As asters have got tight connections to MTs and the length of the MTs may be more than 15 μm on average (Fig. 3.5.b,), the crucial step was the MT shortening protocol. Classically, MT shortening could be achieved by cold treatment [242] , but taxol induces cold-resistance of MTs[243]. Therefore, I modified one original tubulin purification protocol where MTs were stabilized with taxol[239] and I was able to create short segments of MTs with a maximum length of 2 μm. This also enabled separation of MTs from asters and later to the affinity purification of MTs based on their connection to γTuRC.

As it is demonstrated in Fig. 3.6.a, MTs cluster together, which is a common behaviour of MTs in solution. The distribution of MT seeds is not regular on the grid, where some meshes have got more MTs compare to other meshes (Fig. 3.6.b,). I also observed differences in the number of MT seeds between preparations, where in Fig. 3.6.b, upper two meshes are from preparation with highly active LSS, and the lower two meshes are from two different preparations with extracts of lower activity. This induces variability between preparations as well as the location of MTs on the grid.

Nevertheless, the sample fulfils the criteria for further analysis. The MT seeds are approximately a maximum of 2 μm long and well spaced on grids without creating crossing railway structures (Fig. 3.6.b,). The number of seeds from highly active LSS was sufficient for cryo-EM grid preparation. By closer look at MT ends, I could identify distinct cap-like structure characteristics of γTuRC-capped MTs at the minus end (Fig. 3.6.d,).

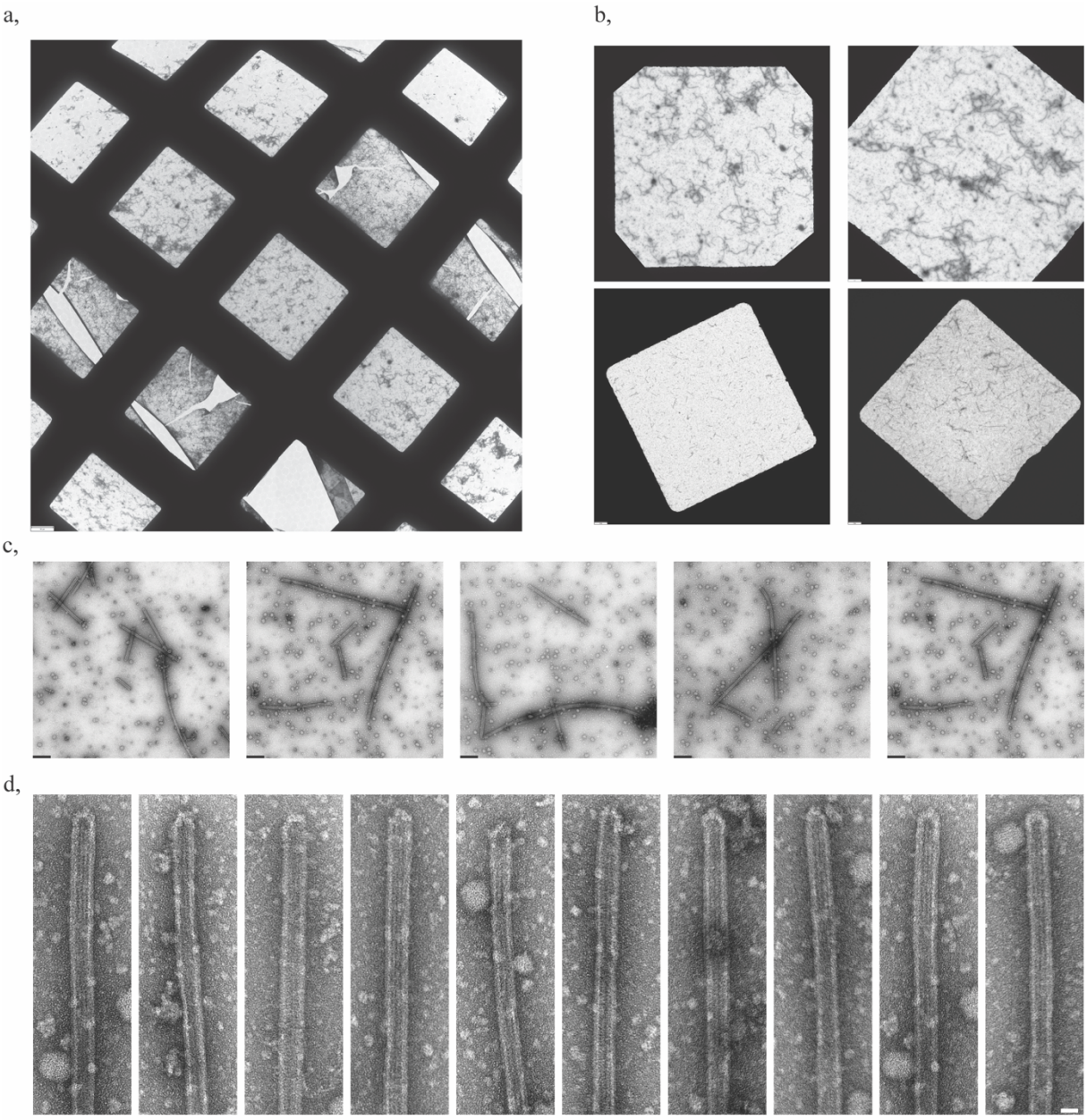

Fig. 3.6.: γTuRC capped MTs minus ends isolated from *Xenopus leavis* LSS expresed the satisfactory purity. a, Negative stain EM (NS EM) meshes pictures showing the distribution of purified MTs. Scale bar 10 µm. b, Representative pictures of the NS EM meshes of three indipendent MTs purifications representing the differences between preparations depending on the LSS quality. Scale bar 3 µm c, Zoomed images of purified MTs. Scale bar 25 nm. d, Representative MT minus ends with a cap-like structure of MT end indicating presence of γTuRC. Scale bar 20 nm. NS EM performed by Annett Neuner.

Additionally, the quantity of γTuRC-capped microtubules is increased in the *X. leavis* LSS preparation compared to preparations from HEKT293 cell purifications or *in vitro* recombinantly created γTuRC-capped minus ends. Therefore, I decided to focus on the *X. leavis* source of γTuRC-capped MTs for cryo-EM analysis as one of the most suitable sources.

2.1.3.1. Influence of Ran GTP on the quantity of γTuRC capped MT minus ends

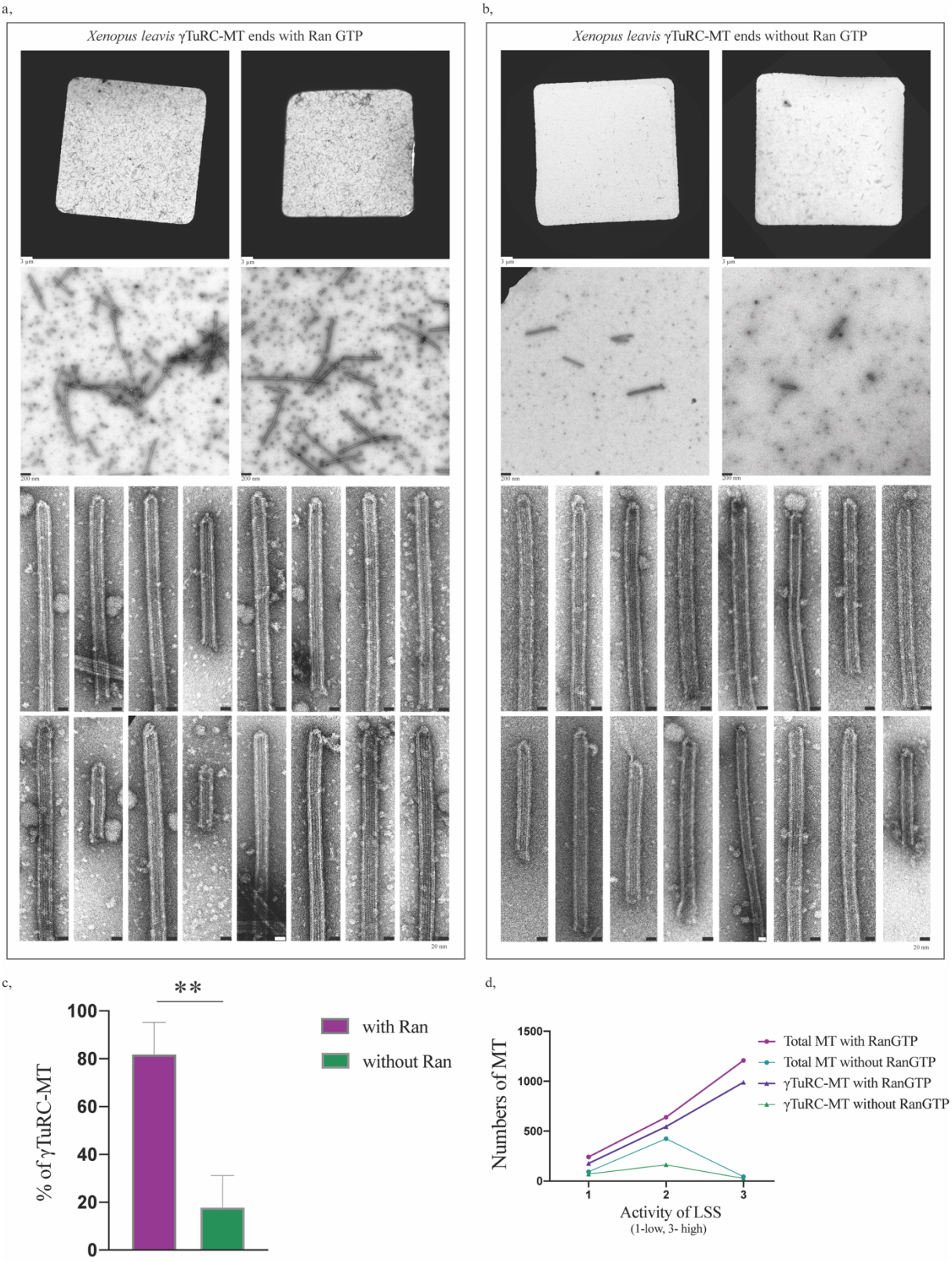

Fig. 3.7.: RanGTP significantly increase the γTuRC dependent MT nucleation in *Xenopus leavis* LSS. a, The isolated *X. laevis* γTuRC MT minus ends created via Ran(Q69L) activation of chromosomal MT nucleation. Upper picture : NS EM meshes representing the amount of MTs created with inflence of Ran(Q69L), scale bar 3µm. Middle picture: a magnified image representing the spreading of MT seeds. Scale bar 200 nm. Lower picture: the representative images of MTs with cap like structure representing the presence of the γTuRC. Scale bar 20 nm. b, The purified *X.l.* γTuRC minus ends without the influence of the RanGTP activation pathway. Upper picture: NS EM meshes representing the distribution and amount of MTs created without influence of Ran(Q69L), with a scale bar of 3µm. Middle picture: a magnified image representing the spreading of MT seeds, with a scale bar of 200 nm. Lower picture: the representative images of MTs with cap like structure representing the presence of the γTuRC. Scale bar of 20 nm. c, 82% of assmbled MTs are created via RanGTP activation pathway.. T-test, p= 0,0041. d, The efficiency of MT assembly is dependednt on quality of the LSS, where the LSS with elevated aster formation tendencies have got higher amout of γTuRC capped MTs and overal assembled MTs content. NS EM performed by Annett Neuner.

Three factors can influence MT nucleation in my purification protocol of *X. leavis* γTuRC-capped MT minus ends: i) RanGTP, ii) taxol and iii) temperature. So, it was crucial to address the factors that influence formation of γTuRC-capped MTs.

MTs are temperature-dependent, dynamic structures. Tubulin assembly into MT polymers is induced *in vitro* by the presence of GTP and is normally optimal at the body temperature of the animal from which tubulin was purified from. The same may also apply during the purification of γTuRC-capped MTs *from X. leavis* LSS, where endogenously GTP and RanGTP activation promote MT nucleation at 20°C. The body temperature of nucleation is a stable factor, which should not be changed to achive optimal performance.

Taxol incorporates into β-tubulin and stabilizes the binding between heterodimers. It stabilizes the MT seeds, which then function as nucleation cores for elongation and multiplication. The impact of Taxol could potentially result in the formation of new MT seeds within LSS, alongside pre-existing MT seeds generated by RanGTP activation, or it may enhance the effect of RanGTP. It is important to emphasize that in this purification protocol, I cannot omit the presence of taxol, because of its crucial role in the stabilization of MTs. Noting that taxol is added after 20 min of initiated nucleation. Without taxol stabilization, MTs may depolymerize during purification and in this way it can influenced the efficiency of the purification.

Therefore, I investigated the effect of RanGTP upon MT nucleation in the presence of taxol and triggered by the body temperature of the tubulin source. MT nucleation also occus when RanGTP is not added, as it is demonstrated on the negative stained grids (Fig. 3.7.b,), but significantly less than during MT purification with RanGTP (Fig. 3.7.a,). The number of

MT seeds can be compared also in the distribution of MT seeds on mesh (Fig. 3.7.a,b, middle part). In both preparations, I observed cap-like structures at the MT minus end as summerized in the gallery (Fig. 3.7.a,b, lower part).

Upon quantification, approximately 18% of cap-like structures were generated in the absence of RanGTP. Importantly, 82% of MT minus ends with a cap-like structure were produced in response to RanGTP (Fig. 3.7.c,). Therefore, I can conclude, that the major contributor to the production of MT minus ends with a cap-like structure is RanGTP.

I observed differences depending on LSS quality characterized by its MT aster forming ability. The yield of MT minus ends with a cap-like structure from highly active LSS was more than 97% compared to the purification from the same extract without RanGTP. With middle or low-quality LSS this yield reduced to approximately 75% (Fig. 3.7.d,).

2.2. Structure of XL γTuRC -capped MT minus ends

2.2.1. Cryo-EM manual picking and first densities of γTuRC-capped minus ends

I worked in close collaboration with Dr. Stefan Pfeffer's group, particularly with Bram Bermeulen, for cryo-EM analysis of γTuRC capped MT minus ends.

The γTuRC-capped MT minus end preparation from *X. leavis* was suitable for Cryo-EM single particle analysis. It fulfilled the criteria about a high concentration of MT seeds as well as the length of MTs. Nevertheless, not every preparation led to the creation of highly concentrated MTs with acceptable distribution on grids. Therefore, successful preparation suitable for further analysis was only prepared from highly active *Xenopus leavis* LSS, with a high yield of MT seeds.

As demonstrated in Fig. 3.8.a, we may observe the plus and the minus end in one MT as well as some MTs without cap-like structures. I and Bram Vermeulen have manually picked MT with a cap-like structure on their end (Fig. 3.8.a,- green circle, Fig. 3.8.b,- zoomed-in picture on structure). About 9382 particles were collected from 4 datasets. Bram Vermeulen selected 2579 particles with defined plane rotation and position of the minus end (Fig. 3.8.c,). The 3D model showed cylindric densities with cap structure on top reflecting the position of γTuRC. The alignment of the γTuRC spokes did not work properly due to structural similarities

among its GCPs. As a result, low resolution and misalignment were observed at the position of γTuRC and the MT site (Fig. 3.8. d,e,).

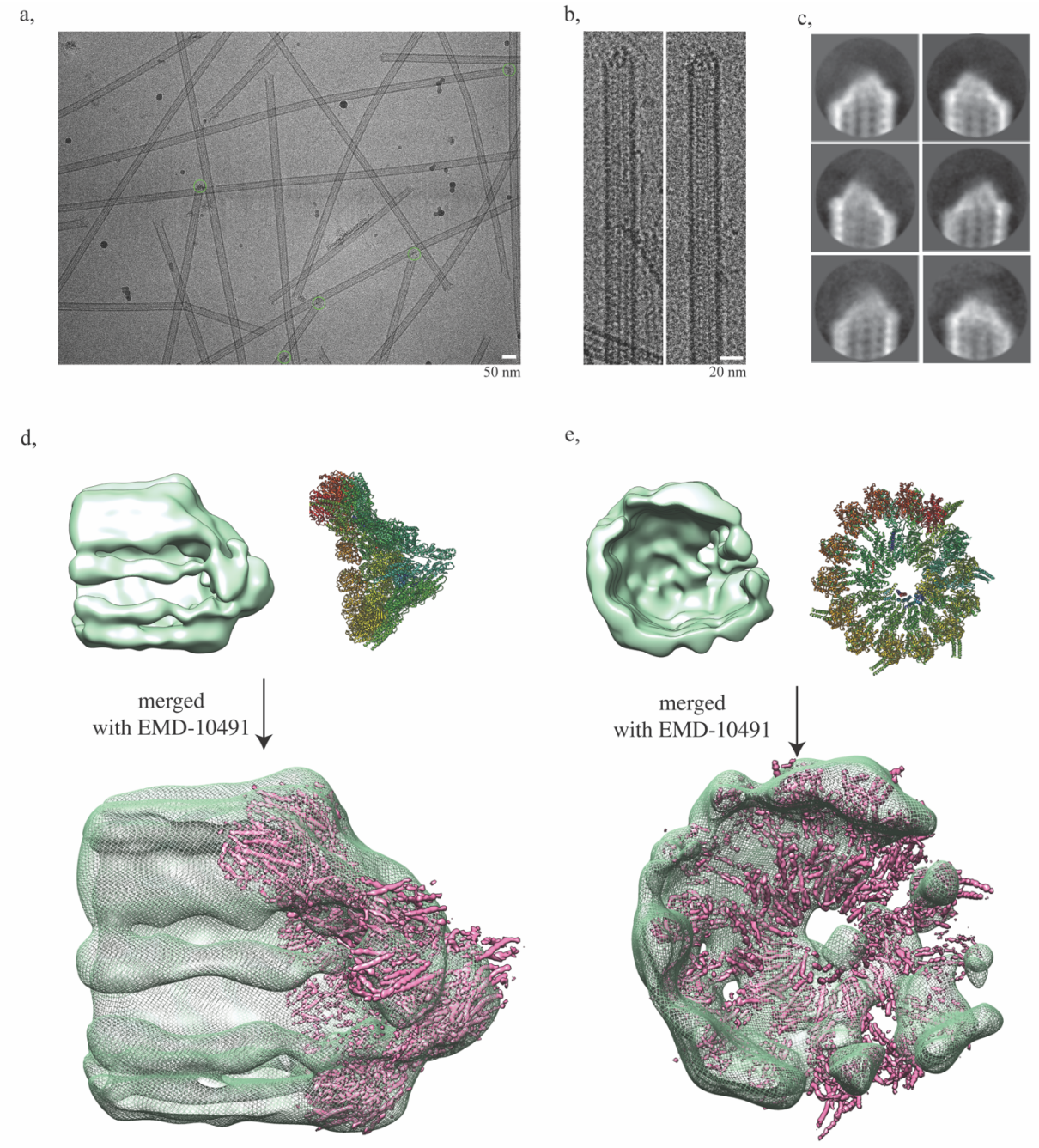

Fig. 3.8.: Cryo-EM structural analysis of *Xenopus leavis* γTuRC capped minus ends. a, a representative picture of cryo EM micrograph showing the manually picked particles for further γTuRC capped minus ends reconstruction. The scale bar is 50 nm. b, Magnified image of selected capped MTs. Scale bar 20 nm. c, Representativs of the 2D classes of γTuRC capped MTs, mask diameter 38 nm. d, e, Side and top view of the first 3D densities of analysed γTuRC capped MT minus ends compared to the map of isolated γTuRC (PDB- 6FT9) (top picture) and initial densities superposed with densities of isolated γTuRC (EMD-10491) (low picture). Cryo-EM grids were prepared by Annett Neuner and Bram Vermeulen, and data acquisition and first densities analysis was performed by Bram Vermeulen.

For improvement of the analysis, Bram Vermeulen performed a 3D re-definement of the densities with isolated *X. leavis* γTuRC as reference (EMDB 10491,[53]) with missing GRIP2 domain and γ tubulin at spoke 5 and 6. This refinement came to limitations due to the low number of particles indicated by incorrect determination of some particles spoke register. Therefore, additional 3D refinements were performed with the supplementation of approximately 30 000 particles from *Xenopus leavis* native γTuRC, accessible in our lab. As control, 30 000 γTuRC particles with removed GRIP2 domain and γ-tubulin at spoke 5 and 6 were used. After the refinement, isolated γTuRC particles were removed from the further analysis and was gained correctly aligned γTuRC with recovered GRIP2 domain and γ-tubulin at spoke 5 and 6. This analysis reached a resolution of 23 Å for the γTuRC site and 32 Å on the MT site. These resolutions enabled a further geometrical analysis of conformations.

2.2.2. γTuRC transformation at the MT minus end

23 Å resolution by 3D reconstruction focused on γTuRC (Fig. 3.9.a,) enable spoke-wise rigid-body docking of *Xenopus leavis* atomic model (PDB 6FT9) (Fig.3.9.b,). After that, the conformation of γTuRC at MT minus end was compared to two known conformations of γTuCs, which are the vertebrate γTuRC (PDB 6FT9-mol map) with an asymmetric structure to MTs and crosslinked budding yeast γTuSC ring (mol map of PDB 5FLZ) with compatible symmetry to MTs serving as a model of "closed" γTuC. Compared to the isolated ring, γTuRC at minus ends undergo a conformational change in the character of movement toward the middle axis of the structure (Fig. 3.9.c,), but still not reaching the symmetrical conformation of "closed" γTuC (Fig. 3.9.b,).

Where spoke 1 and spoke 14 are overlapping in the "closed" conformation of the isolated γTuRC ring, the position spoke 14 is dislocated at γTuRC at capped MTs (Fig.3.9.c,d,).

Upon schematic comparison of γ-tubulin positions at these three conformational examples, it is observed that there is conformational similarity of the γTuRC from spoke 1 to spoke 10. Major arrangements are observed from spokes 11 to 14 (Fig. 3.10.a,). The pitch distance of γ-tubulin at the capped γTuRC at a MT reduces by around 2 nm at position 14, and from spoke 13 to 11 it is reduced by approximately 1.2 nm to achieve a closed conformation similar to the isolated ring (as shown in Fig. 3.10.b,). The angle of the γ-tubulin pitch positions

in the closed ring compared to the other two models is about 5° at positions 13 and 12 at γTuRC capped minus ends. The reduction at spoke 14 is about 11° (Fig.3.10.c,). Consistent with previous geometrical parameters, also the distance of γ-tubulin molecules and positions are reduced and move toward the close conformation in horizontal and in vertical directions (Fig. 3.10.d,e,).

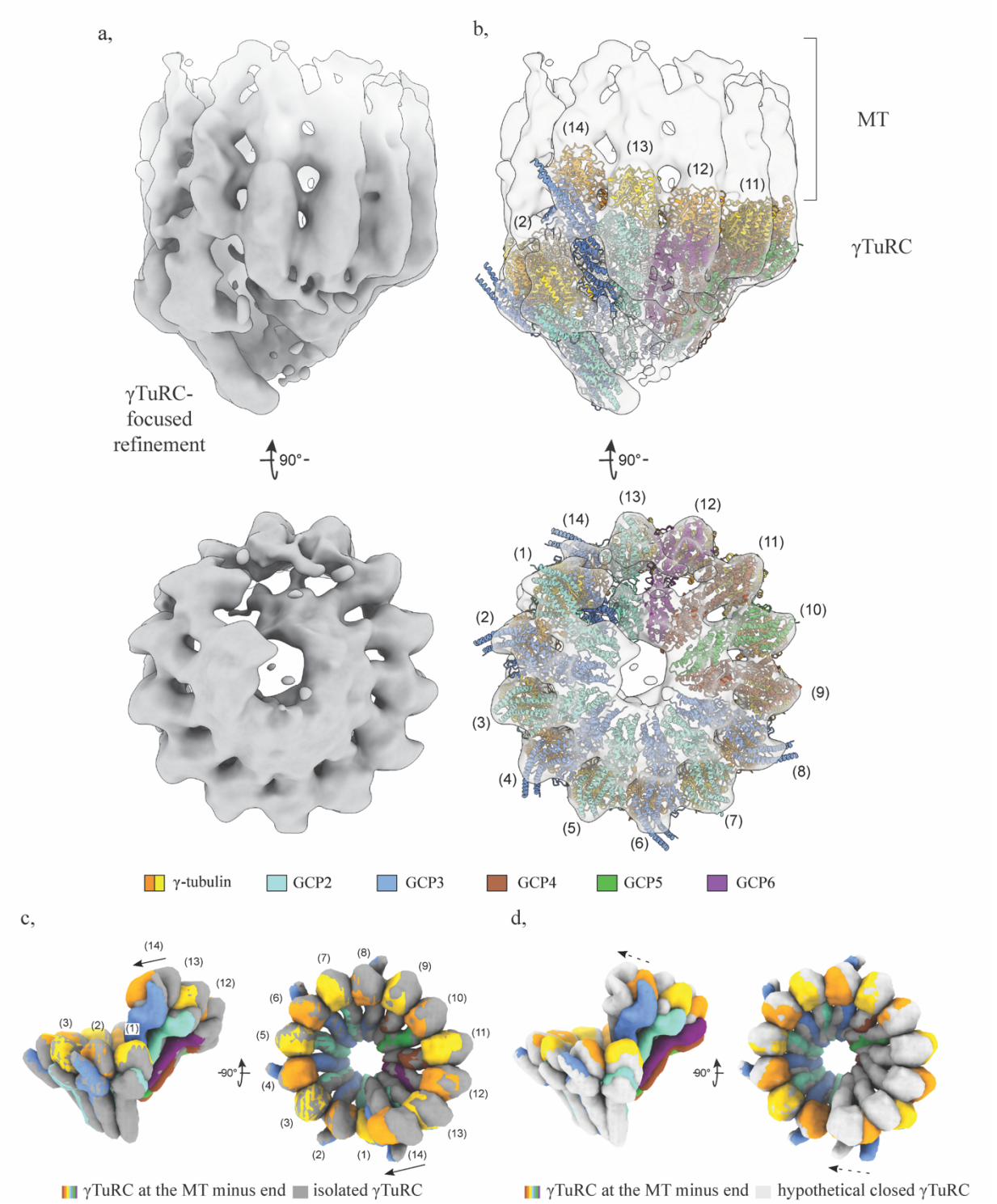

Fig. 3.9.: Analysis of γTuRC focused refinement of capped MT minus ends densities. a, The 3D reconstruction focusing on refinement of γTuRC at MT end with blended densities of MT site. b, Spoke-wise rigid body fitting of the atomic model of *X. leavis* γTuRC (PDB 6TF9) without γTuRC's luminal bridge densities. Colors representing isolated and MTs capped γTuRC are illustrated in the image. c,d, Visual demonstration of the structural conformation differences between *X. leavis* γTuRC at MT minus ends and *X. leavis* isolated γTuRC (PDB 6FT9, with omitted luminal bridge) and to hypothetical closed γTuRC (model is based on budding yeast ring of γTuSCs – PDB 5FLZ). Comparism indicate that γTuRC undergoes the conformational rearragment to to partially closed architecture, but still not reaching the closed conformation compatible with 13 pt MTs. Colouring as indicated. Figure components were created by Bram Vermeulen. Published in [240].

The discovery that vertebrates' γTuRC differs from budding yeast γTuSCs ring in terms of its asymmetry to MTs was unexpected. Based on the presented data, when nucleation occurs, the γTuRC experiences a conformational change seeking to achieve the MT symmetry of the "closed" γTuC, but not reaching it completely. This misalignment might have a physiological function in the regulation of MT nucleation and microtubule turn-over factor in evolutionary more advanced systems.

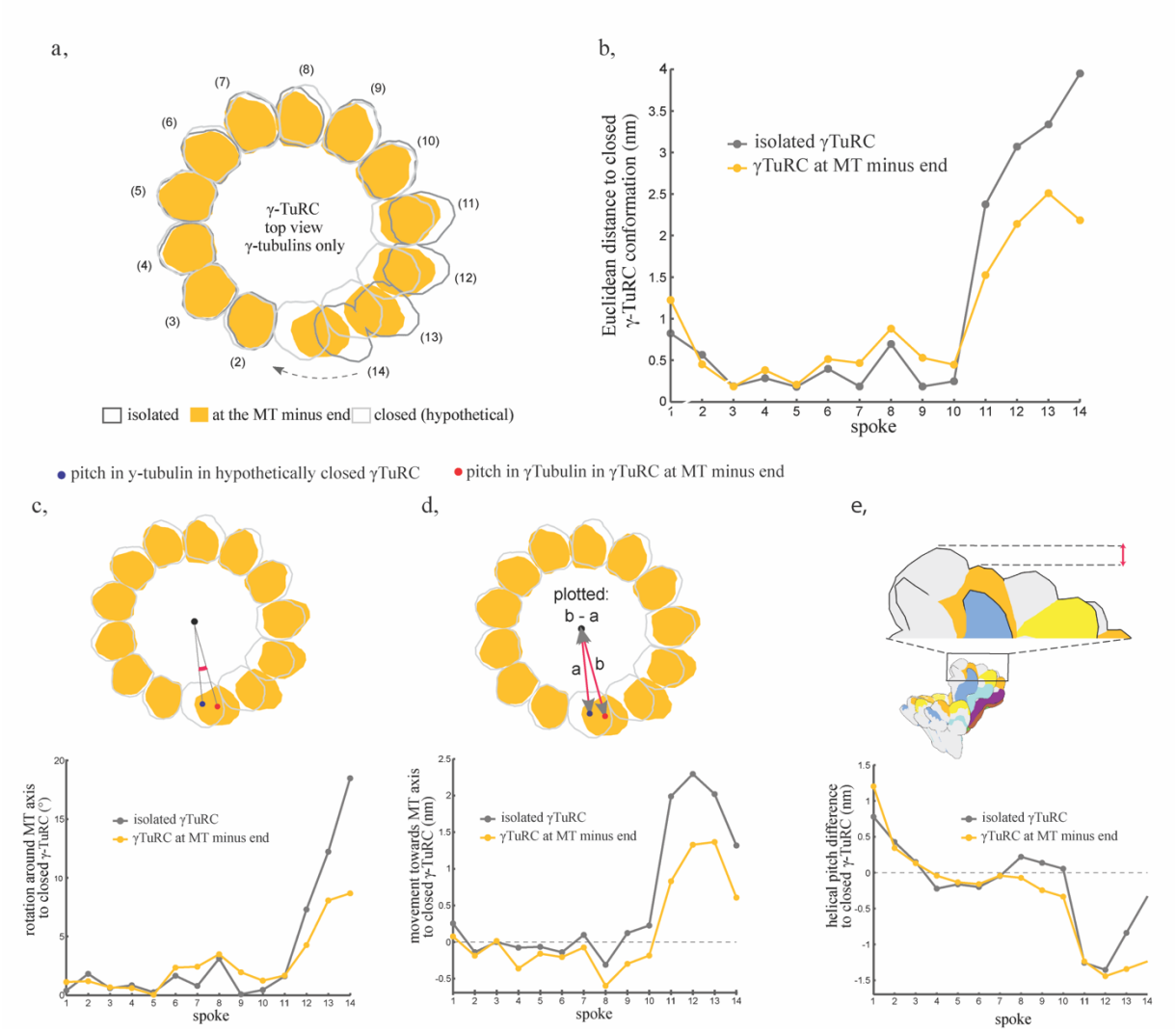

Fig. 3.10.: Geometrical analysis of structural reaargmanet of γTuRC at MT minus end . a, The scheme of γ-tubulin position in hypothetical closed γTuRC (light grey), γTuRC at MT minus end (orange) and *X. leavis* isolated γTuRC (PDB 6FT9, dark grey). Arrow indicates the required movement to achieve closed conformation. b, The meassurment of the distance, which the centres of the γ-tubulin need to undergo to reach the closed conformation (y=0) , isolated *X. leavis* isolated γTuRC (dark grey) and γTuRC at MT minus end (orange). The highest differences are from spoke 11 to spoke 14. c, The angle of the pitch of γ-tubulin of hypothetical closed γTuRC and the pitch of γ-tubulin of the γTuRC at the MT minus end (orange) or *X. leavis* isolated γTuRC (dark grey). Data show that angle of the γTuRC at the MT minus is decreased in attemto to reach closed conformation. d, The substraction of distances of pitch of γ-tubulins to the center of γTuRC in case of isolated and MT capped γTuRC compared to closed conformation e, the helical pitch differences indicating the movemnt of γTuRC at MT minus end to reach the closed γTuRC conformation. Figure components and geometrical analysis were created by Bram Vermeulen. Published in[240].

2.2.3. MT transformation and protofilament numbers

An interesting question is what happens with MT protofilaments in close proximity to γ-tubulin. Therefore further 3D refinements were focused on the nucleation MT site. Finally a resolution of 32 Å was achieved.

Based on the 3D structure there are 13 distinct densities growing from the γTuRC axis corresponding to the αβ-tubulin protofilaments (Fig. 3.11.a,). This observation is in line with Moiré pattern analysis and also computational analysis (Fig. 3.11.c,d,). According to Moiré pattern analysis 90.9% of the analysed MTs consisted of 13 protofilaments, the rest are unidentified numbers. Computational analysis confirmed that 96.9% were composed by 13 protofilaments.

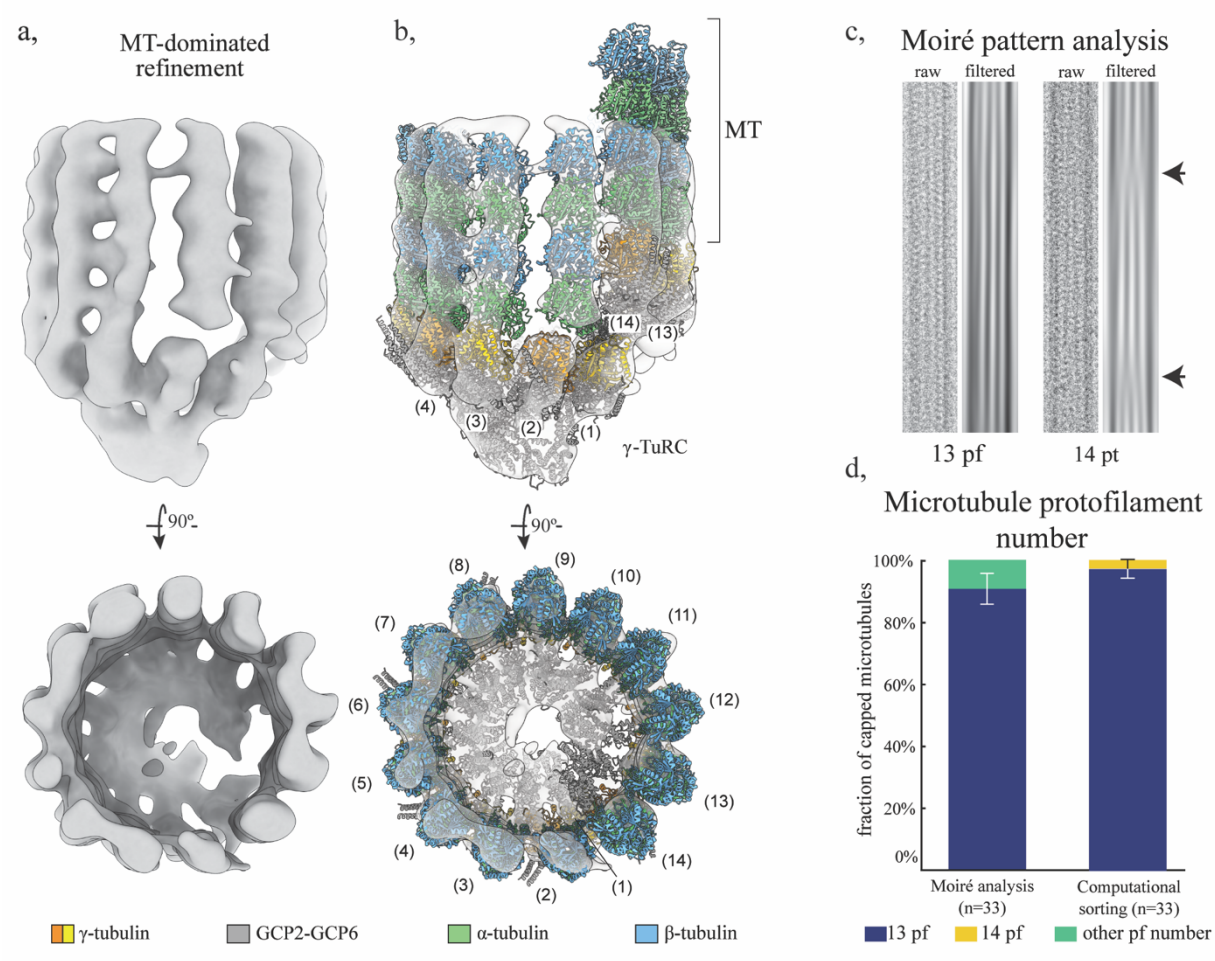

Fig. 3.11.: Analysis of MT focused refinement of capped MT minus ends densities. a, The 3D reconstruction of the final refinement MT at its minus end capped with γTuRC. b, Protofilament-wise fitting of MT into the final refinement of γTuRC capped minus end. Colour of γ-tubulin and αβ tubulins and spokes numbers as indicated. c, Represantative micrographs cut-outs of MTs showing raw and the Moire pattern filtered examples of 13 and 14

protofilaments (pf) MTs (obtained from γTuRC -capped MT). Arrows indicate the Moire pattern characteristi. d, Results of Moire pattern analysis shows that more than 90% of the MTs are created by13 pt, computational particle sorting analysis demonstrate that more than 96.9% of the MTs are assemblied by 13 pt. Error bars show standard deviation. Figure components were created by Bram Vermeulen. Published in[240].

32 Å resolution enabled rigid body docking of protofilaments based on prior knowledge of inter-protofilament contacts. This enabled the generation of the 3D model in the MTs axis that accurately described the obtained cryo-EM densities for all protofilaments except at spoke 2. The protofilament for spoke 2 had to be fitted separately (Fig. 3.11.b,).

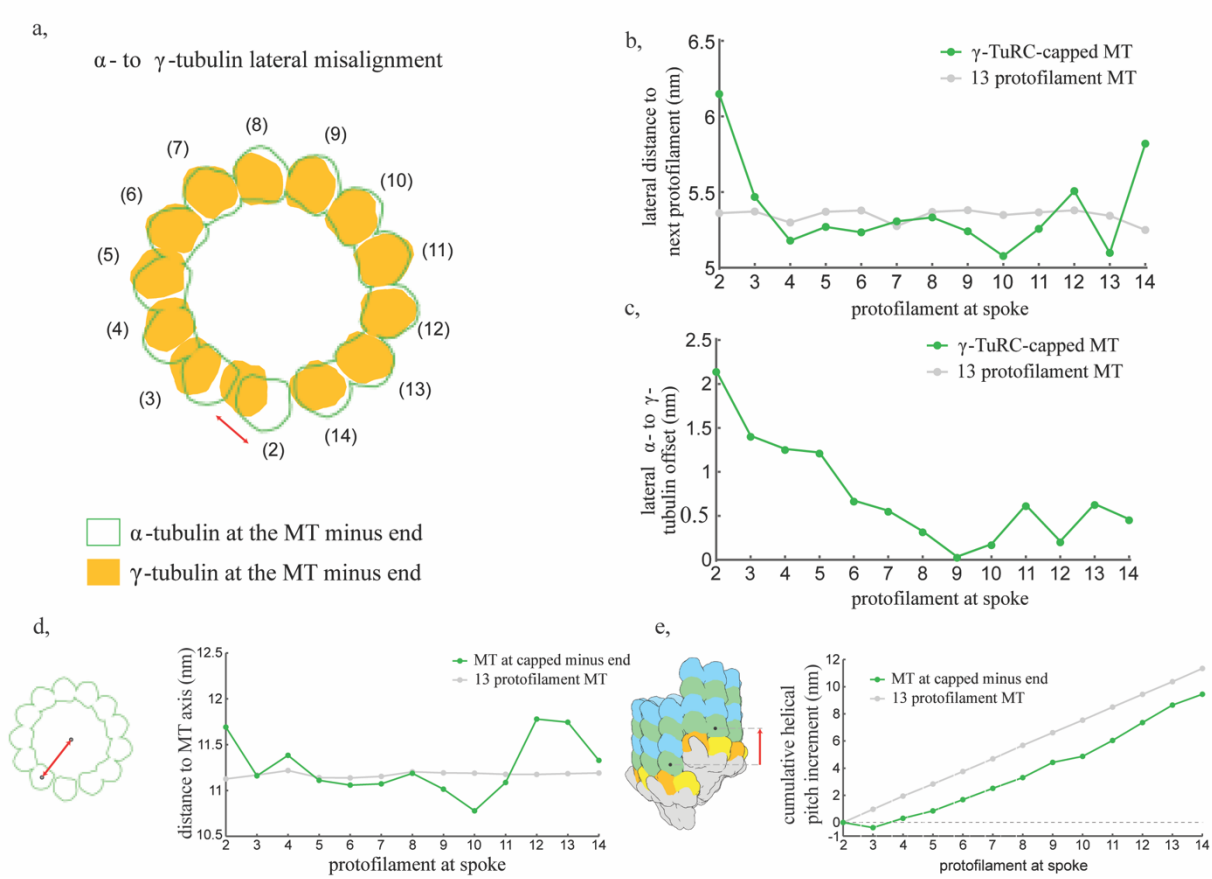

Fig. 3.12.: Geometric analysis of MT protofilaments at the MT minus-end close to the γTuRC. a, The outline of the position of γ-tubulin (orange) of γTuRC and α-tubulin (green) of MT at γTuRC capped microtubules minus end. b, Lateral distance between protofilament number n and its lateral binging protofilament (n+1). Comparison between 13 pt MTs and MTs at the proximity to the γTuRC. c, The gap between γ-tubulin of γTuRC and the first α-tubulin (green) of the emerging MT pt at corresponding γTuRC spokes. d, The distance between the center of MTs and the first α-tubulin subunit of the corresponding MT pt at the γTuRC capped minus end (green) compared to 13 pt MT. e, Examination of the pitch increment of the α-tubulin of the MT pt at spoke 2 to the MT pt's α-tubulins at following spokes. Figure components and analyses were created by Bram Vermeulen. Published in[240].

A schematic comparison reveals a mismatch between the contacts of the γ-tubulins at γTuRC and the first α-tubulins at microtubules minus end (Fig. 3.12.a,).

This discrepancy is characterised by the following geometrical analyses, where the lateral distance between the protofilaments at spoke 2 is prolonger approximately by 0.8 nm to spoke 3 and about 0.57 nm to spoke 14 compared to distances between regular 13 pt MTs (Fig. 2.12.b,). The distance between γ-tubulin of γTuRC and the first α-tubulin is increased by about 2 nm at spoke 2 and it also varies from 1.45 nm to 0.5 nm at spokes 3 to 7 (Fig. 3.12.b,) (γTuSC site). The distance of the pitch of tubulins and the middle axis of MZs is deviated at spokes 2 by about 0.6 nm and at spokes 12 and 13 by 0.7 nm. Capping with γTuRC triggers also a deviation in distance between pitches of α-tubulin and the middle axis of MTs by spokes 2, 12 and 13 in the range of more than 0.5 nm (Fig. 3.12.d,). The cumulative helical pitch increment of α-tubulins, which is linear in the case of 13 pt MTs, also exhibits the linearity deviations associated with decrescent values (Fig. 3.12.e,).

3D reconstruction of γTuRC capped MT minus ends showed that the geometry of the MT adapts partially to the asymmetry of γTuRC. Particularly in increments of distance to the MT axis and also by the increment of lateral distance between protofilaments. Also the distance between γ-tubulins and α-tubulins is enlarged especially at the GCP2-GCP3 site of γTuRC. These results suggest that interaction between MTs and the γTuRC is weaker compared between α- and β-tubulins dimers in the MT lattice.

2.2.4. The position of the MT seam at the γTuRC capped MT minus end

Inter-protofilament interactions are characteristic of lateral interaction between α - α tubulins and β - β tubulins. The seem of MTs is created by lateral interactions between αβ tubulin interactions (Fig. 3.13.b, left). Based on our 3D reconstruction and rigid body protofilament fitting (Fig. 3.13.a,) it was observed that MT eam may be created with a higher probability between spoke 2 and spoke 14, while the movement of the protofilament at spoke 2 needs adjustment by only 1.3 nm in the distal vertical direction. In contrast, the movement of the protofilament at spoke 2 needs to be adjusted by about 2.2 nm into the proximal direction to achieve seam position between spokes 2 and 3 (Fig. 3.13.b, right).

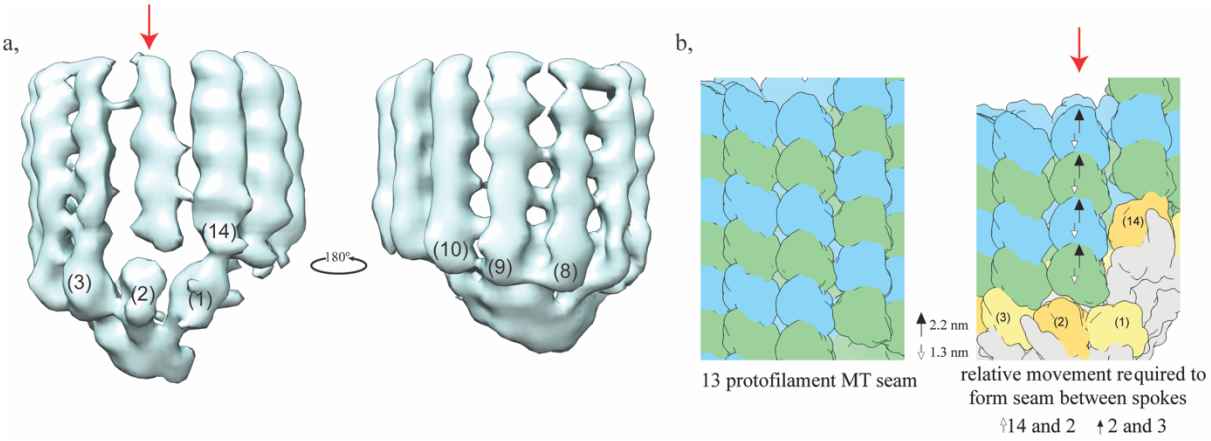

Fig. 3.13.: MT seem position at the γTuRC capped minus end. a, Density map of γTuRC capped minus end shoving the missaligned protofilamet at spoke 2 (red arrow) compar to the symetrical arragment at spokes 8 to 10. b, Layout of MT seam with lateral α to β tubulins interactions in regular 13 pt MT (left), outline of α and β tubulins of the pt at spoke 2 and neighbouring pt at spokes 3 and 14 interacting with γTuRC shows the direction of the repositioning neccesarry to achieve tubulin's seam conformation. The position of spoke 2 is demonstrated by a red arrow. Figure 3-13b was created by Bram Vermeulen. Piblished in[240].

2.3. CAMSAP2 protein recognizes γTuRC-capped MT minus ends

2.3.1. Binding of CAMSAP2 to recombinant γTuRC-capped MT minus ends and its influence on MT nucleation in vitro

The observed misalignment of the MT lattice at the boarder to the γTuRC, which persist to be asymmetric, might have physiological implication. The surface of the microtubule lattice creates epitopes which are recognized by MAPs (MT-binding proteins). The interphase between protofilaments differs at the minus end, middle part and plus end of the MT accompanied by different hydrolytic stages of GTP. Data from 3D reconstruction shows that we have got a misalignment of protofilaments at the proximity to the γTuRC resulting in increased curvature along the longitudinal axis of the protofilaments as well as decreased curvature in the lumen of MTs. These characteristics are recognized by the CAMSAP proteins family when it is binding to MT seeds. To this protein family belong CAMSAP1 to 3 and ASPM. If the assumption that the γTuRC upon nucleation reaches "closed" conformation is correct, as it is in the case of the oligomerized γTuSC, this should create a protofilament arragment similar to the middle segment of MTs and therefore it should be not be a binding site for CAMSAP.

Therefore I decided to test, where CAMSAP2 binds to γTuRC capped MTs and if it colocalizes with γTuRC. For this purpose, I purified CAMSAP2 tagged with GFP from insect cells (Fig. 3.14.e,). To freshly purified recombinant γTuRC capped MT minus ends, I added 200 nM CAMSAP2 and incubated only for 30 seconds to observe the first binding of CAMSAP2 to MTs. After this, the sample was crosslinked and then analyzed by IF.

According to my data, even 30 seconds of incubation were enough for CAMSAP2 to recognize MT minus ends capped with γTuRC. As the gallery of recombinant γTuRC capped minus ends shows, CAMSAP2-GFP signal colocalized with the γ-tubulin antibody signal (Fig. 3.14.a,). Additionally, the distribution of CAMSAP2 signal along the MT lattice demonstrates a significant preference of the CAMSAP2 protein to attach at positions where the γTuRC is situated (Fig. 13.14.b,c,).

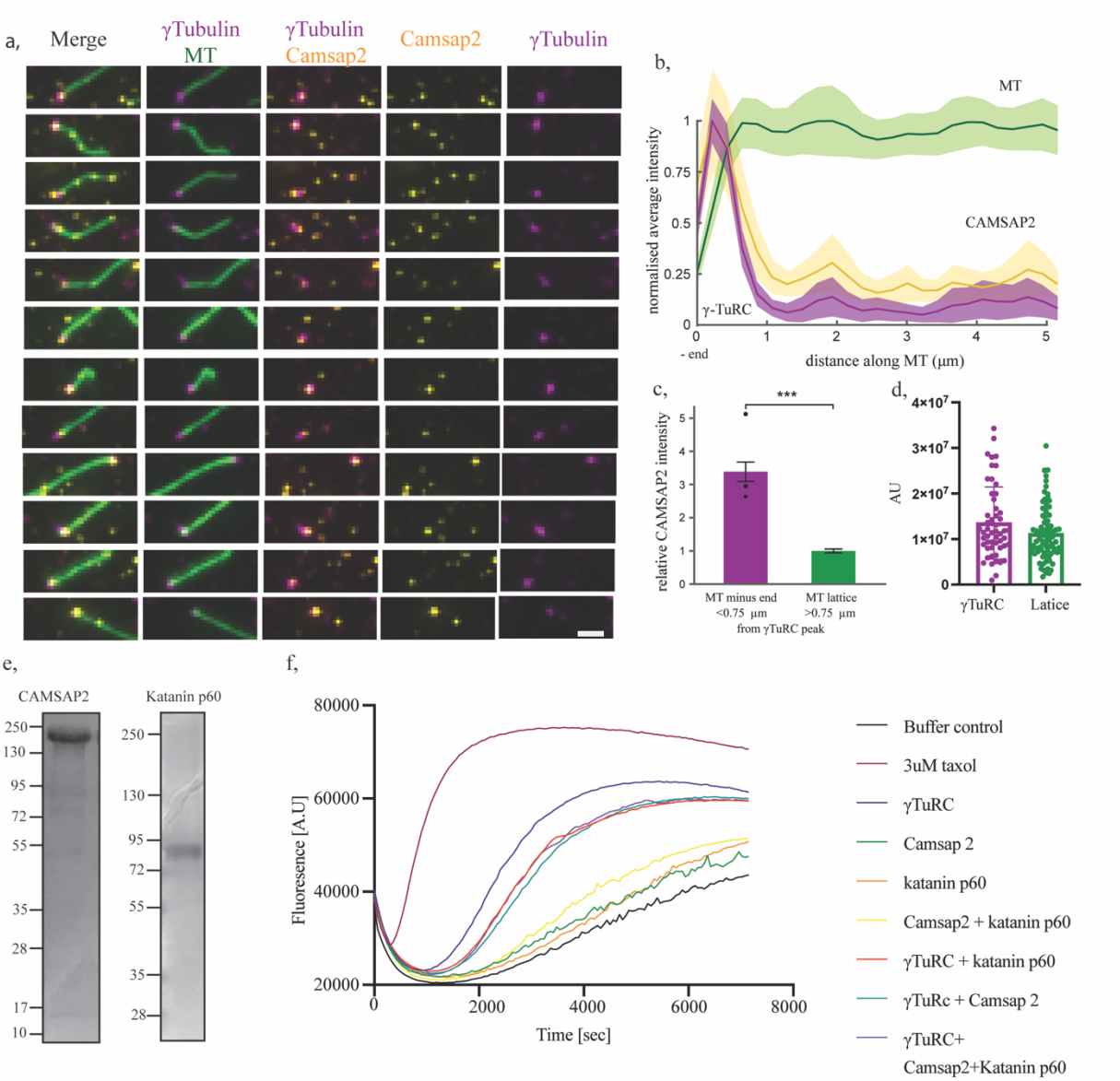

Fig. 3.14.: CAMSAP2 specifically recognises the recombinantly prepared γTuRC capped MT minus end but does not enhance γTuRC MT nucleation activity *in vitro*. a The gallery of selected recombinantly prepared γTuRC capped minus ends shows colocalization of CAMSAP2 (yellow) with γ-tubulin signal (magenta) on MT ends (green). Scale bar 1μm. b, Plot analysis reveils that CAMSAP2 signal colocalized with γ-tubulin signal analyzing the 5 μm length of γTuRC capped MTs (n=65). The blot shows CAMSAP2 binding to the γTuRC site. c, CAMSAP2 signal is significantly higher distributed along the first 0.75 μm of the length of γTuRC -MTs (3 replicates, n=48 MTs, n=53 MTs, n=58 MTs; Welch's t-test). d, Puncta of CAMSAP2 on the MT lattice (n=80) are comparable intensity the CAMSAP2 puncta co-localizing with γTuRC (n=53) (p=0,0541, t-test). e, Images of coomassie-stained SDS page gel showing purified CAMSAP2 and silver-stained SDS page gel with purified katanin p60 indicating the purity of samples. f, *In vitro* fluorescence microtubule nucleation measurement does not reveiled the enhancment of MT nucleation activity influenced by CAMSAP2 and katanin p60. Analysis of b and c were performed by Bram Vermeulen. Published in[240].

As it was recently shown, even the half of the γTuRC (recombinant γTuRC lacking actin and MZT1) can induce MT nucleation in vitro[244]. Hence, it was confirmed through negative stain EM that the γTuRC preparation used for capping MT minus ends comprised of fully assembled γTuRC mostly devoid of γTuRC assembly intermediates (data not shown in thesis, but published[240]).

I can observe the puncta of CAMSAP2 protein with the same intensity at the MT lattice. Considering the purification protocol of recombinant γTuRC capped minus ends, MT fragmentation may occur and will that generate new MT minus and plus ends. Puncta of CAMSAP2 protein may indicate the initiation of this process (Fig. 3.14.d,).

CAMSAP proteins recognize and interact with katanin, a MT severing enzyme. CAMSAP and katanin are potentially crucial for the regulation of MT turnover[19,75,80,81]. Once CAMSAP binds and decorates the MT lattice, katanin is recruited to the CAMSAP and triggers MT severing at this position. This is way CAMSAP stabilizes MT seeds while katanin cuts them into smaller segments, from which every one of them serves as the template for MT elongation.

Therefore, I prepared plasmids coding for the katanin subunit p60, which is recognized by CAMSAP2 and has severing activity. This plasmid was used to create a stable HEKT293 cell line by Onur Karasu with the usage of a sleeping beauty system. I purified katanin p60 subunit after overexpression during mitotic arrest, to get the most active form of the enzyme (Fig. 3.14.e,). I used both proteins to investigate their effect on MT nucleation with and without γTuRC. In both cases, I did not observe a significant effect of these proteins on MT nucleation in *vitro* (Fig. 3.14.f,).

2.3.2. CAMSAP2 recognizes *X. leavis* γTuRC-capped MT minus ends

γTuRC capped minus ends may be different in recombinant systems compare to native sources in posttranslational modification as well as in conformational changes due to them. For this reason, I have verified if CAMSAP2 is also able to bind to native γTuRC capped minus ends from *Xenopus leavis* source. Due to differences in the preparation of both samples, mainly due to the small size of microtubule seeds, I was not able to use fluorescence microscopy. The limitation on our microscope is about 200 nm, everything below this size is recognized as one signal, or it is possible to recognize two different signals between which is the distance of about 200 nm. The size of microtubule seeds varies between 100 nm to 2 µm. Therefore together with Annett Neuner, we optimized the protocol for double labelling negative stain EM for investigation of the binding of CAMSAP2 to native *Xenopus leavis* γTuRC capped minus ends.

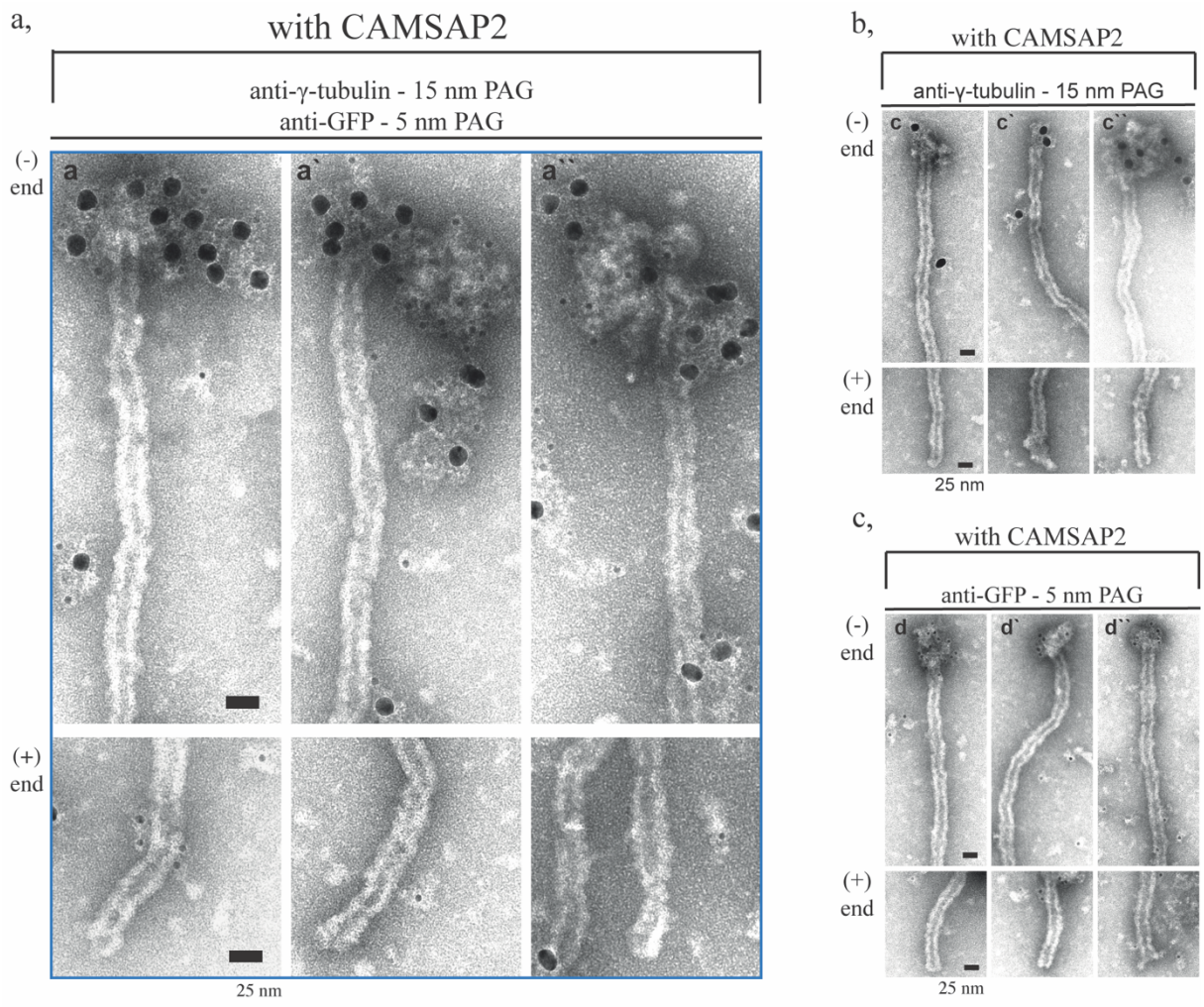

Fig. 3.15.: *Xenopus laevis* γTuRC capped MT minus ends are recognized by CAMSAP2 a, NS EM images showing the double immuno labbeling of native Xenopus leavis γTuRC capped MT minus ends, showing the co-

localization of γ-tubulin signal with CAMSAP2-GFP at the MT end (top). The lower part shows plus end of the MT which is label free. Labelling is with γ-tubulin antibody coupled with 15 nm PAG (gold particle) and anti-GFP antibodies labelled with 5 nm gold particles. b,c, Control samples with single labelling are confirming the specifity of antibodies via recognition of one MT end. Labelling as indicated. b, single controle of γ-tubulin antibody c, single controle of anti-GFP antibody. Double labelling NS EM was performed by Annett Neuner.

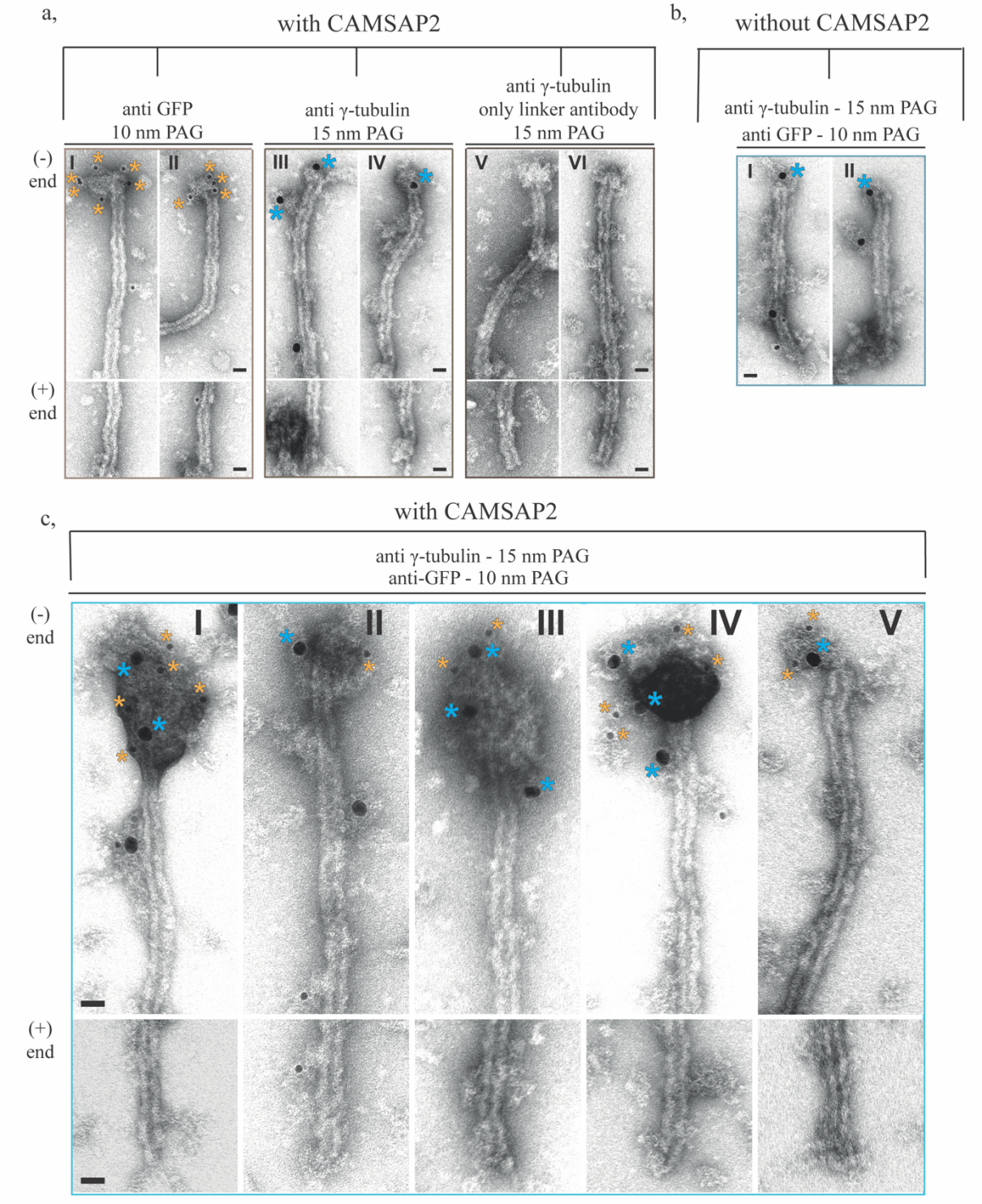

Fig. 3.16.: The CAMSAP2 protein can identify *X. laevis* γTuRC-capped MT minus end. The speacifity of CAMSAP2 binding to the γTuRC capped MT minus endswas verified with different set up of antibody labelling. Mouse γ-tubulin antibody was identified with an anti-mouse secondary antibody coupled to 15 nm gold particles and goat anti-GFP antibody was recognized with an anti-goat secondary antibody coupled to 10 nm gold particles. a, Control samples with the single labeling with antibodies: I-II goat anti-GFP and anti-goat-10 nm gold; III-IV mouse anti-γ-tubulin and anti-mouse-15 nm gold; V-VI only anti-mouse-15 nm gold. Scale bars: 25 nm. b, Double labelling of *X. laevis.* γTuRC capped MT minus ends without CAMSAP2 showing signal only for γ-tubulin at the MT minus end. Scale basr: 25 nm. c, Double labelling of *X. laevis* γTuRC capped MT minus ends incubated with CAMSAP2. Blue asteriks indicates the position of γ-tubulin signal, which colocalizes with CAMSAP-GFP (orange asteriks). Scale bars: 25 nm. Double labelling NS EM was performed by Annett Neuner in collaboration with me. Published in[240].

Even the short incubation time of CAMSAP2 protein with freshly purified *X. leavis* γTuRC capped minus ends was enough to accumulate the CAMSAP2 signal to the position of γTuRC at MT minus ends (Fig. 3.15.a,; Fig. 3.16.c,).

To verify the specificity of the signal, me and Annett Neuner decided to follow two different approaches how to detect the proteins. In the first case, we detected γ-tubulin with anti-γ-tubulin antibodies. The first antibodies were detected with secondary antibodies conjugate to 15 nm PAG. The GFP was recognised by an specificly modified anti-GFP antibody that can be directly conjugated with 5 nm PAG (without usage of 2nd antibody)(Fig. 3.15.a,). The negative stain analysis of the labelled MTs resulted in a strong, electron dense signal on the capped MT minus end because of the antibody accumulation that was stained by UrAc.

A second approach was the use of anti-γ-tubulin antibody and its corresponding anti-mouse secondary antibody conjugated with 15 nm PAG and goat-anti-GFP and anti-goat secondary antibody conjugated with 10 nm PAG. Both signals colocalize at the MT end (Fig. 3-.6.c,). The single labelling confirmed the specificity (Fig. 3.16.a,) as did the control without added CAMSAP2 protein (Fig. 3.16.b,)

According to the expression database, CAMSAP2 mRNA is expressed in *Xenopus leavis* and expression of other CAMSAP proteins varies during development stages. The ASPM, mitotic member of CAMSAP protein family, is expressed in Xenopus leavis eggs extracts[245,246].These set of proteins are involved in the regulation of MTOCs. With this experiment, I could confirm the specificity of interaction between CAMSAP2 and γTuRC capped minus ends also in other biological systems and the specificity of the first interaction, where the accumulation of CAMSAP2 signal is in proximity to γTuRC.

2.3.3. Effect of CAMSAP2 and katanin p60 subunit on aster formation in *Xenopus leaves* extract

I did not observed an impact of CAMSAP2 and Katinin p60 on MT nucleation in vitro (Fig. 3.14.f,), which may be explained by lacking activation factors that are present in the *in vivo* system. Therefore I decided to investigate their effect in *X. leavis* egg extract.

One hypothesis is that the CAMSAP2 and katanin p60 might influence MT turnover by stabilization of MT seeds, multiplication of MT seeds or by severing longer MTs[83,84,86]. If this hypothesis is correct, the expected result would be the increased mass of MT asters, as I can confirm by the increased diameter of asters (Fig. 3.17.a,b,). Surprisingly, both components also induced not only an increase in the mass of asters but also their numbers (Fig. 3.17.c,). The influence of exogenous components is limited to the amount of active endogenous factors, such as activation factors or tubulin accessibility to polymerize.

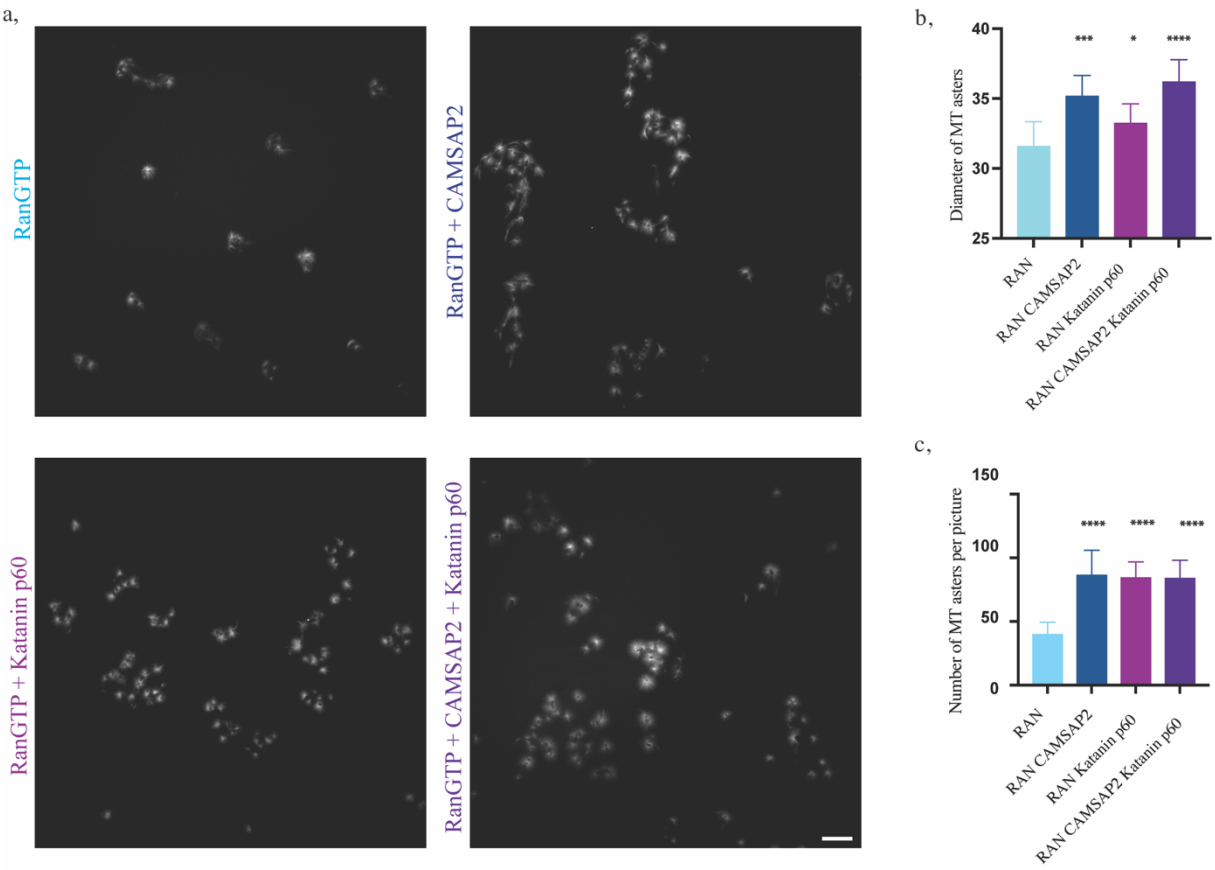

Fig. 3.17.: Influence of CAMSAP2 and Katanin p60 on RanGTP chromosomal MT nucleation verified via LSS MT aster formation. a, Selected fluorescence images of the MT asters created via Ran(Q69L) in the presence of 100 µM CAMSAP2 and 80 µM Katanin p60. Scale bar: 100 µm. b, The average diameter of the MT asters is increased in the presence of CAMSAP2 as compared to the influence of Katanin p60 alone. t-test, $p_{(CAMSAP2)}$= 0,0001, $p_{(Katanin\ p60)}$= 0.0298 , $p_{(CAMSAP2+\ Katanin\ p60)}$ < 0.0001. c, The average number of the MT asters

per picture is increased in the presence of CAMSAP2 and Katanin p60. t-test, $p_{(CAMSAP2)} < 0{,}0001$, $p_{(Katanin\ p60)} < 0{,}0001$, $p_{(CAMSAP2+\ Katanin\ p60)} < 0{,}0001$.

2.4. Actin as *bona fida* structure of γTuRC

2.4.1. Confirmation of actin presence inside of the *Xenopus leavis* γTuRC

At the beginning of my PhD, I participated in a study to determine the structure of vertebrates γTuRC. In this study, Erik Zupa was able to identify the positions of all GCPs and γ-tubulins, but two densities remained unresolved. Both of them were in the lumens of the γTuRC (Fig. 3.18.a,b, -shown as red and pink). One of the segments had a globular shape (red) with proximity to γ-tubulin and the other one had a helical arrangement (pink, described as α-a helical domain of luminal bridge).

Analysis of the purified γTuRC by mass spectrometrie idenfied besides GCPs and γ-tubulin NEDD1, NME7 or MZT1. However, NEDD1, NME7 or MZT1could not be fitted into these densities.

Surprisingly, LFQ mass spectrometry analysis showed that actin molecule also co-purified with other γTuRC components to a relative stoichiometric abundance of 0.8 molecules[53]. Comparing the structure of actin with unsolved densities produced an unambiguous fit in the globular segment of luminal densities. Therefore, I and Annett Neuner verified the presence of actin inside γTuRC via immunofluorescence analysis (Fig. 3.18.c,d,). Considering the size of γTuRC of 37 nm and the size of primary and secondary antibodies reaching approximately 20 nm, an optimized protocol involved light SDS extraction of γTuRC after fixation and before antibody addition. This led to better accessibility of epitopes and therefore the actin colocalisation events were increased to 40.2% of the total GCP6 signal.

As the centrosomes regulate not only MT nucleation but also nucleation of actin filaments[247,248], I have investigated if the presented actin inside of γTuRC may undergo conformational change and nucleat actin filaments via fluorescence actin polymerisation assay. Whereas the ARP2/3-VCA complex that served as positive control and showed robust actin filament nucleation activity *in vitro*, the γTuRC did not trigger actin filament assembly (Fig. 3.18.e,).

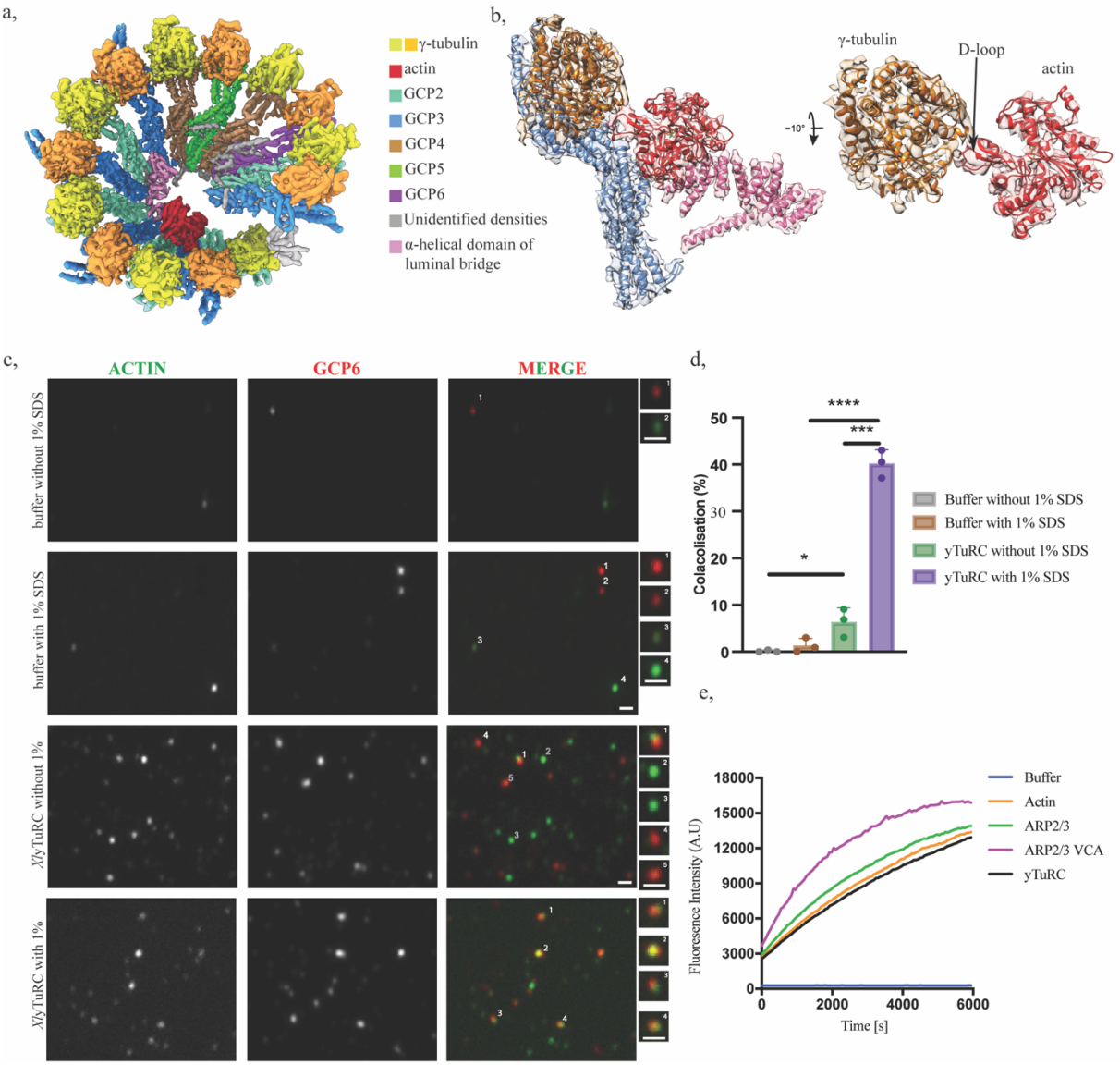

Fig. 3.18.: Actin is the *bona fida* structure of the vertebrates γTuRC. a, Structure of *Xenopus leavis* γTuRC with indicated components. Modified from [53]. b, Position of actin in close contact with GCP3-bound γ-tubulin and the luminal bridge of γTuRC. The D-loop of actin is in contact with γ-tubulin. Modified from[53]. c, Immunofluorescence analysis of *Xenopus leavis* γTuRC with anti-GCP6 and anti-actin antibodies indicates colocalization of both proteins. 1% SDS was used to facilitate the reachability of actin epitopes inside the γTuRC. Co-localization of the signals of actin and GCP6 is demonstrated in zoomed images. Scale bars: 20 nm. Published in[53] d, The 40,l'% of the GCP6 signal co-localize with actinsignal, 3 independent experiments (nGCP6=2678). Without SDS treatment, actin epitope is deeply embeded in lumen of γTuRC which is reflected laso with lower colocalisation events. (6.4%, nGCP6= 2568). *, P=0.024; ***, P=0.0002; ****, P<0.0001. Published in[53] e, Actin polymerization assay. Arp2/3 VCA actin polymerisation activation confirms the functionality of essey. γTuRC is not able to facilitate the actin polymerisation. Fluorescence measurement of pyrene labelled-actin polymerization (2 μM) in the presence of 0.5 nM Arp2/3, 15 nM VCA domain of WASP and 0.5 nM γ-TuRC. Data show the mean of 5 measurements. Published in[53].

2.4.2. IDo of GCP6 as a potential component of the luminal bridge

The second part of the inside segment of the γTuRC is α helical segment, which is in close contact with the actin molecule and extends to the position of GCP6 inside of γTuRC (Fig. 3.19.a,b,).

From obtained densities, we could not resolve the position of N termini of GCPs and the large Insertion Domains (IDo) of GCP5 and GCP6. IDo of GCP5 consists of 120 aa residues which are predicted to be unordered. The IDo of GCP6 contains 868 aa and was predicted to be helical right after the Grip 1 domain (Fig. 3.19.c,).

I have successfully expressed and purified the *X. leavis* variant of the anticipated helical segment of IDo, xGCP6 $^{546\text{-}794}$. The CD spectrum verifies the helical arrangement present in this protein construct (Fig. 3.19.d,e,). I have tried to crystalize this construct together with Jürgen Kopp and Gunter Stier, but this attempt was not successful. For this, I optimize the construct, so they were less flexible and in addition I used different tags. All crystallization attempts were unsuccessful. That suggests that this helical part may still have got flexibility.

Meanwhile, the group of Prof. Kapoor was successful in the crystallization of N-termini of GCPs with bound MZT1, where they could confirm the fold formation in yeast but also in the human system[63,64]. These two components created α-helical fold which resembled the helices in the luminal bridge and were able to fit into their unresolved densities [66,249].

I could not resolve the function and position of the IDo domain of GCP6. Even with the development of artificial intelligence and predictions (Alpha fold), I could not resolve the structure of the predicted helical part, not even in the context of full length GCP6 (Fig 3.19.f,). Alpha fold recognizes it as one extended helix, even so, according to the predictions there are parts with low helical predictions (Fig. 3.19.c,). According to the prediction, the IDo should localized inside of γTuRC, where the part 1 of IDo co-precipitates with GCP2 and GCP5[53]. Mutations in the IDo sequence are associated with microcephaly, which may suggest the involvement of this part in the regulation of MT nucleation[250].

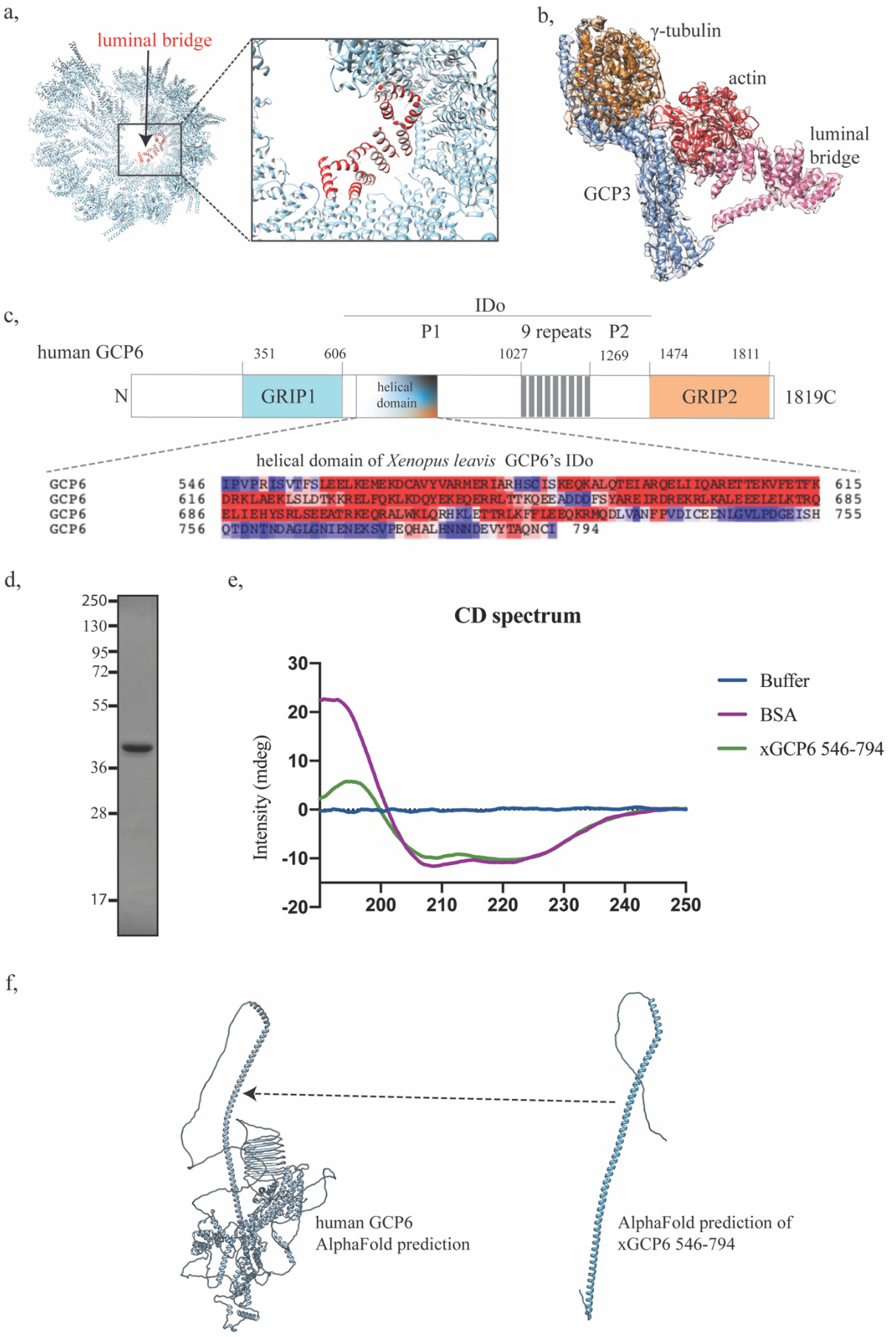
a,
luminal bridge
b,
γ-tubulin
actin
luminal bridge
GCP3
c,
IDo
P1
9 repeats
P2
human GCP6
351
606
1027
1269
1474
1811
N
GRIP1
helical domain
GRIP2
1819C
helical domain of Xenopus leavis GCP6's IDo
GCP6 546 IPVPRISVTFSLEELKEMEKDCAVYVARMERIARHSCISKEQKALQTEIARQELIIQARETTEKVFETFK 615
GCP6 616 DRKLAEKLSLDTKKRELFQKLKDQYEKEQERRLTTKQEEADDDFSYARETRDREKRLKALEEELELKTRQ 685
GCP6 686 ELIEHYSRLSEEATRKEQRALWKLQRHKLETTRLKFFLEEQKRMQDLVANFPVDICEENLGVLPDGEISH 755
GCP6 756 QTDNTNDAGLGNIENEKSVPEQHALHNNNDEVYTAQNCI 794
d,
250
130
95
72
55
36
28
17
e,
CD spectrum
Intensity (mdeg)
30
20
10
0
-10
-20
200
210
220
230
240
250
Buffer
BSA
xGCP6 546-794
f,
human GCP6
AlphaFold prediction
AlphaFold prediction of
xGCP6 546-794

Fig. 3.19.: Analysis if the insertion Domain (IDo) of GCP6 could be potential part of γTuRC's luminal bridge a, Helical composition of the luminal bridge inside the γTuRC are shown in red. b, Distribution of the luminal bridge is from GCP6 covering the lumen of γTuRC till the position of actin molecule at spoke 3 (GCP3). Modified from [53] c, Domain composition of GCP6, between GRIP1 and GRIP2 domain is the insertion domain (IDo), subdivided into part1 of IDo, middle part is created with 9 repeats and close to the C terminus is part 2 of the IDo. GCP6 part 1 is predicted to have high helical composition from amino acids 546 to 794. *X. laevis* 546-794 helical. Prediction made by Erik Župa and published in [53] d, Protein of *X. laevis GCP6*$^{546-794}$ was expressed in *E. coli* BL21 ril.The Coomassie-stained gel confirm the purity of the sample and its suitability for circular dichroism analysis. Published in [53] e, Circular dichroism (CD) analysis of *X. laevis* GCP6$^{546-794}$ confirmt that this part has got helical composition comparable to BSA (consisting of α-helices). Spectra are from three independent biological experiments. Published in [53] . f, Alfa Fold analysis of whole human (GCP6) and *X.l.* GCP6 546-794 amino acids show comparable prediction of the helical structure of the IDo helical part but without any folding segmentation. Structure of GCP6 is from UniProt Q96RT7-GCP6, Segement of GCP6 of IDo separatly analysed by Bram Vermeulen.

2.4.3. Recombinant actin-deficient γTuRC and its activity *in vitro*

A new advantage in the investigation of the function of actin in the γTuRC was enabled by the development of a human recombinant γTuRC system by Martin Würzt in our laboratory[62,235].

Closer analysis identified that the last 2 helices formed by the GCP6 N-terminus creates a binding site for actin in γTuRC (Fig, 3.20.a,b,). By deletion of these two helices actin binding was abolished and surprisingly the γTuRC with minor conformational deviations assembled (Fig .3.20.c,)[62]. This result suggests that actin is not necessary for the assembly of the γTuRC.

I investigated the influence of actin deficiency on the MT nucleation activity of γTuRC. An *in vitro* experiment allows meassuring the single effect of components such as actin-deficient γTuRC. That means I could observe the basic nucleation activity of the γTuRC. I applied two different methods. One based on spinning down crosslinked MTs and counting their amount at different time points and second one based on flourescence measurment of nucleation during 60 minute time interval. Neither with the first, nor with the second method I could obeserve significant deteriations in MT nucleation activity of recombinant and purified γ-TuRC$^{\Delta N56-GCP6}$ compare to wild type γ-TuRC (Fig. 3.20.d,e,f,).

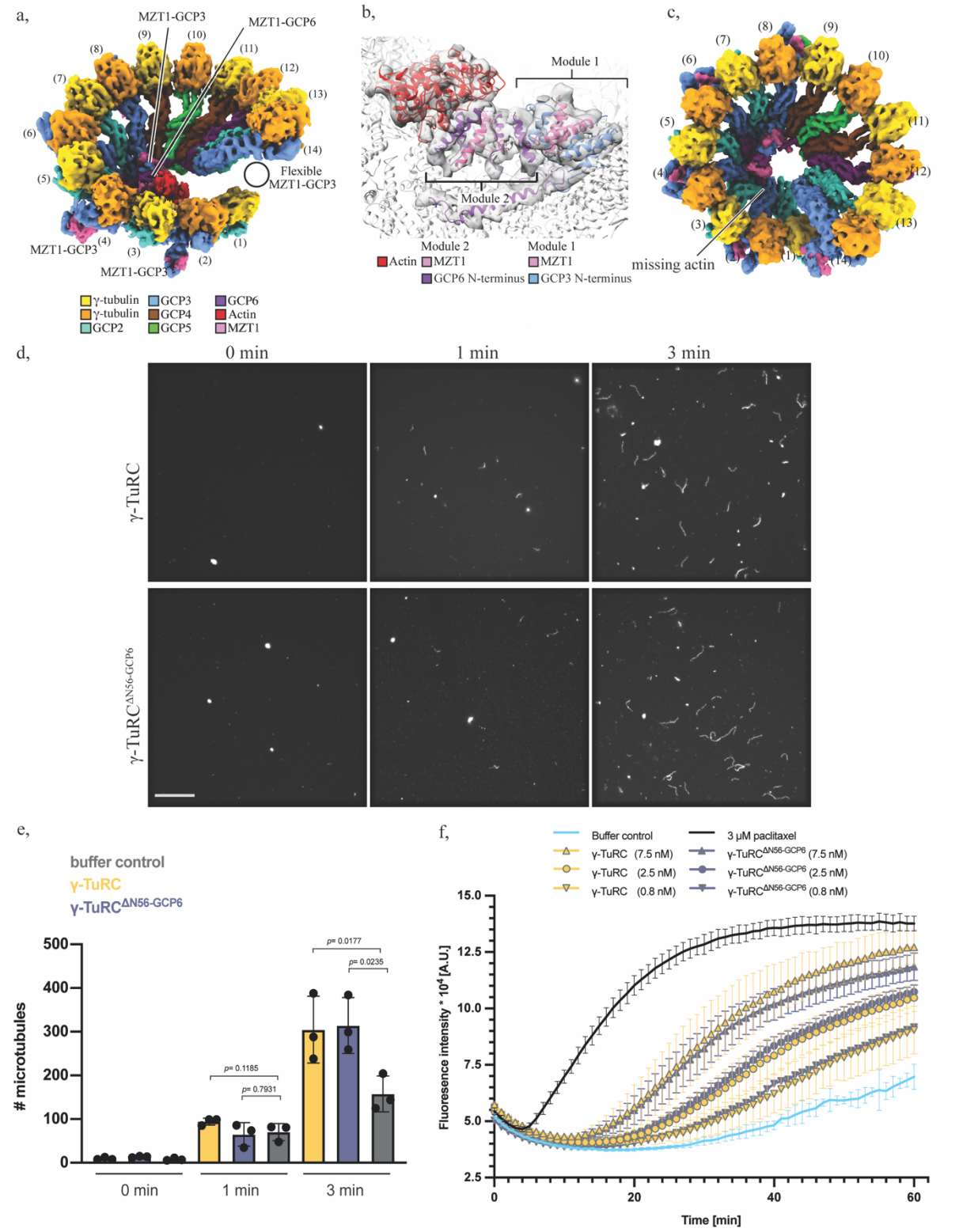

Fig. 3.20.: Luminal bridge components creates the binding interphase for the actin in the lumen of the γTuRC. a, The actin molecule is deeply embedded into the structure of the γTuRC. On the lateral side it contacts with γ-tubulin at spoke 3 and on lumenal site it is in contact with the luminal bridge. b, Crystallization of the N-termini of GCPs with MZT1 [63,64] confirm that these components creates the luminal bridge. The N-termini of GCP6 and GCP3 with 2 molecules of MZT1 create the helical segments of the luminal bridge. Modified from[62] c, Deletion of the N-56 aa terminus of GCP6 disrupted the binding of actin to the γTuRC as confirmed by cryo-

EM. Modified from [62] . d,e, An *in vitro* MT nucleation assay. MTs were nucleated either with recombinant WT γ-TuRC or γ-TuRC$^{\Delta N56\text{-}GCP6}$ containing 7 nM pig brain αβ-tubulin (5% Cy3-labelled tubulin) or with buffer control at an αβ-tubulin of 20 μM containing 5% Cy3-labelled tubulin. Individual MTs were counted. Colouring as indicated Published in [62].d, Fluorescence images taken at 0 min, 1 min, and 3 min were provided for comparison. Scale bar: 20 μm. e, The mean and standard deviation (showing as bars) of the counted MTs, alongside the individual counts (as dots) for each of the three replicates of a given condition. f, Fluorescence based *in vitro* MT nucleation assay comparing concentration influence of recombinant WT γ-TuRC and γ-TuRC$^{\Delta N56\text{-}GCP6}$ on MT nucleation. The mean with standard deviation is depicted for buffer control (blue), 3 μM Paclitaxel as a reference (black), and three different concentrations of γ-TuRC (yellow) and γ-TuRC$^{\Delta N56\text{-}GCP6}$ (purple) samples, with each having four replicates. The concentration is correlated to the amount of γ-tubulin in the sample estimated via the immunoblots of recombinant human γ-tubulin. Recombinant γ-TuRC was obtained from Martin Würzt and cryo-EM was performed by Erik Župa. Data published in[62].

Previosly, isolated γTuRC incubated with DNAaseI, which should interact with the D-loop of actin and in this way interupts the binding of actin to γTuRC, declined MT nucleation activity. But the source of the γTuRC was meiotic arrested *Xenopus leavis* extract, where the components of microtubule nucleation pathway are active. Hence, this γTuRC may be considered as more active as recombinant γTuRC[53].

2.4.4. Actin -deficient γTuRC and its function inside cells

To confirm that actin deficiency does not affect the assembly of the γTuRC also *in vivo*, I purified γTuRC from HEKT293 cells expressing *FLAG-tagged* wild type GCP6 or γ-TuRC$^{\Delta N56\text{-}GCP6}$. In the *in vivo* system actin is also not necessary to assemble the γTuRC judging by averaged classes of γTuRC from negative stain EM analysis (Fig. 3.21.a,).

Enrico Atorino investigated the phenotype of actin-deficient γTuRC *in vivo* in RPE1-hTERT cells. Upon investigation was discovered that actin-deficient γTuRC express delay in re-nucleation assey, which suggests some defects in first stages of nucleation reaction (Fig. 3-21b). This deleay express itself in slowing down of cell cycle, expecially in delays in mitotic spindle assembly and chromosomal aligment[62].

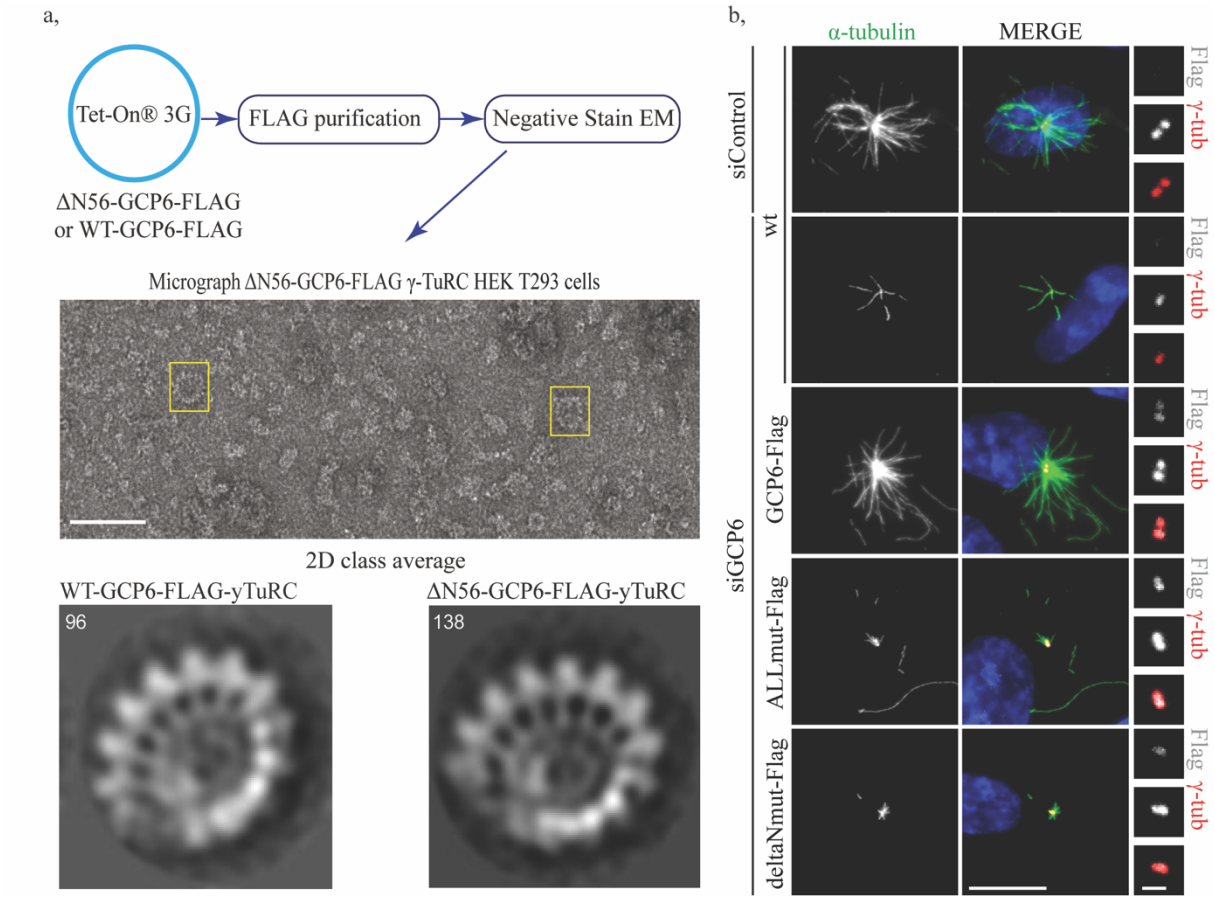

Fig. 3.21.: Acting deficient γTuRC is fully assembled and ehibits defects at the speed of MT nucleation in *in vivo*. a, Negative stain EM analysis of WT γ-TuRC or γ-TuRC$^{\Delta N56\text{-}GCP6}$ ("actin-deficient γ-TuRC") purified via C-terminal-FLAG- GCP6 from HEKT293 cells. Top: Schema of the purification procedure. Representative NS EM image shows individual particles (yellow boxes) on micrographs (middle picture, scale bar 100 nm) and a 2D class average (bottom picture) demonstrate that γ-TuRC$^{\Delta N56\text{-}GCP6}$ is structurally intact and comparable to wild-type γ-TuRC. b, Immunofluorescence images of *in vivo* MTs re-nucleation from centrosomes (marked by γ-tubulin) showing reduction of MT numbers and length between γ-TuRC and γ-TuRC$^{\Delta N56\text{-}GCP6}$. RPE1 cells were treated with GCP6 siRNA expressing either siRNA resistant WT *TUBGCP6-FLAG* (GCP6-Flag) or mutant (ALL (R35D, K38D, K39E, Y42A, F46A); dN (ΔN56-GCP6) – with FLAG tag) *GCP6* constructs. Colouring as indicated. Cell lines and *in vivo*, MT renucleation assay was created by Enrico Antorini, NS EM was done by Annett Neuner and NS data analysis was made by Martin Würtz. Data published in[62].

2.4.5. Actin density in the γTuRC is present also after MT nucleation

By investigating the observed 3D reconstruction of *Xenopus leavis* γTuRC capped minus ends, I can also observe the density corresponding to actin.

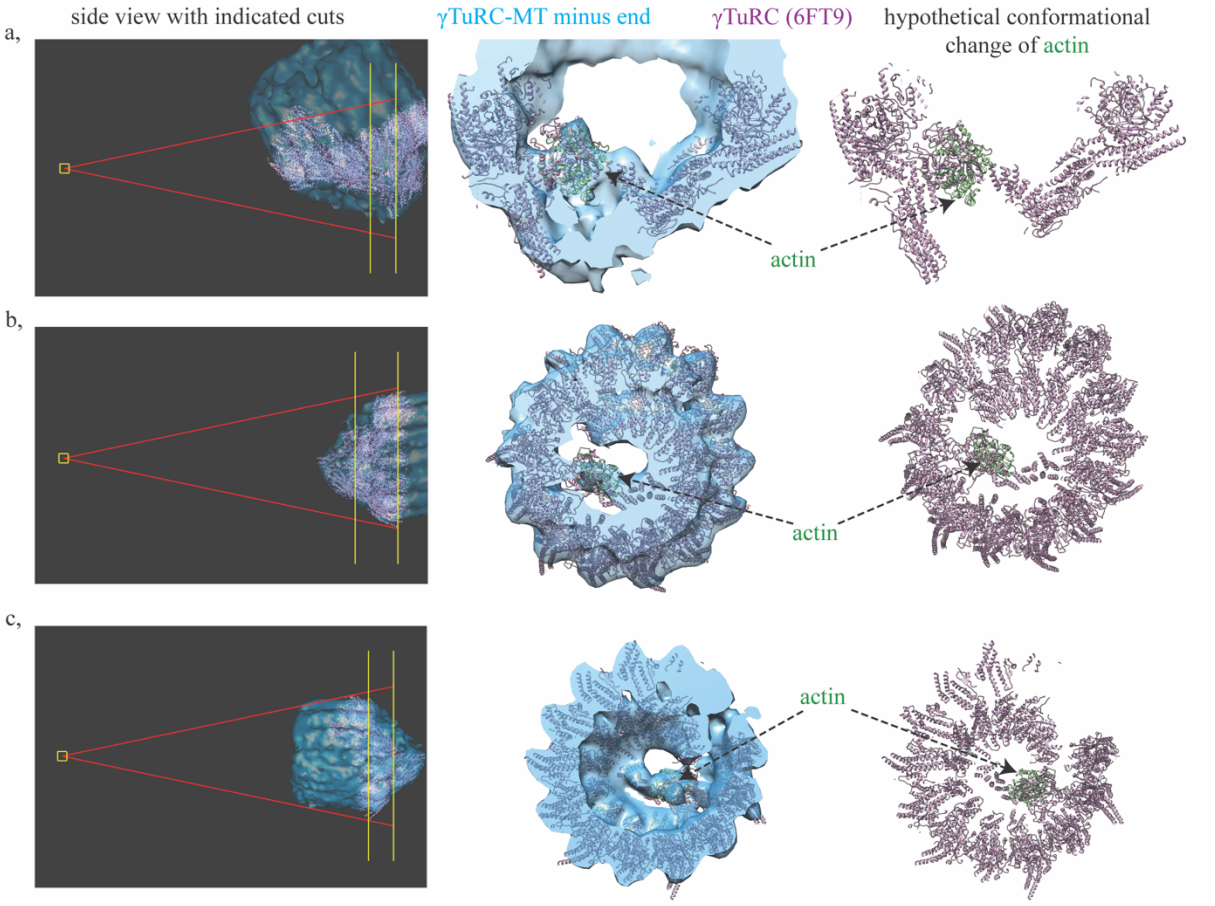

Fig. 3.22.: Actin density is presented in γTuRC capped minus end. The view of the position of the actin and luminal bridge densities inside of γTuRC capped minus end (blue with fitted the *X. laevis* γTuRC model (PDB 6FT9)-violet) indicates a conformational change of actin inside of the γTuRC capped minus end (green). a, side view b, bottom view c, top view.

By comparing the position of actin in an adjusted molecular map of isolated native *Xenopus leavis* γTuRC and in the position of actin in the γTuRC after nucleation, alternation corresponding to supposed conformational changes may be noticed (Fig. 3-22). Changes in actin conformation should be accompanied by changes in luminal bridge conformation. Regrettably, the recent 3D reconstruction resolution of γTuRC capped minus ends does not allow further analysis.

2.4.6. Drosophila melanogaster γTuRC and actin

During my study, I have also investigated the fate of γTuRC in another organism. *Drosophila melanogaster* assembles both variants of γTuCs (oligomerized γTuSC and γTuRC), which means it has got active γTuRC as well as γTuSC[251]. Therefore, in collaboration

with Prof. Sylvia Erhardt and her student Janina Luitz, we focused to obtain ring complexes from the *Drosophila*. In a first attempt, we focused on *Drosophila melanogaster* S2 cells, which expressed endogenously N-terminal tagged *FLAG-GCP2*. From this system, I purified successfully γTuRC. The structure of γTuRC was confirmed by negative stain EM (Fig. 3.23.a,). By comparing the structures of vertebrate (*Xenopus leaves*, PDB 6FT9) and *Drosophila* melanogaster γTuRC, I could observe a persistent density at the position of actin comparable to the vertebrate's system (Fig. 3.23.b,). Unfortunately, the number of purified rings was not sufficient for cryo-EM analysis. By upscaling of cell amount in an attempt to concentrate more γTuRC on beads, I have observed significantly increased ribosomal contamination. Ribosomes were observed as well in γTuRC purification from other systems, albeit in smaller quantities[53,54].

For this reason, I and Janina Luitz decided to switch the system from S2 cells to *Drosophila melanogaster* embryos. For that purpose, was created *Drosophila melanogaster* cell line with endogenously expressed N-termini *FLAG-GCP2*. I have collected embryos and snap-frozen them. For the purification of γTuRC, I have optimised the protocol with the aim to remove ribosomes. I have added cyklohexamine, which causes the release of amino acid chains from ribosomes, and with the ultracentrifugation step I tried to clarify the supernatant from abundant ribosomes. This measure resulted in a decrease in ribosomal contamination in the γTuRC purification process. Purification of γTuRC from embryos led to an increased amount of well-defined γTuRC classes as judged by negative stain EM (Fig 3.23.c,).

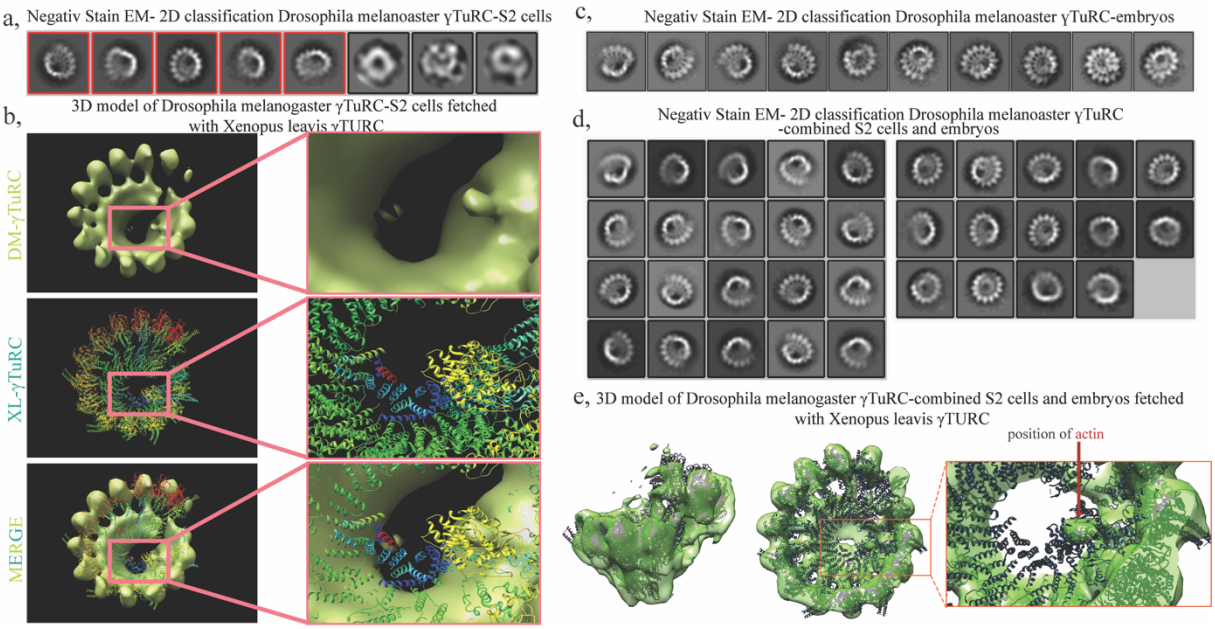

Fig. 3.23.: Density corresponding to the position of actin in vertebrates TuR is also presented in *Drosophila melanogaster* γTuRC a, The NS EM 2D classification of *Drosophila melanogaster* γTuRC. γTuRC was purified via *FLAG-GCP2* expressed in the *D. melanogaster* S2 cell line. b, 3D model of *Drosophila melanogaster* γTuRC (yellow) created from NS EM datasets, fitted with *Xenopus laevis* γTuRC (PDB 6FT9). The zoomed images display expanding density comparable to the position of actin in the vertebrates γTuRC. c, The NS EM 2D classification of *Drosophila melanogaster* γTuRC purified embryos via *FLAG-GCP2* overexpressed in the *Drosohila melanogaster* flies line (pUbi-GCP2-FT). d, The combination of 2D densities of both NS EM datasets from the S2 cell line as well as from embryos in an attempt to increase particle number to get better resolution. e, 3D model of *Drosophila melanogaster* γTuRC from combined datasets with increased resolution confirm the observation of the density at the position of actin in vertebrates γTuRC. Negative stain EM was performed by Annett Neuner and EM data analysis was performed by Bram Vermeulen and Ariani S. Rahadian.

Eventually, the master student Ariani S. Rahadian continued this project, who combined all negative stain EM datasets and created a collection of classes leading to the observed 3D reconstruction of *Drosophila melanogaster* γTuRC (Fig. 2.23.d,e,). Also in this reconstruction, a persistent density at the position of vertebrate actin was observed. During her master study, Ariani S. Rahadian could neither confirm or exclude actin binding to GCP6/MZT1 as this was observed for vertebrate N-GCP6/MZT1[62]. Reasons for that may be multiple, such as the different binding properties of the *Drosophila melanogaster* N-GCP6/MZT1 to the purified rabbit actin or the possibility that in *Drosophila melanogaster* γTuRC contains another protein which resembles the actin fold such as actin-like proteins. Further information is provided in the master thesis of Ariani S. Rahadian.

3. Discussion

I have taken part on the discovery of the structure of the vertebrate γTuRC. Dr. Peng Liu was able to purify the γTuRC from *Xenopus leavis* egg extract. A surprising observation was the finding that the vertebrate γTuRC is asymmetric relative to the 13 protofilaments of the MT lattice and the presence of one molecule of actin inside the γTuRC. These observations were confirmed by 2 additional publications on the structure of the human γTuRC. Recombinantly prepared γTuRCs also had the same architecture. The source of all analyzed γTuRCs were vertebrate systems. To answers if this architecture is specific for vertebrates or for γTuRC as per se, I have purified γTuRCs from *Drosophila melanogaster* embryos and S2 cell lines. *Drosophila melanogaster* is one of the systems, that should have two distinct γTuCs, the γTuSC and the γTuRC. Negative stain analysis showed that *Drosophila melanogaster* rings have the same symmetry as vertebrates γTuRC including the presence of a density corresponding to the actin binding site (Fig. 3.23.).

To answer the questions that I have defined in aim of the study, I have established a protocol for the isolation of γTuRC attached to the MT minus end. Collaborating with the Pfeffer lab, I analyzed the structure of γTuRC capped MT minus ends. In next the chapters I will discuss the challenges with establishing the protocol, then the structural observations on γTuRC MT minus end including the actin repositioning, and I would like to propose a model for the function of the γTuRC and future directions with proposed experiments.

3.1. Challenges with purification of γTURC capped MT minus ends

I have started with purified *X. leavis* γTuRC and tried to nucleate MTs from it. As it was reported, the number of MT seeds increase in the presence of γTuRCs but it was challenging to estimate how many of them are capped with the γTuRC[53]. Other studies confirm my observation that the γTuRC does not have a strong nucleation capacity in *in vitro* conditions [38,54,59,67,244,252–255]. With tomography approach, it estimated that most of the MT ends were uncapped. With experiments using the non-hydrolysable GMPCPP, an equivalent of GTP, I could not significantly increase MT seed production by γTuRC. The reasons for this could be that GMPCPP creates conformational changes in tubulin in favor of the assembly of 14

protofilaments, which may be not compatible with γTuRC properties[255]. With the development of a recombinant system [62,235,256], I could verify that the activity of the recombinant γTuRC is comparable to native *Xenopus leavis* γTuRC and I observe γTuRC capped MT minus ends (Fig. 3. 2.). This observation led to the development of a purification protocol of recombinant γTuRC MT minus ends from *in vitro* nucleation condition. The numbers of purified particles were insufficient for cryo-EM analysis. This protocol is suitable for fluorescence analysis with the possibility of different tagging methods or modifications of γTuRC for future developments in the field.

Therefore, I have focused on the development of protocols of purification of γTuRC capped MT minus ends from *in vivo* conditions. I focused on two events where massive MT assembly is occurring, namely centrosomal or chromosomal spindle assembly during mitosis or meiosis. Both protocols lead to successful MT minus ends purification, but better yields were achieved using the *Xenopus leavis* egg extract (Fig.3.4 and 5.). For further cryo-EM analysis capped MT minus ends were prepared from *Xenopus leavis* egg extract. Another advantage of this preparation is its ability to maintain the active pathway of chromosomal microtubule assembly, thus accurately reflecting physiological conditions.

During the revision process of publication, the structure of γTuRC capped MT minus ends, the protocol was criticized. It was hypothesized that the phenotype that I observe was induced by the paclitaxel or by the mild shortening protocol. My colleagues Bram Vermeulen and Qi Gao were able to confirm that the observed phenotype was not influence by paclitaxel via exchanging it with docetaxel (DTX)[257]. Also, by analyzing the γTuRC capped MT minus ends without implementing the shortening protocol, the same phenotype was observed[240].

Recently two additional studies were published focusing on the structural analysis of γTuRC capped MT minus ends [258,259]. Unlike my approach, they utilized in vitro nucleated γTuRC. To increase efficiency of γTuRC nucleation activity, both studies used a modified version of α-tubulin, that interacts with γ-tubulin. The mutation was in GTP binding site of α-tubulin reducing GTPase hydrolysis are and thereby stabilizing MTs. In yeast cells was observed a very similar mutation (D252A and E255A) characteristic with the disrupted microtubule dynamics. These MTs were unable to depolymerise, which was lethal to the cells [260]. A corresponding amino acid exchange in human α-tubulin where glutamic acid (Glu) at position 254 was exchanged for alanine was used by the Prof. Surrey laboratory in human α-tubulin. These MTs were stable and were not able to hydrolyse GTP[261]. Structural analysis of MTs assembled by this mutated α-tubulin showed that the mutation does not affect α-tubulin

structure but affects MT lattice behaviour compared to wild type[262]. Through the substitution of Glu254 with Asp (E254D) in α-tubulin, GTP hydrolysis was significantly decelerated, resulting in rare instances of catastrophe occurrence [261]. However, the effect of this mutation was not verified via structural analysis of the MT lattice. This slow hydrolysable α-tubulin was used for nucleation assay with γTuRC in both studies. Brito et al. observed increase of nucleation rate of γTuRC from 0.1% of γTuRC with wild type α tubulin to 10% with α^{E254D} tubulin[259]. With usage of the same mutant variant Aher et al. observed increment of colocalization of MT seeds with γTuRC signal from 0.5% in wild type tubulin to 92% in E254D tubulin within the same conditions [258]. Further, Brito et al. as well limited grow of plus end with involvement of artificial created β-tubulin binding protein DARPin. DARPin limited the MT plus end growth. It was easier to identify the MT minus end on shorter MTs. In addition, DARPin stimulated MT nucleation in vitro by γTuRC. Using DARPin combined with α-tubulin^{E254D}, MT nucleation activity increased to 90%. To increase the nucleation rate, Aher et al. involved supplementation of the MT nucleation reaction with chTOG prior to cryo-EM analysis (Aher et al., 2024).

Compare to my protocol both published studies use *in vitro* conditions with defined protein composition. Usage of non-naturally occurring α-tubulin helped them to increase the nucleation rate from γTuRC, but as well as additional factors influencing tubulin behavior were necessary. Both studies achieved the stabilization of α- and γ-tubulin binding and decreasing tubulin dynamics influence by GTP hydrolysis. How this is reflecting the *in vivo* conditions is questionable. I personally believe that both structures, *in vitro* and mine *in vivo* γTuRC capped minus ends, are correct and reflect different reaction stages.

3.2. Structure of γTuRC capped minus end

γTuRC capped MT minus ends created by *in vivo* conditions via activation of the chromosomal MT nucleation pathway nucleated MTs with 13 protofilaments from spoke 2 to spoke 14 of γTuRC (Fig.3.11.)[240]. The two studies with *in vitro* assembled γTuRC capped α^{E254D}-MT also observe 13 protofilaments [258,259]. This agrees with what has been observed in most eukaryotic cells [9]. Spoke 1 of γTuRC overlaps with spoke 14 and in this way γ-tubulin of spoke 1 is not accessible for MT nucleation. This arrangement of γ-tubulin molecules is comparable to the structure of rings formed by oligomerization of the γTuSC [46,50,240,258,259,263].

The position of the seam, where α- and β-tubulins interact laterally, should started from the interface between spoke 2 and 14 (Fig.3.13) [46,50,240,258,259,263]. Interestingly, the MT protofilament from spoke 2 is bound by the N-terminus of a GCP3-MZT1 module at the lateral site of spoke 14 [240,264]. In the *in vitro* study with mutant α-tubulin and DARPin, Brito et al. could observe different stages of closure of the seam, where in a final step the seam is created by binding of N-GCP3/MZT1 to the first α-tubulin attached to spoke 2 [259]. This suggests a role of the N-GCP3/MZT1 module in γTuRC closure and stabilization of the MT cylinder. As protofilaments got longer, the lateral interactions between α- and β-tubulins became more stable [258,259].

In vitro study observed that the first protofilaments assembled from spoke 1 to 9, then accompanied the structural rearmaments of the last spokes of the γTuRC with the formation of more protofilaments. They characterize these stages as early closer and closed stage [259]. The second study observed the structure comparable to the closed stage, where geometry of the γTuRC ring was in symmetrical arrangement to the MT [258]. Comparing it to our observation, I can conclude that we observe the similar process to the first steps observed by Brito et al. But from the mechanical point of view, I would suggest that I observe reverse process. From spoke 8 to spoke 14 of γTuRC, I observe a slight rearrangement towards a partially closed conformation with increasing distance up to spoke 14 (Fig. 3.9. and 3.10.). This is accompanied with an increase in distance between α- and γ-tubulins from spoke 2 to spoke 8. In addition, the lateral gap between the protofilament at spoke 2 to its neighbors is increased, suggesting reduced later binding between these protofilaments at the MT minus end (Fig. 3.12) [240].

Comparing early closed, closed[258,259] and mine asymmetric arrangement of partially closed γTuRC architecture[240], I could conclude some mechanical interpretations discussed in next chapter.

3.3. γTuRC undergoes structural rearrangement upon microtubule assembly

GTP hydrolysis is main crucial step influencing the behavior of microtubules. γ tubulin as well as β-tubulin have GTP activity, that influence the MT dynamics[179,190,254,261,265]. Disruption of the dynamic behavior of MTs is lethal for the cells. This is used in treatment of cancer, where the microtubule stabilization drug taxol that stabilizes MTs is commonly used.

Microtubule assembly can be characterized as enzymatic reaction. Simplified, every enzymatic reaction needs input materials, optimal reaction conditions and an optimal time point when the reaction is completed. Steps of the nucleation reaction are binding of αβ-tubulin in the GTP stage to another αβ-tubulin dimer or to γ-tubulin. Next, GTP is hydrolyzed and afterwards catastrophe occurs. The GDP stage is characteristic for its highly instability and keeping protofilament assembled in microtubules might be depended on lateral interactions and protective GTP cap. All steps should be accompanied by corresponding conformational changes. This basic enzymatic reaction takes place at multiple points during MT assembly, contributing to an increase in complexity.

Structural analysis of native γTuRC capped minus ends from *Xenopus leavis* egg extract shows partial closure of the γTuRC. Brito at al. using a modified α-tubulin, that slows down GTP hydrolysis, shows two stages of γTuRC closure: early stage where spoke 14 and 13 are dislocated, and fully closed upon complete protofilament assembly[259]. Aher et al. used almost the same strategy as Brito et al. but showing only fully closed conformation[258], probably because they did not limited MT length by DARPin.

In my opinion all three studies show the same events but at different time points. Our structure is based on my purification protocol using RanGTP induced γTuRC capped minus ends, not omitting activation and regulation pathways as well as not influencing the properties of the γTuRC. This allows natural spindle assembly within 20 minutes. Taxol binds to β-tubulin [183]. Even when α- and β-tubulin have about 60% similarity [266], taxol does not recognize α-tubulin. The effect of taxol on the γ-tubulin is not known. But even if when it binds to γ-tubulin, its effect is in stabilization of interdimer interaction. On nanomolar level, taxol also repairs and stabilize the damaged MT lattice[267]. Notably with DTX the same γTuRC phenotype was observed. The shortening protocol, using Ca^{2+} ions as main component to prevent repolymerization and slight mechanical stress also did not influence the MT minus end structure [240].

Observing that *in vitro* studies show early closure and full closure of γTuRCs under condition of disrupted GTP hydrolysis accompanied with short reaction times (from 1 minutes to 3 minutes), I would characterise them at early binding stages, from the beginning of protofilament formation to the point of GTP hydrolysis to GDP but not allowing conformational rearrangement to reach natural "relaxed" position of GDP tubulin. It was observed that *in vitro* MT nucleation with purified αβ tubulins and γTuRC after prolonged time the de-attachment of γTuRC from stabilized microtubules occurs [254]. My protocol allowed full

spindle assembly with all regulations up to 20 minutes. After 20 min paclitaxel was added for additional 10 min, where I can assume that full reaction and assembly of MT seeds occurred and with taxol I have stabilised the MTs.

Notably, I observe on one γTuRC site dislocation of γ-tubulins at spokes 2 to 7 from α-tubulins, whereas on the opposite site from spokes 10 to 14 was mostly closed (Fig.3.12.). Between spokes 2 to 9 the first MT protofilaments bind in the in vitro reaction[259]. Considering the parameters of enzymatic reaction, this means binding of γ-tubulin to α-tubulin occurs followed by GTP hydrolysis at γ-tubulin site, the binding of the GDP form is instable. Based on this consideration, I would hypothesize that nucleation starts from spoke 2 in two dimensions – vertical along the γ-tubulins and horizontal by adding the additional αβ dimers to protofilament, creating the sheet of protofilaments. By growing in these two dimensions lateral interactions occur that stabilize the tubulin sheet. The tubulin sheet is closed at the seam position.

I can hypothesize that from spoke 2, where the α- and γ-tubulin interaction is longest, GTP hydrolysis at γ-tubulin site would occur as first. GTP hydrolysis at γ-tubulin at spokes 3,4,5, etc. would follow. GTP hydrolysis could possible manifest in changes of α-tubulin and γ-tubulin interaction leading into weakening of their binding comparable to inter-αβ-dimers interactions.

At the same time, I observed a conformational modulation of the γTuRC. Full closure of the ring is achieved via repositioning of spoke 14 to achieve the compatibility to microtubule tube[258,259]. In our study, it is visible that spoke 14 is de-attached from MT symmetrical arragment and promoting this movement to neighboring spokes 13, 12 and 11 (Fig. 3.10). At these spokes I think that GTP hydrolysis occur as the last, and therefore the interaction between γ-tubulin and growing MT protofilament is still stable. Repositioning of spoke 14 of γTuRC and its neighbours again to the direction of the open conformation of isolated γTuRC, may help and facilitate the observed de-attachment of MT protofilaments from γ-tubulins at spokes 2 to 5 where the lateral γ- and α-tubulin offset is the highest (Fig. 3.12.a,c,).

GTP properties of γ-tubulins as well as dynamic interactions inside the microtubule lattice may influence the stability of γTuRC binding to created MT tube.

In my protocol of purified native γTuRC capped minus ends, I could not omit the influence of other factors which may contribute to “relaxed” stage of γTuRC. From mass spectrometry analysis, it is known that these minus ends carry the augmin complex [240]. The

augmin complex promotes MT branching by stabilization of γTuRC on a preformed MT lattice. It is present in asters in *Xenopus leavis* eggs[268]. Augmin -NEDD1 binding site to γTuRC is not known[269] but may be as well at the position comparable to the position of CM1 binding site on the interface of spoke 12 and 13 and that way influencing the flexibility of γTuRC spokes.

3.4. -TIPs recognize the features at interphase of γTuRC – MT minus end

It is observed that hydrolysis of GTP affects primarily the flexibility and conformation of the inter-dimer interface, without a strong impact on the shape or the flexibility of αβ heterodimer [187,266]. GTP hydrolysis may also destabilize the binding of γTuRC to microtubules. Separation of microtubules may start at seam where depolymerization of microtubules probably also starts [188]. In presence of MT binding proteins such us CAMSAP2, the de-capping of the microtubule minus end was obsedved[255]. Even so without the presence of MAPs, the release of microtubules seeds from γTURC was observed within 10 min reaction times by TIRF microscopy [254]. In the presence of MAPs this time is reduced to approximately 2 min [255]. It suggests that the observed curvature bending of protofilaments at the seam position in native preparations, possibly cause by GTP hydrolysis, leads into creation of MT lattice surface recognizable by -TIPs. Interestingly, the position of γ-tubulin inside the spindle does not change and it localizes at the center of spindle. CAMSAP stabilizes microtubule minus ends and it was observed that CAMSAP-MTs can move from the center of the MT aster [19,87] to the periphery of MT aster when overexpressed in cells upon cell division. Considering this observation together with observed release of γTuRC from CAMSAP decorated MTs, I would suggest that this mechanism may explain the stable position of the γTuRC at the center of the mitotic spindle.

I have verified that CAMSAP recognizes the MT minus end as well in RanGTP induced γTuRC capped minus ends (Fig. 3.15 and 3.16), but also in *in vitro* conditions with predefined proteins content (Fig.3.14). *In vitro* recognition of γTuRC by CAMSAP protein suggest, that CAMSAP recognize changes in microtubule lattice at the MT minus end. This observation agrees with published data that CAMSAP2 binds to γTuRC nucleated microtubules and upon decoration of microtubule lattice it induces the γTuRC de-attachment from MTs[255]. Interestingly, the CDK5RAP2 suppress CAMSAP binding to γTuRC microtubule minus ends

and release of γTuRC. Comparing it with structural data, we may understand that process even better [255]. CM1 motive of CDK5RAP2 is binding at interface od spoke 12 and 13 [59], giving it perfect position to modulate the rigidity of γTuRC spokes. When γTuRC would be in closed conformation, it would not create the changes in α-tubulin position closed to the γ-tubulin, that CAMSAP may be recognizing [81].

I could not confirm the enhancement of microtubule seed production with fluorescence-based nucleation with CAMSAP and katanin p60 subunit in *in vitro* conditions (Fig. 3.14.f,). Using it in experiment with *Xenopus leavis* egg extract, I could observe increase in microtubule nucleation activity (Fig.3.17), suggesting that *in vitro* we are missing some regulatory step leading to turn over of the γTuRC. Interestingly, ASPM protein, a family member of CAMSAPs that is expressed in mitosis, is also expressed in *Xenopus leavis* eggs during all stages of frog growth [245,246]. ASPM presence in eggs may be involved in support of spindle assembly during meiosis, comparable to its effect in somatic cells during mitosis [76,77,80].

3.5. Actin as integrated part of the γTuRC

Function of actin inside the γTuRC was puzzling from the point of its discovery. Actin is deeply embedded in γTuRC structure. From first densities which were observed in structural analysis of *Xenopus leavis* γTuRC, the candidates were actin-like protein and actin. I could confirm with immuno-fluorescence the association of actin with the γTuRC. I have tested if γTuRC may initiate the polymerization of actin [247]. The D-loop of actin is not in a favorable position to bind to another actin molecule[59]. However, I could not exclude the potential conformational flexibility leading to increased accessibility of the D-loop. Whatsoever, I could verify that γTuRC does not significantly influence actin polymerization[53]. Surprisingly, with development of recombinant system for γTuRC expression in insect cells, was discovered that γTuRC expression system omitting human actin, would still have a densities corresponding to actin at spoke 2 [256]. By further analysis it was discovered that the γTuRC recruits actin from insect system, suggesting its importance for the assembly. I have established in collaboration with Janina Luitz from the Erhardt lab, the purification for *Drosophila melanogaster* γTuRC. I have observed that *Drosophila melanogaster* γTuRC has a structural arrangement and resemblance similar to the vertebrate γTuRC. Analyzing the *Drosophila melanogaster* γTuRC

purified from two different sources, I also observe the density where actin normally localizes in the vertebrate system (Fig. 3.23).

Actin could be important for the assembly of the γTuRC. However, the discovery that the γTuRC assembled even when the two helices from the N-terminus of GCP6 was removed, corresponding to the actin binding site at N-teminus GCP6-MZT1 [62]. This created an actin-deficient γTuRC that was fully assembled with smaller differences in the flexibility of the first two spokes. Even actin-deficient γTuRC, which I purified from human cells, showed fully assembled γTuRCs (Fig.3.21a). So, actin is not necessary for γTuRC assembly[62].

Second model was that actin is important for microtubule nucleation. Wieczorek et al. created *in vitro* system a "half" γTuRC that assembled with no bound actin [244]. By TIRF microscopy analysis, they surprisingly found that even these half rings were able to nucleate MTs in vitro as the recombinant wild type γTuRC. But this analysis could not provide the answers to protofilament composition of microtubules due its limited resolution. But it provided the proof, that actin is not essential for the basic γTuRC nucleation activity. By having fully assembled actin-deficient γTuRC, I have tested its capability of nucleation with two different approaches: counting the microtubules seed in short period of time and fluorescence measurement catching the whole process (Fig.3.20.). Between full composed γTuRC and actin-deficient γTuRC, I could not observe any significant differences. These results are not surprising considering that γTuRC is a poor MT nucleator *in vitro* and may lack other regulatory components[38,53,54,59,253,254]. In the *in vivo* set up, using a γTuRC lacking the actin binding site in GCP6, Dr. Enrico Atorino observed that the mitosis in these cells was defective with misalignment of chromosomes. Re-nucleation experiment showed that actin- deficient γTuRC have got delays in MT assembly (Fig. 3.21.b,)[62]. This suggests that actin may play a role in the regulation of γTuRC nucleation in cells. Slowing down the initial steps MT nucleation by γTuRCs will force the spindle assembly machinery to find compensation mechanism for which cells need time. Delays may lead to accumulation of failures with disrupted function perhaps not only on cellular level, but also on tissue level, leading to as microcephaly during brain development.

When I purified the γTuRC capped minus ends from meiotic *Xenopus leavis* egg extract, the γTuRC still contained a luminal bridge but underrepresented the densities for actin (Fig.3.22). Aher et al. were able to nucleate the γTuRC on grids and they were able to observe the luminal bridge densities including actin but only in subset of γTuRC capped minus ends[258].

Brito et al. could observe the luminal bridge density only in early partially closed stage but actin was not detected at this point. In the closed staged even the densities of the luminal bridge disintegrated. The density for actin was not observe at all[259]. Brito et al. hypothesized that actin is disassembled or flexible to achieve better accessibility of spoke 14 to closed position. That way the actin molecule should act as an inhibitor of γTuRC activity. Whereas they compare it to data from actin deficient γTuRCs from our laboratory [62]. Considering his claim, the output of this hypothesis should be that actin-deficient γTuRC should be better nucleators, but my *in vitro* data and the data from Dr. Enrico Atorino' s *in vivo* spindle assembly claims opposite effect. Moreover, in RanGTP induced γTuRC, I could observe the actin densities.

Considering the different biochemical approaches and corresponding changes in γTuRC, I suggest that Brito et al. were able to get early assembled γTuRC with protofilaments bound to the first 9 spokes, which were for time being stable and for simplicity I would call them an early stage of γTuRC nucleation. Then by binding all 13 protofilaments and longer microtubule formation, both studies observed closure of the γTuRC[258,259]. Brit et al. and Aher et al. studies fixed the γTuRC binding to microtubules via usage of slowly hydrolysable α-tubulin. This did not allow the relaxation of γTuRC via full transition of GTP hydrolysis and consequently to start the de-attachment of the microtubule. What I think I observe in our dataset are mostly stable intermediates at the start of de-assembly. For simplicity I would call this conformation relaxed state.

In my hypothesis actin functions is in assisting the γTuRC dependent nucleation by rearmament of γTuRC subunits and established microtubule compatible conformations, in particular stages:

First, upon αβ-tubulin protofilaments to γTuRC, actin would interact with an addition partner to stabiles the reposition of GCPs at 10 to 14 spoke. This partner potentially could be IDo of GCP6 (Insertion domain between GRIPs domains of GCP6) that normally is on the opposite site of the γTuRC. At this stage it is necessary the reposition of luminal bridge.

In closed stage, actin and luminal bridge are dissociated from their stable position and highly flexible and therefore is not possible to identify these densities by cryo-EM.

Upon coming to relaxed stage (partially closed observed in RanGTP chromosomal pathway[240]) the luminal bridge is coming back to its original position and pulling with itself the actin molecule as well. Actin is the last part which would be returned to its position around he time of the MT release or disassembly.

This function may also explain the observed defects in actin-deficient γTuRC at early stages of microtubule nucleation (Fig. 3.21.b)[62] resulting in defects in spindle assembly. What triggers actin rearmament is still unknown. Hypothetically, IDo of GCP6 could be reasonable candidate for this interaction. Densities of IDo were never identified, not in native vertebrates γTuRC nor in high resolution recombinant systems[53,54,59,235,256,264], suggesting high flexibility of IDo. By Alfa Fold prediction of GCP6 structure (Fig. 3.19.f,) and observation some unidentified densities at luminal site of GCP6 may suggest that the position of the IDo could be also at the luminal site of γTuRC (Fig. 3.19f). Interesting, mutations were identified in some parts of IDo, which are associated with microcephaly [270–272], further supporting my hypothesis. The IDo of GCP6 may also be involved in regulation of γTuRC activity via for example phosphorylation or activation by other factors. PRIDE human phosphoproteom showed that the IDo contains 5 phosphorylation sites – phosphoserine at position S831 in part1 of IDo, S1237 as a part of the 9 repeats, but also in part 2 of IDo at positions S1296, S1381 and S1397 [273]. In particularly is interesting the mutation at position E1368K associated with microcephaly [272], which is close to the phosphorylation sites of the IDo - S1381 and S1397.

4. Conclusion

γTuRC upon MT nucleation undergoes conformational changes to adopt architecture compatible to the microtubule lattice. Whereas with γTuRC capped MT minus ends created via RanGTP chromosomal pathway and purified, I could observe the misalignment of MT protofilaments, that is recognized by CAMSAP2 protein[240]. Limiting GTP hydrolysis, two studies show early closed and closed conformational structure of γTuRC in *in vitro* conditions[258,259]. Comparing these two structure and biochemical approaches, I think that γTuRC upon nucleation reach the closed conformation compatible to 13 pt MTs, but GTP hydrolysis influence the stability of the binding between γ- and α- tubulins leading into dissociation of protofilaments from γTuRC. The beginning of this process, I consider that I observe in mine preparation of RanGTP induced γTuRC capped MT minus ends. This hypothesis could be supported with observation of MT release from γTuRC within prolonged time[254] or within influence of CAMSAP proteins[255]. I could confirm presence of actin inside of γTuRC and verified that actin is not requirement for γTuRC assembly[62,240]. Its function

seems to be in microtubule nucleation, where I could observe the repositioning of actin inside of lumen γTuRC.

5. Future prospective

The proper answers for actin function should be still investigated. The cryo EM data may support the hypothesis presented by me earlier, but it has a limitation in scale of the interpretation. Cryo-EM structures are like snapshot of average densities of whole set of the used particles. Tracking the changes of actin reposition may be challenging with "static" methods. In principle something like single particle analysis, such as TIFR microscopy, would be suitable. But TIRF microscopy does not reach necessary resolution. I estimate that the range of actin movement is in between 5 to 10 nm. With the new MINFLUX system, it could be possible to measure actin within the γTuRC directly. A challenge would be to establishing the measurement system as it is TIRF at MINFLUX that allows to start the γTuRC nucleation reaction directly at MINFLUX microscope.

It could be manageable, if we could regulate the temperature in the measuring chamber and start the reaction at 37°C. A second problem that needs to be overcome is the increment of the *in vitro* γTuRC dependent nucleation events. It could be inspiring to use the non-hydrolysable α-tubulin, as was used by Brito et al. and Aher et al.[258,259]. In this case we could observe changes from initiation to microtubule compatible symmetry, but no relaxation stage. This system can provide information about direction of change, and I could assume that the reverse process is accompanied by reaching the relaxation stage of γTuRC. Labelling of the γTuRC is already established by me using the SNAP or StrepII tag at MZT2, which incorporates into γTuRC by interaction with the N-terminus of GCP2. So it is possible to identify stable positions of MZT2 within γTuRC assuming that its exterior binding to GCPs would not be affected by nucleation event in the *in vitro* set up. For SNAP and streptavidin, it is possible to buy MINFLUX specific dyes. Secondly, it is necessary to label actin, which may be more challenging as the label molecule should be as small as possible. As a possible candidate I would consider the actin chromobody modified with StrepII tag. MINFLUX approach would be time consuming and required more attempts to get reasonable results but may provide the information about the actin movement upon MT nucleation.

Upon question what initiate the actin rearrangement:

1. Could it involve external factors?
2. Could it be IDo effect?
3. Could it be initiated with mechanical force of the GCPs rearrangement?

For answering the first question, I would perform IP experiment with usage γTuRC in native and actin-deficient variant with mitotic cell lysate. As the binding may be transient, I would consider modifying the protocol from the binding assay of chTOG to γTuRC[35]. The eluates I would send for mass spectrometry analysis and screen for proteins which are lacking in the actin-deficient set up compared to from WT γTuRC variant. For γTuRC recombinant variants bound to beads or also HEK293 cell variants expressing native GCP6 or delta-N-GCP6 with modifying of my established purification protocol could be used [62]. Considering that Brito et al. observed that rearmament in the *in vitro* set up with usage of native γTuRC from Hela-Kyoto cells [258] and Aher et al. used recombinantly prepared γTuRC and they could observe in subset of their data actin[258], it may suggest that no external impute is needed.

If it is not possible to identify the possible candidate by mass spectrometry, I would assume that the candidate is IDo of the GCP6. I have tried to do pulldown of actin with helical part of IDO, but this was unsuccessful. Therefore, I would suggest using the entire IDo, what could be difficult, because more than half of the sequence is disordered. If it could be expressed and purified in proper fold, I would repeat the actin pull down assay. If I could confirm actin binding, I would try to analyse the binding amino sequence with crosslinking mass spectrometry. This binding could be dependent on some activation mechanism, for example phosphorylation by Aurora A or PLK1 kinase. For this reason, I would go to the mammalian cell expression system with arrest of cells in mitosis using a mitotic lysate for IP experiments. We know from experiences that purified centrosomes still carry the PCM. So, purified centrosomes with attached PCM, where the factors for activating the MT nucleation are the most concentrated, could be used as starting material for for IP experiments.

Perhaps would be interesting to do experiments with deletion of amino sequences containing serin phosphorylation site in IDo of GCP6 in *in vivo* conditions and observe if the behaviour of the γTuRC would be comparable to actin-deficient γTuRC phenotype.

It is worthy to consider that actin movement is triggered with mechanical force of GCPs rearmament.

Other investigating pathway should focus on γTuRC binding partners, such augmin, chTOG, and the still not discovered binding sites of NEDD1 and NME7. From expertise in our lab, an obvious candidate for further investigation in context of MT nucleation and branching

could be augmin. We should combine the knowledge of the augmin structure and γTuRC at minus ends. Massive branching occurs in spindle assembly in *Xenopus leavis* egg extract. To support and increase augmin-γTuRC-MT branching I would add recombinant augmin to induce aster formation with labelled tubulin, stabilise the asters with taxol or DTX. After spindle assembly, I would pellet the microtubule asters via centrifugation and resuspended the pellet and use it for cryo EM tomography. Labelling of MT asters would help with identification of the position where the lamella should be prepared. The analysis should be focused on the centre of the aster, where also the labelling would be more intensive. The γTuRC is also enriched in the centre of the asters and therefore also targeted by the analysis. Also, the purification protocol of γTuRC capped microtubule minus ends may lead into a dataset with branched microtubules. Knowing both structures, I would focus on creating the automatic screening process in data analysis.

6. Materials and methods

6.1. Materials

6.1.1. Chemicals

Chemicals used in my study were produced by Sigma-Aldrich, Thermo-Fischer scientific, AppliChem, Roth and Merck unless otherwise stated.

6.1.2. Equipments

Table 1.: Instuments

Instrument	*Producer*
CLARIOstar	BMG Labtech
Jasco J715 spectropolarimeter	JASCO
Nikon Ti-E fluorescence microscope	Nicon
JEOL JEM1400	Joel
Widefield microscope Delta Vision	GE (Applied Precision)
Sonicator UW 200	Bandelin
Sonicator UP100H	Hielscher
Biorupter Plus	Diagenode
RC 6 Plus centrifuge	Sorvall
Rotor S100-AT3	Sorvall
Rotor S120-AT2	Sorvall
Äkta system	Cytiva
SDS page equipment	Bio-Rad
WB equipment	Bio-Rad
pH meter	Sartorius
Titan Krios Thermo Fisher/FEI	Thermo Fisher/FEI
Vitrobot Mark IV	Thermo Fisher/FEI
Talos L120C TEM	Thermo Fisher

6.1.3. Buffer and reagents

Buffers and reagents recipes are mentioned by corresponding methods.

6.1.4. Enzymes

Table 2. Enzymes

Enzyme	*Producer*
Gibson Assembly® Master Mix	NEB Cat no. E2611
NEBuilder® HiFi DNA Assembly Master Mix	NEB Cat no. E2621S
T4 ligase	NEB Cat no. M0202S
Restriction enzymes	NEB
Q5® High-Fidelity DNA Polymerase	NEB Cat no. M0491

6.1.5. Kits

Table 3.: Kits

Name	*Producer*
QIAquick® Gel Extraction Kit	QIAGEN Cat. # 28704
Plasmid Mini Kit	QIAGEN, Cat. N. 12123
PierceTM Silver Stain Kit	Thermo ScientificTM , Number 24612
The fluorescence-based Tubulin Polymerization assay kit	Cytoskeleton Inc, Denver Com Cat. # BK011P

6.1.6. Primary antibodies

Table 4.: Antibodies

Target Protein	*Animal*	*Producer*
X.laevis γ-tubulin	rabbit polyclonal	produced by Oliver Gruss, homemade, epitop is the C-terminal EYHAATRPDYISWGTQDK peptide

Human γ-tubulin	mouse polyclonal	Sigma Aldrich, GTU-88
GCP4	rabbit polyclonal	homemade, against full-length GCP4
anti-human GCP6	guinea pig	homemade, against ?
anti-Human γ-tubulin	guinea pig	homemade, against full length recombinant γ-tubulin
Xgrip109 (GCP3)	rabbit polyclonal	homemade, from Prof. Yixian Zheng
anti-Actin	rabbit monoclonal	Sigma Aldrich A2066
anti-ß-Actin	mouse monoclonal	Sigma Aldrich A5316
anti-MBP	rabbit monoclonal	Proteintech: Cat no : 15089-1-AP
anti-Katanin p60	mouse monoclonal	R/D Systems Catalog #: MAB7100
anti-DYKDDDDK (Flag)	mouse monoclonal	Cell signaling Cat no : #8146
anti-DYKDDDDK	rabbit polyclonal	Proteintech, Cat no : 20543-1-AP
anti-GFP	mouse monoclonal	Roche, Cat no : 11814460 001
α-tubulin	mouse monoclonal	Sigma-Aldrich
α-tubulin	rabbit polyclonal	Proteintech, Cat No. 11224-1-AP
b-tubulin	rabbit polyclonal	Proteintech, Cat No. 10068-1-AP

6.1.7. Secondary antibodies

Table 5.: Secondary antibodies

Secondary antibody	*Source*	*Producer*
HRP-conjugated anti-rabbit	donkey	Jackson 711-035-152
HRP-conjugated anti-rabbit	donkey	Sigma
HRP-conjugated anti-mouse	donkey	Jackson 715-035-151
HRP-conjugated anti-guinea pig	donkey	Jackson 706-405-148

Alexa Fluor 480/555/647 anti-rabbit	donkey	life technologies
Alexa Fluor 480/555/647 anti-mouse	donkey	life technologies
Alexa Fluor 647/555 anti-guinea pig	goat	life technologies

6.1.8. Plasmids

Table 6.: Plasmids

Name	*Description*
pET28b-TOG6-CTD	human chTOG domain 6 and C-terminal domain with HIS TAG, from Addgene #29480, kanamycin
pET28b-TOG5-TOG6-CTD	human chTOG domains 5 and 6 and C-terminal domain with HIS TAG from Addgene #29480, kanamycin
pET28B-TGO6-CTD-emiRFP	human chTOG domain 6 and C-terminus with HIS TAG and emiRFP gene from Addgene #29480, kanamycin
pETM44-TGO5-TOG6-CTD	human chTOG domains 5 and 6 and C-terminus with MBP TAG from Addgene #29480, kanamycin
pETM44-TGO6-CTD	human chTOG domain 6 and C-terminus with MBP TAG from Addgene #29480, kanamycin
pFastBac-CAMSAP1-emiRFP	recloned Addgene #59036, GFP exchanged for emiRFP with infusion system, ampicilin
pFastBac-CAMSAP1-SNAPTag	recloned Addgene #59036, GFP exchanged for SNAP with infusion system, ampicilin
pFastBac-CAMSAP2-emiRFP	recloned Addgene#59037, emiRFP added behond GFP with infusion system, ampicilin
pFastBac-Camsap2-SnapTag	recloned Addgene#59037, SNAP added behond GFP with infusion system, ampicilin
pFastBac-Camsap3-SnapTag	recloned Addgene #59038, GFP exchanged for SNAP with infusion system, ampicilin
pESA-SBDonor-TRE3GV-KATNA1-SNAP3	Addgene #89316 DNA of KATNA1 - p60 subunit of katanin, rat DNA, added into sleeping beauty donor vector with SNAP TAG on C-terminus, prepared HEK293 cell stable line with DOX expression of katanin p60-Flag purification, ampicilin

pESA-SBDonor-TRE3GV-KATNA1-SNAP	Addgene #89316 DNA of KATNA1 - p60 subunit of katanin, rat DNA, added into sleeping beauty donor vector with SNAP TAG on C-terminus, prepared HEK293 cell stable line with DOX expression of katanin p60-flag purification, ampicilin
pESA-SBDonor-TRE3GV-Spastin-emiRFP	Addgene #134461 DNA of spastin,human DNA, added into sleeping beauty donor vector with emiRFP plus FLAG on C-terminus, prepared HEK293 cell stable line with DOXY expression of spastin-flag purification, ampicilin
pESA-SBDonor-TRE3GV-Spastin-SNAP	Addgene #134461 DNA of spastin,human DNA, added into sleeping beauty donor vector with SNAP plus FLAG on C-terminus, prepared HEK293 cell stable line with Dox expression of spastin-flag purification, ampicilin
pattBsatIIISense-Flag-Tev-SG5-DM GCP2	*Drosophila melanogaster* DNA of *FLAG-GCP2* cloned into pattBsatIIISense vector, to incorporate *FLAG-GCP2* into DM flies genome, *pUbi-GCP2-FT* flies by Erhardt lab, ampicilin
pET28b-HS-Cm1-50-100-WT	human CM1 motive with lengt from 50-100 amino acids, kanamycin
pET28b-XLCM1-50-100-WT	*X. leavis CM1* motive with 50-100 amino acids, kanamycin
pET28b-XLCM1-50-100-F75A	*X. leavis* CM1 motive with 50-100 amino acids with F75A modification that inactivates CM1, kanamycin
pMT V5 HIS C-FLAG.TEV.SG5-GCP2	*D. melanogaster* DNA of *FLAG-GCP2* cloned into pMTV5-C-HIS vector; to incorporate *FLAG-GCP2* into DM S2 cells genom, ampicilin
pGEX6p-xPH-StrepII	published in Liue et al. 2019, *X. leavis* predicted helices in P1 of GCP6's IDo with N-GST and C-StrepII, ampicilin
pGEX6p-xPredicted helices	*X. leavis* predicted helices in P1 of GCP6's Ido with N-GST more information in Liu et al. 2019, N-GST, ampicilin
pGEX6p-xloop P1	*X. leavis* P1 of GCP6's Ido with N-GST, more information in Liu et al. 2019, N-GST, ampicilin
pGEX6p-xloop P2	*X. leavis* P2 of GCP6's Ido with N-GST, more information in Liu et al. 2019, N-GST, ampicilin

pGEX6p-x8rep.	*X. leavis* 8 repeats of GCP6's Ido with N-GST, more information in Liu et al. 2019, N-GST, ampicilin
pET26b-xPredicted helices	*X. leavis* predicted helices in P1 of GCP6's Ido with N-GST more information in Liu et al. 2019, C-HIS, kanamycin
pET26b-xloop P1	*X. leavis* P1 of GCP6's Ido with N-GST, more information in Liu et al. 2019, C-HIS, kanamycin
pET26b-xloop P2	*X. leavis* P2 of GCP6's Ido with N-GST, more information in Liu et al. 2019, C-HIS, kanamycin
pET26b-x8rep	*X. leavis* 8 repeats of GCP6's Ido with N-GST, more information in Liu et al. 2019, C-HIS, kanamycin
pFastBac-xPH	*X. leavis* predicted helices in P1 of GCP6's Ido with N-GST more information in Liu et al. 2019, C-HIS, kanamycin
pETHIS17	screening vector from Gunter Stier (BZH) - crystalization screening
pESA-SBDonor-TRE3GV-KATNA1-RFP	Addgene #89316 DNA of KATNA1 - p60 subunit of katanin, rat DNA, added into sleeping beauty donor vector with RFP TAG on C-terminus, prepared HEK293 cell stable line with DOX expression of katanin p60-flag purification, ampicilin
pESA-SBDonor-TRE3GV-KATNA1-SNAP	Addgene #89316 DNA of KATNA1 - p60 subunit of katanin, rat DNA, added into sleeping beauty donor vector with SNAP TAG on C-terminus, prepared HEK293 cell stable line with DOX expression of katanin p60-flag purification, ampicilin
pESA-SBDonor-TRE3GV-Spastin-emiRFP	Addgene #134461 DNA of spastin, human DNA, added into sleeping beauty donor vector with emiRFP plus FLAG on C-terminus, prepared HEK293 cell stable line with DOX expression of spastin-flag purification, ampicilin
pESA-SBDonor-TRE3GV-Spastin-SNAP	Addgene #134461 DNA of spastin, human DNA, added into sleeping beauty donor vector with SNAP plus FLAG on C-terminus, prepared HEK293 cell stable line with DOX expression of spastin-flag purification, ampicilin
pACEBac1-DM-Tub23-ST	*Drosophila melanogaster* Tub23 cloned into pACEBac1 with Infusion system

pETM44-XHP-C6	screening contruct for *X. leavis* predicted helices of ID of *GCP6*, T4 ligation with NcoI and XhoI, Construct 6,kanamycin
pETM44-XHP-C10	screening contruct for *X. leavis* predicted helices of ID of GCP6, T4 ligation with NcoI and XhoI, Construct 10, kanamycin
pETM44-XHP-C12	screening contruct for *X. leavis* predicted helices of ID of *GCP6*, T4 ligation with NcoI and XhoI, Construct 12, kanamycin
pETM44-XHP-C24	screening contruct for *X. leavis* predicted helices of ID of GCP6, T4 ligation with NcoI and XhoI, Construct 24, kanamycin
pETM44-XHP-C26	screening contruct for *X. leavis* predicted helices of ID of GCP6, T4 ligation with NcoI and XhoI, Construct 26, kanamycin
pETM44-XHP-C29	screening contruct for *X. leavis* predicted helices of ID of GCP6, T4 ligation with NcoI and XhoI, Construct 29, kanamycin
pACEBac1-TUBA1B intra HIS.dna	Human *TUBA1B*, gene from Roostalu et al., 2020, eLife recloned into MultiBac system, gentamycin
pACEBac1-TuBB3 G2SG2 FLAG.dna	Human *TUBB3*, gen from Roostalu et al., 2020, eLife recloned into MultiBac system, gentamycin

6.1.9. Primers

Table 7.: Primers

Construct	*Name of primer*	*Sequence*
pACEBac1-DM TUB23C-C-G5s-3C-StrepII.dna	Tub23c, fwd	TAATAAAAAAACCTATAAATATGCC CAGCGAAATTATTACAC
	Tub23c, rev	TCGAGACTGCAGGCTCTAGATTACT TTTCAAATTGTGGGTGGCTCCAACC GCTGGGTCCCTGAAACAACACTTCC AACGAGCCACCACCACCTCCGCTAC CCGCAGAGGTAAC
pACEBac1-TUBA1B intra HIS Martin strategy.dna	Tuba1BintraHIS fwd	TAATAAAAAAACCTATAAATATGA GAGAGTGCATTTCAATC

	Tuba1BintraHIS rev	TCGAGACTGCAGGCTCTAGATTAGT ACTCTTCTCCTTCTTC
pACEBac1-TuBB3 G2SG2 FLAG Martin strategy.dna	TUBB3 fwd	TAATAAAAAAACCTATAAATATGCG CGAAATAGTTCACATC
	TUBB3 rev	TCGAGACTGCAGGCTCTAGATTATT TATCGTCGTCATCCTTG
pattBsatIIISense-Flag-Tev-SG5-DM GCP2.dna	patt-GCP2 fwd	GCAGAATAATCCACGGGTACCATG GATTACAAAGACGATGATGACAAA GGTAGTGAAAACCTCTATTTTCAAG GCTCGGGCGGTGGCGGAGGTATGA GTAAACCCCATGCGC
	patt-GCP2rev	TCAGGGGTGACCACCGGTGCGGCC GCTTAGCCACCCGGTACCCTC
pESA-SBDonor-TRE3GV-KATNA1-emiRFP.dna	KATNA1 fwd	ATCGATACGCGTGCGCCACCATGAG TCTTCTAATGATTACTGAG
	KATNA1rev	CTTCCGCCATTGCACCTGCACCAGC TCCGCATGATCCAAACTCAAC
	emiRFPrev	TGGATCATGCGGAGCTGGTGCAGGT GCAATGGCGGAAGGATCCGTC
	emiRFP fwd	GCACCTGCACCAGCTCCTGCGCTCT CAAGCGCGGTGATC
pESA-SBDonor-TRE3GV-KATNA1-SNAP.dna	katSnapTAG fwd	TGGATCATGCGGAGCTGGTGCAGGT GCAATGGACAAAGATTGCGAAATG AAAC
	katSmapTAG rwv	GCACCTGCACCAGCTCCTGCTCCCA GACCCGGTTTACC
pESA-SBDonor-TRE3GV-Spastin-emiRFP.dna	SpastinRFP fwd	ATCGATACGCGTGCGCCACCATGAA TTCTCCGGGTGGACGAG
	SpastinRFPrev	CTTCCGCCATTGCACCTGCACCAGC TCCAACAGTGGTATCTCCAAAGTCC

	emiRFPSP fwd	TACCACTGTTGGAGCTGGTGCAGGT GCAATGGCGGAAGGATCCGTC
	emiRFPSP rev	GCACCTGCACCAGCTCCTGCGCTCT CAAGCGCGGTGATC
pESA-SBDonor-TRE3GV-Spastin-SNAP.dna	SpastinRFP fwd	ATCGATACGCGTGCGCCACCATGAA TTCTCCGGGTGGACGAG
	SpastinRFPrev	CTTCCGCCATTGCACCTGCACCAGC TCCAACAGTGGTATCTCCAAAGTCC
	SNAPSP fwd	TACCACTGTTGGAGCTGGTGCAGGT GCAATGGACAAAGATTGCGAAATG AAAC
	SNAPSP rev	GCACCTGCACCAGCTCCTGCTCCCA GACCCGGTTTACC
pET26b-8 repeats .dna	PET 8 repeats fwd	CTTTAAGAAGGAGATATACATATGA TGACCCAAGTATCACAAGGC
	PET 8 repeats rev	GGTGATGGTGATGGTGGTGGGATCC GGGCCCCTGGAACAGAACTTCCAG GTGCACTTCCGATTCAGAC
pET26b-xloop P2+seq.dna	PetxLoopP2 fwd	CTTTAAGAAGGAGATATACATATGA GTTCCAACTCAACGATTC
	PetxLoopP2 rev	GGTGATGGTGATGGTGGTGGGATCC GGGCCCCTGGAACAGAACTTCCAGC ATAAGGACTGGCAGTGAC
pET26b-xloopP1+seq.dna	Petxloop p1 fwd	CTTTAAGAAGGAGATATACATATGT TGTGTTGCCCGAAGCATTATATC
	Petxloop p1 rev	GGTGATGGTGATGGTGGTGGGATCC GGGCCCCTGGAACAGAACTTCCAG ACAAGCGATGGGTTTAAGAATTG
pET26b-xpredicted helices+seq.dna	PerXPH fwd	CTTTAAGAAGGAGATATACATATGA TCCCGGTTCCACGTATTTC

	PerXPH rev	GGTGATGGTGATGGTGGTGGGATCC GGGCCCCTGGAACAGAACTTCCAG AATGCAATTCTGTGCGGTG
pFastBac-CAMSAP1-emiRFP.dna	BAC-CAM1-fwd	GAGCTAATGAGTGCCCACATG
	BAC-CAM1-rev	TGGATCCATGGCGCCCTGAA
	RFP.C1-rev	TTCAGGGCGCCATGGATCCAATGGC GGAAGGATCCGTC
	RFP.C1-fwd	ATGTGGGCACTCATTAGCTCGCTCT CAAGCGCGGTGATC
pFastBac-CAMSAP1-SNAPTag.dna	C3.SNAP-fwd	TTCAGGGCGCCATGGATCCAATGGA CAAAGATTGCGAAATGAAAC
	C1.SNAP-rev	ATGTGGGCACTCATTAGCTCTCCCA GACCCGGTTTACC
pFastBac-CAMSAP2-emiRFP-with GFP inside presented.dna	CAm2-VBAC-fwd	GGATCCGGGGATGCTGCAGA
	CAm2-VBAC-rev	GGCGCCCTGAAAATACAGGT
	RFP-C2-fwd	ACCTGTATTTTCAGGGCGCCATGGC GGAAGGATCCGTC
	RFP-C2-rev	TCTGCAGCATCCCCGGATCCGCTCT CAAGCGCGGTGATC
pFastBac-Camsap2-SnapTag-with GFP presented inside.dna	C2.SNAP-fwd	ACCTGTATTTTCAGGGCGCCATGGA CAAAGATTGCGAAATGAAAC
	C2.SNAP-rev	TCTGCAGCATCCCCGGATCCTCCCA GACCCGGTTTACC
pFastBac-Camsap3-SnapTag.dna	BAC-CAM3-fwd	GAGCTCGTGGAAGCGGCGCC

pFASTbac-HTa-xph-c-stop.dna	xph-c-pFB-fwd	TGTATTTTCAGGGCGCCATGGATCC GTCGCTGGAAGAACTTAAAG
	xph-c-pFB-rev	CTCGTCGACGTAGGCCTTTGAATTC TTAATTGGCGACAAGGTCTTG
pGEX-6P-CDK5RAP2-1-100aa.dna	CM1-1-100-fwd	TCTGTTCCAGGGGCCCCTGGGATCC ATGGACTTGGTGTTGGAAG
	CM1-1-100-rev	GCCGCTCGAGTCGACCCGGGAATTC TCATTTGTAGATATGTTCAGTGG
pGEX-6p-xph-c-stop.dna	xph-c-GST-fwd	TCTGTTCCAGGGGCCCCTGGGATCC TCGCTGGAAGAACTTAAAG
	xph-c-GST-rev	GTCGACCCGGGAATTCCGGGGATCC TTAATTGGCGACAAGGTCTTG
pGEX-6PI-8 repeats NEW.dna	8 repeats fwd	TCTGTTCCAGGGGCCCCTGGGATCC ACCCAAGTATCACAAGGC
	8 repeats rev	GTCGACCCGGGAATTCCGGGGATCC GTGCACTTCCGATTCAGAC
pGEX6p-xloopP1.dna	GxLoopP1-fwd	TCTGTTCCAGGGGCCCCTGGGATCC TTGTGTTGCCCGAAGCATTATATC
	GxLoopP1-rev	GTCGACCCGGGAATTCCGGGGATCC ACAAGCGATGGGTTTAAGAATTG
pGEX6p-xloopP2.dna	GxLoopP2-fwd	TCTGTTCCAGGGGCCCCTGGGATCC AGTTCCAACTCAACGATTC
	GxLoopP2-fwd	GTCGACCCGGGAATTCCGGGGATCC CATAAGGACTGGCAGTGAC
pGEX6p-xpredicted helices.dna	GXPH fwd	TCTGTTCCAGGGGCCCCTGGGATCC ATCCCGGTTCCACGTATTTC
	GXPH fwd	GTCGACCCGGGAATTCCGGGGATCC AATGCAATTCTGTGCGGTG
pMT V5 HIS C-FLAG.TEV.SG5-GCP2.dna	GCP2 (DM).TEV.SC.fwd	TGTGGTGGAATTCTGCAGATATCAT GGATTACAAAGACGATGATGACAA AGGTAGTGAAAACCTCTATTTTCAA

		GGCTCGGGCGGTGGCGGAGGTATG AGTAAACCCCATGCGC
	GCP2 (DM)rev	TCGAATGGGTGACCTCGAGCGGCCG CTTAGCCACCCGGTACCCTC
PETM44-XPHC-C29	XPHC-29-FWD	GAAGTTCTGTTCCAGGGGCCCATGG GACCGAAGCATTATATCTGTTGG
	XPHC-29-rev	AGTGGTGGTGGTGGTGGTGCTCGAG TTAGTCCACCGGAAAATTGGC
PETM44-XPHC-C26	XPH 24 26 fwd	GAAGTTCTGTTCCAGGGGCCCATGG GAATCCCGGTTCCACGTATTTC
	XPH 26 rev	AGTGGTGGTGGTGGTGGTGCTCGAG TTAAATGCAATTCTGTGCGGTG
PETM44-XPHC-C12	XPH 12 10 fwd	GAAGTTCTGTTCCAGGGGCCCATGG GACCACGTATTTCCGTGACC
	XPH12 rev	AGTGGTGGTGGTGGTGGTGCTCGAG TTATTCTTCGCAAATGTCCAC
PETM44-XPHC-C10	XPH10 rev	AGTGGTGGTGGTGGTGGTGCTCGAG TTAATTGGCGACAAGGTCTTG
PETM44-XPHC-C6	XPH 6 fwd	GAAGTTCTGTTCCAGGGGCCCATGG GATCGCTGGAAGAACTTAAAG
	XPH 6 24 rev	AGTGGTGGTGGTGGTGGTGCTCGAG TTAATCGTTATTGTTATGCAGC

6.2. Methods

6.2.1. Molecular biology methods

6.2.1.1. Molecular cloning

DNA inserts were amplified with Q5 High Fidelity DNA Polymerisa (NEB) following the manufactured protocol. Fragments were separated on 2% (w/v) agarose gel and purified from it with QIAquick® Gel Extraction Kit (QIAGEN Cat. # 28704). Pursuant to the manufactured

protocol and eluted with 30 µl of ddH_2O. Concentration was measured on a NanoDrop® spectrophotometer. Fragments were inserted into vectors with Gibson Assembly® Cloning Kit, NEBuilder® HiFi DNA Assembly Cloning Kit (NEB), T4 ligation (NEB) or InFusion cloning (Takara) system subsequent to producers' protocols.

6.2.1.2. DNA plasmids purification

For small scale plasmid production 5 ml *E. coli* DH5α cells were cultivated with proper antibiotics overnight at 37ºC in LB. The cells pellet was resuspended in 0,5 ml S1 buffer followed by alkaline lysis using 0,5 ml of S2 buffer. Proteins and chromosomal DNA were precipitated by concentrated potassium acetate in 0,5 ml of S3 buffer. Solution with denaturated cells were centrifuged for 20 000 g, 15 min, 4ºC and the supernatant with the plasmid DNA was used for further purification. DNA was precipitated with 800 µl of 2-propanol and pelleted with 20 000g, 15 min, 4ºC. The DNA pellet was resuspended in 50 µl of ddH_2O. For midi preparation, cells were cultivated in 100 ml LB medium and pelleted. Plasmid isolation was performed following the protocol of the Plasmid Mini Kit from QIAGEN (Cat. N. 12123).

6.2.1.3. SDS PAGE electrophoresis

Samples were mixed with Laemmli buffer (50 mM Tris-HCl pH 6.8, 2% SDS, 10% glycerol, 0,02% bromphenol blue, 100 mM DTT) and loaded onto 5% stacking gel, 10%, 12% or gradients resolving gels (Bio-Rad, Mini-Protean™, Nummer 4568036, Nummer 4568046, Nummer 4568086). These gels were used depended on the protein size. Electrophoresis was performed with Criterion™ Vertical Electrophoresis Cell (Bio-Rad) in SDS running buffer (25 mM Tris, 192 mM glycine, 0,1% SDS) **at** 90 to 130 **V**.

6.2.1.4. Western blot

Transfer of proteins from SDS page gel onto Immobilon®-P PVDF membranes (Merck Millipore) was performed with the Trans-Blot Turbo transfer system (Bio-Rad, Number 1704150) with maximal voltage of 100 volts, for 20-40 min. The membrane was washed 2 times in TBS-T buffer (25 mM Tris-HCl pH7,5, 150 mM NaCl, 0,05% Tween-20) and then blocked for 30-60 min in 5% ((w/v) skim milk in TBS). Before incubation with primary antibodies, the membrane was washed two times with TBS-T buffer and incubated with

antibodies diluted in 5% skim milk in TBS-T buffer with 1 mM NaN_3 for overnight at 4°C or 4 h at room temperature. Membrane was washed three times with TBST buffer and incubated for 1 h with secondary antibodies diluted in 5% skim milk in TBTS without NaN_3. Before visualisation, the membrane was washed three times with TBST and incubated for 5 min with chemilumiscence solution for HRP-conjugated antibodies (ClarityTM, Estern ECL Substrate, 1:1). Visualisation was performed with Odyssey® Infrared Imaging System (LI-COR Biosciences)

6.2.1.5. Coomassie staining

The SDS-PAGE gel was washed 3 times with ultrapure water and transferred into Coomassie solution (0.1% (w/v) Coomassie, 50% (v/v) methanol, 10% (v/v) acetic acid). The gel and solution were warmed till boiling and let to cool down to room temperature. Coomassie solution was exchange with de-staining solution (40% (v/v) methanol, 10% (v/v) acetic acid) and de-stain at room temperature with shaking till bands became visible.

6.2.1.6. Silver staining

For staining of the proteins with lower abundance the Pierce™ Silver Stain Kit (Thermo Scientific™, Number 24612) was used following the manufacturer's instructions. Shortly, the gel was washed 2 times for 5 min at RT with water. Fixation of the gel was performed with two washes in 30% ethanol, 10% acetic acid for 15 min. Fixation solution was washed away with two washes in 10% ethanol for 5 min, then two times for 5 min in water. Gel was sensitized for 1 min using manufacturer's solution (Sensitizer Working Solution, diluted 500 times) and wash twice with water. Staining was performed within 30 min by incubation in a solution containing 50 times diluted Stain Working Solution. Gel was washed twice with water and developed till there were visible bands using 50 times diluted Developer Working Solution. Development was stopped by washing with 5% acetic acid for 10 min.

6.2.2. Cell biology methods

6.2.2.1. Transformation and cultivation of E.coli

For *E. coli* plasmid transformation, cells were incubated together with plasmids on ice for 20 min, then transferred to 42°C water bath to induce heat-shock for 60 sec, which induces

permeability of the membrane and allows insertion of the plasmid into the cell. Cells were afterwards incubated on ice for 2 min. 1 ml of LB medium was added and let the cells to regenerate at 37°C, shaking for 60 min. Cells were spined down for 5 min at 900 rpm. The pellet cells were resuspended in 100 µl LB medium and plated on plates with the required antibiotics. Plates were cultivated at 37°C, overnight. For plasmid purification single colonies were used. For protein production all colonies from the plate were used. For plasmid production *E.coli* DH5α was used and cultured in LB medium at 37ºC overnight with shaking. For protein purification *E. coli* strains BL21-CodonPlus (DE3)-RIL or Rosetta were used, cultivated in 2YT medium with shaking at 37°C till reaching an optical density at 600 nm of 0.5–0.8. Protein production was induced with 0.2 mM isopropyl β-D-1-thiogalactopyranoside (IPTG) and cells were further cultivated at 18°C or 16°C overnight, or at 25°C or 30°C for 5 h. Cells were collected, washed with PBS and stored at -80°C till purification.

6.2.2.2. Insect cells cultivation and protein production

Bacmid production was executed following the guidelines outlined in the MultiBac™ manual (GENEVA Biotech version 5.1). Viruses were produced in Sf21 insect cells with corresponding bacmids for γTuRC components (*2xFLAG-TUBGCP5*, *TUBGCP6*, *TUBGCP4, TUBG1, ACTB, TUBGCP2, TUBGCP3*, *MZT1, MZT2B, RUVBL1 and RUVBL2)* [62,65] or *CAMSAP2-GFP-6HIS* in pFastBac vector with induction of cellfectin II reagent (Thermo Fisher Scientific). Viruses were amplified in 30 ml till reaching concentration $1x10^6$ cells/ml and diluted in 1:100 in 100 ml Sf-900 III medium supplemented with (100 units/ml penicillin/100 µg/ml streptomycin, Thermo Fisher Scientific) with Sf21 cells. Infected cells were incubated at 27°C for 60 h. Cells were harvested by 800 g centrifugation for 5 min, snap frozen and stored at −80°C till purification.

6.2.2.3. HEK T293 cell cultivation

Stable HEK T293 cell lines with *WT-TUBGCP6*-FLAG and *ΔN56-TUBGCP6*-FLAG were prepared by Dr. Enrico Antorini with usage of the Retro-X™ Tet-On® 3G Inducible Expression System (Clontech)[62]. Cells were selected in medium containing 0,05 µg/ml of Puromycine (Invivogen) for 5 d. Stable cell lines with Katanin p60 were prepared by Dr. Onur Karasu using of Sleeping Beauty System Donor[274–276] vectors were electroporated together

with SB100X transposase vector in ratio 1 to 1. To enrich the content of cells with electroporated vectors, cells were incubated for 2 d with 100 µg/ml Zeocin (# R25001; Invitrogen) regularly every 10 cell's passaging. Both stable cell lines were kept at -80ºC, before use they were thawed and let expanded. Cells were incubated at 37°C with 5% CO_2 in growth medium (DMEM/F-12 (Gibco) supplied with 10% v/v foetal bovin serum (FBS), 2 mM L-glutamine, 1% penicillin/streptomycin) with addition of paxitaxel in case of γTuRC-capped minus ends, or nocodazole (Sigma-Aldrich) in case of purification of γTuRC or katanin p60 in active from, described in detail by purifications.

6.2.2.4. Drosophila melanogaster S2 cells cultivation

Schneider 2 (S2) cells with stable expressed *FLAG-GCP2* coned into the pMTV5-C-HIS vector were produced and maintained by Janina Luitz from Prof. Erhardt (Karlsruhe) by collaboration. Cells were cultivated in Schneider's *Drosophila* medium (Gibco) supplemented with 10% (v/v) Fetal Bovine Serum and 200 µg/ml penicillin and streptomycin in sterile 250 ml Erlenmeyer flask at 25 °C. Twice a week cells were splitted or divided for expansion to keep the density to 10^6 cells/ml. Harvesting of the cells were performed by centrifugation at 3000 rpm for 3 min. Cells with medium were kept in cryotubes supplemented with 20% DMSO at -80°C upon use.

6.2.3. Animal methods

6.2.3.1. Maintaining of Drosophila melanogaster flies

pUbi-GCP2-FT flies were produced by microinjected with pattBsatIIISense-Flag-Tev-SG5-DM GCP2 by Bloomington. Flies in stock were kept at 25°C in vials containing fly food (7.2% (w/v) maize, 2.4% molasses, 7.2% (w/v) malt, 0.72% (w/v) agar, 0.88% (w/v) soya, 1.464% (w/v) yeast and acid mix (1% propionic acid + 0.064% orthophosphoric acid), which was exchanged every 2 weeks until use.

6.2.3.2. Collection of Drosophila melanogaster embryos

Flies were kept in collection cages, which on the bottom had got grape juice plates (3.5 g agar in 150 ml H_2O, 50 ml of grape juice). Backing yeast pasta was used for enhancing the

production of the embryos. Two times per day the plates were exchanged, and embryos were collected from them via washing them of the plates with water and collecting of embryos on filtration membrane. Water was removed and embryos were snap-frozen and kept at -80°C till start of the purification procedure.

6.2.4. Biochemical methods

6.2.4.1. MT nucleation methods

6.2.4.1.1. In vitro nucleation

60 µM unlabeled ab-tubulin was mixed with 4% Cy3 labeled ab-tubulin in presence of 12,5% glycerol in 1xBRB80 buffer (80 mM PIPES/KOH pH6.8, 1 mM $MgCl_2$ and 1 mM EGTA) and spined down at 352,860 *g*, 5 min in S100-AT3 rotor (Thermo Fisher Scientific) at 4°C. The supernatant was then mixed with premix containing 1 mM GTP, 12,5% glycerol, 1x BRB80 buffer and with or without required amount of different types of γTuRC in ratio 1:1. The mix was incubated on ice for 30 min and after the polymerization reaction was started at 37°C in a water bath. Incubation time at 37°C was depended on experimental conditions but varied from 1 min to 10 min. The reaction was stopped with 1% glutaraldehyde in 1xBRB80.

6.2.4.1.2. MT aster formation in *Xenopus leavis* extract

Cytostatic factor (CSF)-arrested meiotic *X. laevis* egg extracts preparation was carried out according to a published protocol [238]. By ultracentrifugation at 100 000 g, 60 min at 4°C in a S120-AT2 rotor (Sorvall) a low-speed supernatant was acquired, which was used for further analysis. CSF and later on as well as LSS was provided by Prof. Oliver Gruss. 20 µM Ran(Q69L) and 4 µM Cy3-labelled pig brain tubulin were added to 15-20 µl of LSS on ice and transformed to 20°C water bath for 20 min to induce MT asters formation. For the study of the influence of CAMSAP2 and Katanin p60 proteins, 100 nM CAMSAP2 and 80 nM Katanin p60 were added to the reaction. All additives were diluted to the LSS maximum of 10 % to keep aster formation reaction stable. 3 µl of sample was squash fixed with 3 µl solution containing 50% glycerol, 8% formaldehyde in 1xBRB80 on 12x12 mm coverslip. The sample were examined by fluorescence microscopy (Nikon Ti-E epifluorescence microscope equipment with a 10x objective (0.25 NA, Nikon), a 2048 x 2048 px (6.5 µm) sCMOS camera

(Flash4, Hamamatsu) and a Perfect Focus autofocus system (Nikon), with fitted 542/27 excitation and 600/52 emission filters (Semrock).

6.2.4.1.3. In vitro fluorescence nucleation method

MT nucleation was performed using the fluorescence-based Tubulin Polymerization assay kit (Cytoskeleton Inc, Denver Com Cat. # BK011P) following the manufacturer's instruction. Shortly, 5 µl of γTuRC elution buffer, 5 µl of TuRC or 5 µl of 30 µM paclitaxel was pipetted into 96-well microtiter plate, prewarmed and mixed with 50 µl of tubulin buffer (2 mg/ml porcine tubulin in 80 mM PIPES pH 6.9, 2 mM $MgCl_2$, 0.5 mM EGTA, 1mM GTP, 15% glycerol). The polymerization reaction was triggered transferring the plate to the 37°C chamber of plate reader. Fluorescence was measured at 37°C using a plate reader every 1 min for a period of 60 min (CLARIOstar, BMG Labtech, excitation at F:360-10, emission at F: 450-10).

6.2.4.2. Actin polymerization

Actin labeled with pyrene (obtained from Hypermol, Germany) was dissolved in a standard actin buffer (containing 5 mM Tris at pH 8.0, 0.2 mM CaCl2, 0.2 mM ATP, and 0.5 mM DTT) to reach a final concentration of 2 µM. This solution was left to incubate on ice for 1 h before being centrifuged at 20 000g and 4°C for half an hour. Following this, 20 µl of the pyrene-actin solution in the standard actin buffer (at 2 µM) was combined with 2 µl of γ-TuRC elution buffer (containing 50 mM Na-HEPES at pH 8.0, 1 mM EGTA, 1 mM MgCl2, 100 mM NaC, 0.1 mg/ml γ-tubulin antigenic C-terminal peptide, 1 mM GTP, and 0.02% Tween20) within a reaction system. Arp2/3 (final concentration of 0.5 nM, from Hypermol, Germany), GST-VCA (final concentration of 15 nM, from Hypermol, Germany), and γ-TuRC (final concentration of 0.5 nM) were then added to the reaction system. The resulting mixture was combined with 1/10th of the actin polymerization buffer (consisting of 100 mM Tris-Cl at pH7.5, 500 mM KCl, 20 mM $MgCl_2$, 10 mM ATP) and the fluorescence was recorded at 25°C using a plate reader every minute for a total duration of 100 min (using a CLARIOstar instrument from BMG Lab, with excitation at F:360-10 and emission at F: 450-10). Published in [53]

6.2.4.3. Circular dichroism spectroscopy

Purified xGCP6(546–794) underwent dialysis with a solution containing 50 mM Na_2HPO_4-NaH_2PO_4, 150 mM NaF, at pH8, and this process took place overnight. Afterward, the sample was concentrated using a Vivaspin® 6 centrifugal concentrator from Santorius, achieving a final concentration of 2.6 µM. Circular dichroism spectra were obtained at 25°C utilizing a Jasco J715 spectropolarimeter. A 1 mm path length cell was employed, and spectra were documented in the range of 190 nm to 250 nm, with data points collected every 0.2 nm. This procedure was carried out twice, with the resulting spectra being the mean of 5 scans. Lastly, the CD intensities were reported in mdeg. Published in [53]

6.2.4.4. Preparation of γ tubulin conjugated Dynabeads protein A beads

A home- made XRanPB2 antibody against the c-terminus of *Xenopus leavis* γ-tubulin was created and provided by Prof. Oliver Gruss and verified in[53]. 62,5 µg of the antibody was incubated with 1 ml of Dynabeads protein A beads (Invitrogen™) overnight at 4°C. The beads were then washed twice with 200 mM Na-borate, pH9, and incubated with fresh prepared DMP in 200 mM Na-borate, pH9, (5,2 mg/ml) for 30 min at RT. The crosslinking reaction with DMP was stopped by one wash and incubation for 2 h with 200 mM ethanolamine, pH 8. The beads were then washed two times with 100 mM glycine, pH 2,5 to remove any uncoupled proteins. Finally, the beads were neutralized with two washes with 1xPBS and kept in 1ml of 1xPBS with 1mM sodium azide at 4°C.

6.2.5. Protein purifications methods

6.2.5.1. Purification of γTuRC

6.2.5.1.1. Native γTuRC from *Xenopus leavis*

Cytostatic factor (CSF)-arrested meiotic *Xenopus laevis* egg extracts was prepared as described before, provided by Prof. Oliver Gruss lab and stored in small aliquots at -80°C. Approximately 400 µl of extract was used to bind γTuRC to 180 µl *Xenopus leavis* γ-tubulin antibody crosslinked Dynabeads Protein A and incubated for 30 min at RT. Afterwards beads were washed:

1, three times with CSF buffer- XB buffer (5 mM EGTA, 10 mM HEPES pH7.7, 2 mM $MgCl_2$, 50 mM sucrose, 100 mM KCl, 0.1 mM $CaCl_2$)

2, three times with CSF buffer- XB buffer containing additional 250 mM KCl

3, washed two times with HB 100 buffer 50 mM Na-HEPES pH8.0, 1mM EGTA, 1 mM $MgCl_2$, 100 mM NaCl, 0,1 mM GTP).

Bound γTuRC was eluted with 25 µl of elution buffer (HB100 buffer containing 1 mg ml^{-1} γ-tubulin antigenic C-terminal peptide, 1 mM GTP and 0.02% Tween20) overnight at 4 °C. Published in [53].

6.2.5.1.2. Native γTuRC from HEK T293 cells

HEK T293 cell line expressing *FLAG-WT-GCP6* and *FLAG-ΔN56-GCP6* was produced by Dr. Enrico Antorini . Prepared 1/3 of 15 cm dish aliquots of these cells were stored at –80°C and thawed prior to use. Cells were expanded to five 15 cm dishes and 48 h before harvesting 10 ng/ml Dox was added to the cell medium. Upon harvesting of the cells, they were washed with 1xPBS and resuspend in lysis buffer (50 mM Na-HEPES pH8.0, 1 mM EGTA, 1 mM $MgCl_2$, 100 mM NaCl, 0.1% (vol/vol) TritonX, 0.1 mM GTP and one complete EDTA-free protease inhibitor tablet (ROCHE). Lysis was performed usage of Potter-Elvehjem Homogenizer ((Thermo scientific), 5x times of pushing and rotating of pestle on ice)). Supernatant was extracted by centrifugation at 20,000 × g for 15 min at 4°C. γTuRC was pulled down through its incorporated FLAG-GCP6 variants via magnetic FLAG beads (M2, Sigma Aldrich). Incubation on the beads was for 2 h at 4°C. Beads were washed first one time with lysis buffer and two times with wash buffer (50 mM Na-HEPES pH8.0, 1 mM EGTA, 1 mM $MgCl_2$, 100 mM NaCl, 0.1% (vol/vol) TritonX, 0.1 mM GTP) and eluted with elution buffer

(50 mM Na-HEPES pH8.0, 1 mM EGTA, 1 mM MgCl2, 100 mM NaCl, 1 mM GTP, 0.2 mg/ml 3xFLAG peptide (Gentaur)) for 30 min at 4°C.

6.2.5.1.3. *Drosophila melanogaster* S2 cells- γTuRC

Frozen S2 cell pellets expressing *FLAG-GCP2* were thawed on ice and resuspended in lysis buffer (HB100 buffer (50 mM Na-HEPES pH8.0, 1mM EGTA, 1 mM $MgCl_2$, 100 mM NaCl) supplemented with 0,1 mM GTP, 0,1% Triton X, one cOmplete EDTA-free protease inhibitor tablet)) and after resuspension PMSF was added. Resuspended cells were kept for 10 min, 4°C, rotating, afterwards the cells were sonicated using a Diagenode Bioruptor with 5 cycles of 30 sec on/ 30 sec off, ”LOW” function toggled. Lysates were clarified with 20 000 g centrifugation, 4°C, 15 min. To the lysis buffer equilibrated anti-FLAG M2 Magnetic beads (Millipore Sigma, #M8823), I added the supernatant fraction and incubated the mixture for 2 hat 4°C with rotating. The beads were wash 3x times with HB100 buffer and eluted with HB100 buffer supplemented with 1 mM GTP, 0,02 % Tween 20, 0,5 mg/ml 3xflag peptide. Samples were directly used for Negative Stain EM.

6.2.5.1.4. *Drosophila melanogaster* embryos - γTuRC

Flash frozen pellets of embryos were added to glass tubes of the Potter Homogenizator and let thawed on ice. The pellet was supplemented with lysis buffer (HB100 Buffer (50 mM Na-HEPES pH8.0, 1 mM EGTA, 1 mM $MgCl_2$, 100 mM NaCl) supplemented with 0,1mM GTP, 0,1% Triton X, one cOmplete EDTA-free protease inhibitor tablet and PMSF and 1 to 2000 diluted cycloheximide (Sigma Aldrich) were added after resuspension. Homogenization was performed with 7x up and down movement of pestle. The lysate was clarified by centrifugation at 20 000g at 4°C for 15 min. After centrifugation the upper fat layer was removed with a pipette. For purpose of removal of abundant ribosomes, I performed ultracentrifugation at 150 000 g, 4°C, rotor S120 AT2 (Sorvall) for 20 min. Supernatant was used for binding with pre-equilibrated anti-FLAG M2 Magnetic beads (Millipore Sigma, #M8823) with lysis buffer. After 2 h incubation at 4°C, rotating, beads were washed with first with HB100 + 0,1 mM GTP, second with HB100 + 0,1 mM GTP + 200mM NaCl, and third with HB100 + 0,1 mM GTP.

Elution was performed for 30 min at 4°C with HB100 buffer supplemented with 1 mM GTP, 0,02% Tween 20, 0,5 mg/ml 3xFlag peptide. Sample was immediately used for further analysis.

6.2.5.1.5. Recombinant human γTuRC from SF21 insect cells

Bacmids containing components of γ-TuRC (*2xFLAG-TUBGCP5*, *TUBGCP6*, *TUBGCP4, TUBG1, ACTB, TUBGCP2, TUBGCP3*, *MZT1, MZT2B, RUVBL1 and RUVBL2*) were produced with the MultiBac system (GENEVA Biotech). Cell lysates were produced by sonification (3 times for 1 min, 0,6 amplitude, Hielscher UP50H) in 15 ml of lysis buffer containing 50 mM Tris, pH7.5, 200 mM NaCl, 1 mM $MgCl_2$, 1 mM EGTA, 0.5 mM DTT, 0.1% (vol/vol) Tween-20 with 10 µl Benzonase (Sigma Aldrich) and one cOmplete EDTA-free protease inhibitor tablet (Roche). Cytosolic fraction was collected by centrifugation at 20 000 g for 30 min at 4°C. For tag affinity binding equilibrated anti-FLAG M2 Magnetic beads were used (Millipore Sigma, #M8823), incubated for 1 to 2 h at 4°C on a rotator. Beads were washed first with lysis buffer and then two times with wash buffer (50 mM Tris-Cl, pH7.5, 150 mM NaCl, 1 mM $MgCl_2$, 1 mM EGTA, 0.5 mM DTT). γ-TuRC was eluted from the beads with wash buffer including 0.5 mg/ml 3x FLAG peptide (Gentaur). Published in [62,240]

6.2.5.2. RanGTP purification

A pQE32 vector containing cloned Ran(Q69L) was transformed into *E. coli* competent cells (strain BL21-CodonPlus(DE3)-RIL). At optical density at OD 600 0,5-0,8 the cells growing at 37°C were incubated with 0,2 mM IPTG (Roth) to induce expression. Afterwards the cells were grown at 18°C overnight. Upon harvesting of the cells, pellets were stored at -80°C till purification. Cells were resuspended in lysis buffer (10 mM Hepes pH7.6, 100 mM KCl, 1 mM $MgCl_2$, 5% (v/v) glycerol, 1 mM DTT, 0.1% Triton X-100, cOmplete EDTA-free protease inhibitor cocktail (Roche) and PMSF). Lysis of the cells was performed by sonification (6 x 1 min with 0.8 amplitude, Hielscher UP50H) and the supernatant was clarified via centrifugation at 40 000 rpm for 20 min in a Type 50.2 Ti Rotor (Beckman Coulter). The Ran(Q69L) protein was pulled out with Ni-NTA Agarose beads (Qiagen), 2 h, rotating at 4°C. Beads were wash three times with washbuffer (10 mM Hepes pH7.6, 100 mM KCl, 1 mM $MgCl_2$, 5% v/v glycerol) and eluted with wash buffer containing 300 mM imidazole (Roth). Buffer exchange on HiTrap Desalting column (5 mL, Cytiva) on an ÄKTA go system (Cytiva) operated using the UNICORN software (version 7.6) was performed to remove imidazole. Ran

(Q69L) was concentrated on Amicron® Ultra protein concentration colons (Merk) to reach at least to 240 μM. Ran (Q69L) was aliquoted and stored at -80°C till use. Published in[240].

6.2.5.3. CAMSAP2 purification

N-terminally tagged 6His-GFP-human CAMSAP2 was cloned into pFastBac vector from Addgene (Plasmid #59037). Cellfectin II reagent (Thermo Fisher Scientific) was used to transfect cellfectin II reagent (Thermo Fisher Scientific) for production of baculovirus. Baculovirus infected Sf21 cells grown at 27ºC for 60 h. Afterwards. the cells were harvest by centrifugation (800 g for 3 min), the pellet was flash frozen and stored at -80ºC.
The lysis buffer (50 mM HEPES pH 7.6, 300 mM KCl, 1 mM MgCl2, 1 mM EGTA, 1 mM DTT, 0.1% Triton X-100, cOmplete EDTA-free protease inhibitor cocktail (Roche) and PMSF) was used to resuspend the cell pellet, then cell lysis was performed by sonification for 3 times 1 min at 0,6 amplitude and 0,5 cycle at Hielscher UP50H sonicator. Cytosolic fraction was produced upon centrifugation for 30 min at 20 000 g at 4ºC. Protein was pulled down via Ni-NTA Agarose beads (Qiagen) for 2 h at 4ºC. Beads were washed 3x times with washing buffer (50 mM HEPES pH7.6, 300 mM KCl, 1 mM MgCl2, 1 mM EGTA, 1 mM DTT, 0.1% Triton X-100, cOmplete EDTA-free protease inhibitor cocktail (Roche)) and eluted with wash buffer containing 300 mM imidazole (Roth). Imidazole was removed by buffer exchange through a HiTrap Desalting column (5 mL, Cytiva) on an ÄKTA go system (Cytiva). The protein was aliquoted, flash frozen and stored at -80ºC upon use. Published in[240].

6.2.5.4. Katanin p60 purification

Pellets of HEK T293 cell line with sleeping beauty system integrated katanin p60-emiRFP-FLAG (Addgen, Plasmid # 89316) were thawed on ice and resuspended in lysis buffer (50 mM HEPES pH 7.6, 100 mM KCl, 1 mM MgCl2, 1mM EGTA, 1 mM DTT, 0.1% Triton X-100, cOmplete EDTA-free protease inhibitor cocktail (Roche) and PMSF). Lysis of the cells were facilitated via homogenisation with 5 times pushing the pestle rotating up and down, on ice. After 20 000 g, 30 min, 4 ºC centrifugation was collected supernatant and added to pre-equilibrated anti-FLAG M2 Magnetic beads (Millipore Sigma, #M8823) with lysis buffer and incubated for 2 h, 4ºC with rotating. Beads were washed three times with washing buffer (50 mM HEPES pH7.6, 100mM KCl, 1 mM $MgCl_2$, 1 mM EGTA) and eluted by supplementing

the washing buffer with 0.5 mg/ml 3x FLAG peptide (Gentaur). Sample were aliquoted, flash frozen and stored at -80ºC upon use.

6.2.5.5. Xenopus leavis GCP6 $^{546-794}$ construct purification

For the expression of N-terminal 249 amino acids of the xGCP6-IDo, pGEX-6p1- xGCP6(546–794)-Strep II was transformed into E. coli strain BL21(DE3) Codon plus-RIL. The transformed cells were grown in 2XYT medium and expression of the protein was induced with 0,2 mM IPTG, when the optical density reached 0,5-0,8. After five hours at 25°C, the cells were harvested by centrifugation (4 000 rpm, 20 min), washed with PBS buffer and stored at -80ºC for further use. The cells were resuspended in lysis buffer containing 50 mM Tris-Cl, 150 mM NaCl, 10% glycerol, pH8, 1 mM EDTA, 1 mM DTT, 5 mM ATP, 2 mM $MgCl_2$, 0,1% Triton X-100, 1x cOmplete EDTA-free protease inhibitor cocktail (Roche), 1x PMSF. Afterwards they were lysed by sonification for four times at 90% amplitude pulses for 1 min each time. Cell debris was pelleted by centrifugation at 45 000 rpm for 25 min. After binding of the protein from the centrifuged supernatant to the pre-equilibrated Glutatione Sepharose 4B (MACHEREY-NAGEL) with lysis buffer, the GST-Tag was cleaved by GST 3C protease (EMBL, 50 mM Tris, 150 mM NaCl, 10% glycerol, pH 8, 1 mM EDTA, 1 mM DTT) on the column. The protein from the first affinity purification was afterwards bound to StrepTactin TM Sepharose High Performace (GE Healthcare) and eluted with 2,5 mM desthiobiotin. Published in[53]

6.2.5.6. MT minus ends purification

6.2.5.6.1. Recombinant γTuRC capped minus end

60 µM pig brain tubulin supplemented with 4% Cy-3 labelled tubulin in 1xBRB80 (80 mM PIPES/KOH pH6,8, 1 mM MgCl2, 1 mMEGTA, 12,5% glycerol) was spin down at 352 860 g, 4ºC for 5 min using a S100-AT3 rotor (Thermo Fisher scientific). Supernatant fraction of ab-tubulin was mixed with γTuRC solution (1:4 diluted γTuRC (5-10 nM) in 1xBRB80 with 12,5 % glycerol, 2 mM GTP) in 1:1 ratio. Initial polymerization of MTs was started for 5 min in 37ºC. Afterwards 10 µM taxol was added and let polymerised for additional 5 min. Polymerised MTs were spin down 2 times through 30% glycerol cushion in BRB80, 10 µM Taxol, 0,1 mM GTP at 69 700 g, 30ºC for 20 min. To finally resuspended MTs, 100 mM KCl

was added. MTs were transferred to equilibrated anti-FLAG M2 Magnetic beads (Millipore Sigma, # M8823), incubated for 1 h at RT, washed 3x with 1xBRB80, 100mM KCl, 10 µM Taxol, 1 mM GTP) and eluted with washing buffer supplemented with 0,2 mg/ml 3xFLAG peptide and 0,02% Tween 20 for 1 h at RT. Purified reconstructed γ-TuRC-capped MT minus ends were immediately used for analysis. Published in[240].

6.2.5.6.2. MT minus ends from HEK T293 cells

HEK T293 cell cells with *FLAG-GCP6* were cultivated till it reached 80% confluency, at that point 1 ng/ml doxycycline (Dox) were added to induce production of FLAG-GCP6. 13,5 h before harvesting 1 µM Paclitaxel (Sigma Aldrich) was added to the cells .Cells were harvest and pellets were collected by centrifugation using 1000 rpm (Eppendorf™ Centrifuge 5810/5810 R), RT for 10 min. Cells were resuspended in lysis buffer (1xBRB80, 1 mM GTP, 10 uM paclitaxel, 1x PI, 0,1% Triton) and transferred into glass tube of Potter Homogenizator. The homogenization was performed with 7 times pushing up and down and rotating of pestle in close proximity to ice. Clarified supernatant (20 000 g, 15 min, RT) was added to 36ºC for 15 min. MTs were ultracentrifuged through 30% glycerol cushion (1x BRB80, 30% glycerol, 1 mM Taxol, 0,1mM GTP) for 20 min at 44 000 rpm, RT in S120-AT2 (Sorvall). The pellet was resuspended in binding buffer (1x BRB80, 100 mM KCl, 10 µM Taxol, 1 mM GTP). For 1 h was pellet incubated with equilibrated anti-FLAG M2 Magnetic beads (Millipore Sigma, # M8823) at RT, wash three times with binding buffer and eluted with binding buffer supplemented with 0,2 mg/ml 3xFLAG peptide for 30 min at RT. After elution, the sample was crosslinked with 1% glutaralderhyde and used for further analysis by NS EM by Annett Neuner.

6.2.5.6.3. *Xenopus leavis* γTuRC capped MT minus ends

Cytostatic factor (CSF)-arrested meiotic *X.laevis* egg extracts were prepared according to Chinen et al. and supplemented by Prof. Oliver Gruss[238]. Using ultracentrifugation at 100 000 g for 1 h at 4°C in a S120-AT2 rotor (Sorvall) is prepared low speed supernatant (LSS). Only high quality LSS with higher MT asters formation were used for further purification. The quality of the activity of LSS was verified via induction of aster formation by 20 µM Ran(Q69L) in the presence of 4 µM Cy3-labelled pig brain tubulin for visualisation purpose. LSS together with Ran(Q69L) were incubated for 20 min at 20°C. 3 µl of sample was squash-

fixed on a slide with a 12 x 12 mm coverslip and analysed by fluorescence microscopy (Nikon Ti-E epifluorescence microscope with a 10x objective (0.25 NA, Nikon), a 2048 x 2048 px (6.5 µm) sCMOS camera (Flash4, Hamamatsu) [277] filters (Semrock)). Only the extracts with satisfactory aster formation were used for purification. LSS were incubated with 20 µM of Ran(Q69L), incubated for 20 min in a water bath at 20°C. After that LSS were transformed into new Eppendorf tubue containing 20 µM Paclitaxel (Sigma Aldrich), incubated for an next 10 min at 20 °C in a water bath to stabilise MTs in asters. MT asters were separated from cytosolic components via centrifugation through a 40% glycerol cushion (1xBRB80 (80 mM PIPES/KOH pH 6.8, 1 mM $MgCl_2$ and 1 mM EGTA), 40% glycerol, 10 µM Taxol, 0.1% Triton X-100) for 20 min at 20°C at 53 000 g in a S120-AT2 rotor (Sorvall). Asters in the pellet were gently resuspended with 1xBRB80 buffer (80 mM PIPES/KOH pH 6.8, 1 mM $MgCl_2$ and 1 mM EGTA) supplemented with 1 mM GTP and 10 µM Paclitaxel (Sigma Aldrich). To shorten γTuRC-capped MT minus ends, the asters were fragmented via modification of a previous published protocol of tubulin purification (Vale). Shortly, asters were pipetted through squeezed pipette tip for 5 min on ice with the addition of 3 mM $CaCl_2$. To avoid the precipitation of proteins on the beads, 100 mM NaCl was added. γ-TuRC-capped MTs were separated with anti-γ-tubulin antibodies coupled to Dynabeads Protein A (Life Technologies) for 30 min at RT. Beads were after incubation shortly washed with 1xBRB80 buffer containing 100 mM NaCl and 1 mM GTP. Elution was performed for 2 h at RT with BRB80 containing 0.1 mg/ml γ-tubulin antigenic C-terminal peptide[60], 1 mM GTP and 0.02% Tween 20. The sample was used immediately. Published in[240].

6.2.6. Microscopic methods

6.2.6.1. Negative stain electron microscopy

5 µl of the sample was applied on Copper-palladium 400-mesh EM grids (PLANO GmbH) with a continuous carbon layer of approximately 10 nm, which was prior to use discharged in ACE1 (GaLa Instrumente GmbH). The sample was incubated for 30 sec at RT and blotted on a Whatman filter paper 50 (CAT N.1450-070). Grids were wash three times on a water drop and tree times stained of 3% uranyl acetate containing water drops. Images were acquired on a JEOL JEM-1400 (JEOL Ltd., Tokyo, Japan) operating at 80 kV, equipped with a 4k x 4k digital camera (F416, TVIPS, Gauting, Germany). Micrographs containing the *in vitro* recombinant

human γ-TuRC capped MT and CAMSAP2 or native WT-GCP6 and ΔN56-GCP6 γTuRC from HEK293 cell line were collected on a Talos L120C TEM equipped with a 4k x 4k Ceta CMOS camera (Thermo Fisher Scientific) at a pixel size of 3.28 Å (45,000 x magnification) and a nominal defocus of -2 µm. Processing of images were done on ImageJ 2.0 software by adjusting contrast and brightness. NS EM was performed by Dr. Annett Neuner.

6.2.6.2. Double labelling NS EM

Freshly purified γ-TuRC-capped MT minus ends from *X. laevis* low speed supernatant were incubated at 37ºC with GFP-CAMSAP2 for 30 sec, immediately crosslinked with 0,5 % glutaraldehyde. Carbon-covered copper-palladium 400-mesh grids, to which 5 µl of sample was applied, were glow discharged in ACE1 (GaLa Instrumente GmbH). Sample were applied for 1 min at RT, and rinsed two times on water drops. The grid was incubated with blocking buffer (1.5% BSA in PBS supplemented with 0.1% fish skin gelatin, FSG) for 20 min. After blocking, grids were put on the drop with mouse anti-γ-tubulin antibodies (Sigma; 1:20 dilution) for 30 min and then washed three times with PBS. After that grids were incubated for 20 min with rabbit anti-mouse linker antibody (Abcam; 1:200) and rinsed on three drops of PBS. Subsequently, grids were incubated with Protein A gold conjugate (PAG, 15 nm gold, Utrecht University, Utrecht, The Netherlands) for 15 min. For a second setsof antibodies, grids were blocked for 10 min and incubated with goat anti-GFP antibody (Rockland; 1:20) for 30 min, rinsed with 3 drops of PBS and subsequently incubated with protein A gold-conjugated rabbit anti-goat antibody (1:50; 10 nm gold) for 20 min. After washing three times with PBS, grids were fixed with 1% glutaraldehyde in PBS for 3 min and washed three times with water. Grids were post-stained with 3% uranyl acetate (UA) in water. Excess uranyl acetate was blotted away on Whatman 50 filter paper and let dry on air at room temperature.-Micrographs containing the *in vitro* recombinant human γ-TuRC capped MT and CAMSAP2 were collected on a Talos L120C TEM equipped with a 4k x 4k Ceta CMOS camera (Thermo Fisher Scientific) at a pixel size of 3.28 Å (45,000 x magnification) and a nominal defocus of -2 µm. Double labelling was performed by Dr. Annett Neuner. Published in[240].

Cryo- electron microscopy

Cryo-EM analysis was performed in collaboration with Dr. Stefan Pfeffer group, particularly with Dr. Erik Zupa and Bram Vertmuelen. Protocols for the analysis of native or recombinant

γTuRC were published[53,62]. The protocols for the analysis of γ-TuRC-capped minus ends of *Xenopus leavis* was published[240]. Shortly, samples were applied onto the carbon face of Cu R2/1 grids (200 mesh; Quantifoil), which were prior glow discharged in a Gatan Solarus 950 plasma cleaner for 20 sec inside of a Vitrobot Mark IV (Thermo Fisher/FEI) at 100% humidity and 22°C. Sample was applied and incubated for 30 sec and after that for 0,5 sec blotted and immediately plunge-frozen into liquid ethane and stored in liquid nitrogen. Data were acquired on a Titan Krios (Thermo Fisher/FEI) operated at 300 kV, with a Gatan K3 direct electron detector and a Quantum Gatan Imaging Filter (Gatan) with an energy slit width of 20 eV. Data were processed using RELION 3.1 and beam-induced motion was corrected with MotionCor2. γTuRC-capped MTs minus ends were manually picked through multiple datasets. Particles were subjected multiple rounds of 2D classification. Only the best representing classes were used for further analysis. Prior further analysis, all classes were put in the same orientation according to the MT site. Next, in 2D view all classes were reoriented according to the projection of an artificial reference of 13 protofilament MT lattice by cross-correlation in PyTom[278,279]. In a second round, 3D refinement was created using the cryo EM density of the published native isolated *Xenopus laevis* γ-TuRC (EMDB 10491)[53] as a reference. GRIP2 domain and γ-tubulins of spoke 5 and 6 were removed to serve as a control for bias by Segger tool [280]. To increase the lower resolution that limited the alignment process, particles of native isolated γ-TuRC from *Xenopus laevis* omitting the GRIP2 domain and γ-tubulins of spoke 5 and 6 (datasets 1-3 from[53]) were supplemented. γTuRC-capped minus ends were re-extracted and γTuRC part reached the resolution of 23 Å at the MT minus end. The densities of GRIP2 domain and γ-tubulins of spoke 5 and 6 were intact which confirm that all densities were correctly aligned. This indicates no bias from refence or supplemented particles. For resolution of MT densities, were performed an additional refinement step with absence of supplemented particles and mask covering just MTs. This led to 32 Å resolution.

6.2.6.3. Fluorescence microscopy

In vitro prepared γTuRCs capped MT minus ends were prepared as previously described. For CAMSAP2 binding analysis, 200 nM of GFP-CAMSAP2 were incubated with MTs at 37ºC for 30 sec. All samples were crosslinked after purification or reaction with 0.5% glutaraldehyde. All MTs samples were spined down on a 12 mm coverslip coated with poly-L-lysine (Sigma-Aldrich) through 10% glycerol cushion in 1xBRB80 in a Corex 12 mL glass tube with glass support platform in the bottom via centrifugation at 23 500g for 1 h at 20ºC in

an HB6 rotor (Thermo Fisher Scientific). Coverslip were carefully removed from glass tube with prior removing of cushion with vacuum pump. Fixation was performed with cold methanol for 5 min, coverslips were washed 3 times with1x PBS and blocked with 1xPBS, 10% FBS and 0.1% Triton X-100 for 20 min RT. For identification of γTuRC at the MT minus end anti-γ-tubulin primary antibody (ab27074, Sigma Aldrich) were used, which were incubated for 40 min at RT. Three washes of the coverslip with 1xPBS were used, then corresponding secondary antibody was incubated for 20 minutes at room temperature. In case of CAMSAP2 binding experiment it was 680 donkey anti-mouse (LOT 1853988, Life technologies). Sample was washed three times with PBS and mounted with Mowiol.

In case of IF identification of actin inside *X. leavis* γTuRC, freshly purified γTuRCs were spun down as described above with exception of usage of glycerol cushion. After blocking, coverslips were incubated with 1% SDS in 1xPBS for 5 min at RT. The used antibodies were primary anti-GCP6 genuine pig diluted 1:200 and anti ß-actin mouse (Sigma-Aldrich) diluted 1000x in 3 % BSA. Secondary fluorescence antibodies were donkey anti mouse Alexa 488 and donkey anti genuine pig Alexa 555. Each of them was diluted 1:500 in 3% BSA.

Data were collected on a DeltaVision RT system (Applied Precision, Olympus IX71-based) equipped with a Photometrics CoolSnap HQ camera (Roper Scientific), a 60x/1.42 NA UPlantSAPO objective (Olympus), the softWoRx software (Applied Precision). Exposure times of FITC, TRITC and Cy5 channels were adjusted individually to the fluorescence intensities of respective proteins. Data were analysed with FIJI and Prism (GraphPad v. 9.2.0) software. Published in [240]

6.2.7. Crystallization constructs tools

An online tool was utilized to estimate the boundary of the construct for construct screening Crystallisation Construct Designer 2 (https://ccd.rhpc.nki.nl) .

7. References

1. Ludueña, R. F. Chapter Two - A Hypothesis on the Origin and Evolution of Tubulin. in (ed. Jeon, K. W.) vol. 302 41–185 (Academic Press, 2013).
2. Ludueña, R. F. A Hypothesis on the Origin and Evolution of Tubulin. in 41–185 (2013). doi:10.1016/B978-0-12-407699-0.00002-9.
3. Breuss, M. W., Leca, I., Gstrein, T., Hansen, A. H. & Keays, D. A. Tubulins and brain development – The origins of functional specification. *Molecular and Cellular Neuroscience* **84**, 58–67 (2017).
4. Gadadhar, S., Hirschmugl, T. & Janke, C. The tubulin code in mammalian sperm development and function. *Semin Cell Dev Biol* **137**, 26–37 (2023).
5. Fukushige, T. *et al.* MEC-12, an alpha-tubulin required for touch sensitivity in C. elegans. *J Cell Sci* **112**, 395–403 (1999).
6. Saito, K. & HAMA, K. Structural Diversity of Microtubules in the Supporting Cells of the Sensory Epithelium of Guinea Pig Organ of Corti. *J Electron Microsc (Tokyo)* (1982) doi:10.1093/oxfordjournals.jmicro.a050372.
7. Tucker, J. B., Paton, C. C., Richardson, G. P., Mogensen, M. M. & Russell, I. J. A cell surface-associated centrosomal layer of microtubule-organizing material in the inner pillar cell of the mouse cochlea. *J Cell Sci* **102**, 215–226 (1992).
8. Xu, Z. & Afzelius, B. A. The substructure of marginal bundles in human blood platelets. *J Ultrastruct Mol Struct Res* **99**, 244–253 (1988).
9. Chaaban, S. & Brouhard, G. J. A microtubule bestiary: structural diversity in tubulin polymers. *Mol Biol Cell* **28**, 2924–2931 (2017).
10. Kwiatkowska, M., Popłońska, K., Stepiński, D. & Hejnowicz, Z. Microtubules with different diameter, protofilament number and protofilament spacing in Ornithogalum umbellatum ovary epidermis cells. *Folia Histochem Cytobiol* **44**, 133–8 (2006).
11. Burton, P., Hinkley, R. & Pierson, G. Tannic acid-stained microtubules with 12, 13, and 15 protofilaments. *J Cell Biol* **65**, 227–233 (1975).
12. Roll-Mecak, A. & McNally, F. J. Microtubule-severing enzymes. *Curr Opin Cell Biol* **22**, 96–103 (2010).
13. Cueva, J. G., Hsin, J., Huang, K. C. & Goodman, M. B. Posttranslational Acetylation of α-Tubulin Constrains Protofilament Number in Native Microtubules. *Current Biology* **22**, 1066–1074 (2012).
14. Topalidou, I. *et al.* Genetically Separable Functions of the MEC-17 Tubulin Acetyltransferase Affect Microtubule Organization. *Current Biology* **22**, 1057–1065 (2012).
15. Guardia, C. M., Farías, G. G., Jia, R., Pu, J. & Bonifacino, J. S. BORC Functions Upstream of Kinesins 1 and 3 to Coordinate Regional Movement of Lysosomes along Different Microtubule Tracks. *Cell Rep* **17**, 1950–1961 (2016).
16. Muroyama, A. & Lechler, T. Microtubule organization, dynamics and functions in differentiated cells. *Development* **144**, 3012–3021 (2017).
17. Wu, J. & Akhmanova, A. Microtubule-Organizing Centers. *Annu Rev Cell Dev Biol* **33**, 51–75 (2017).
18. Sanchez, A. D. & Feldman, J. L. Microtubule-organizing centers: from the centrosome to non-centrosomal sites. *Curr Opin Cell Biol* **44**, 93–101 (2017).
19. Jiang, K. *et al.* Microtubule Minus-End Stabilization by Polymerization-Driven CAMSAP Deposition. *Dev Cell* **28**, 295–309 (2014).
20. De Groot, C. O. *et al.* Molecular Insights into Mammalian End-binding Protein Heterodimerization. *Journal of Biological Chemistry* **285**, 5802–5814 (2010).

21. Akhmanova, A. & Steinmetz, M. O. Microtubule minus-end regulation at a glance. *J Cell Sci* **132**, jcs227850 (2019).
22. Akhmanova, A. & Steinmetz, M. O. Control of microtubule organization and dynamics: two ends in the limelight. *Nat Rev Mol Cell Biol* **16**, 711–726 (2015).
23. Maurer, S. P., Bieling, P., Cope, J., Hoenger, A. & Surrey, T. GTPγS microtubules mimic the growing microtubule end structure recognized by end-binding proteins (EBs). *Proceedings of the National Academy of Sciences* **108**, 3988–3993 (2011).
24. Reid, T. A. *et al.* Structural state recognition facilitates tip tracking of EB1 at growing microtubule ends. *Elife* **8**, (2019).
25. Nehlig, A., Molina, A., Rodrigues-Ferreira, S., Honoré, S. & Nahmias, C. Regulation of end-binding protein EB1 in the control of microtubule dynamics. *Cellular and Molecular Life Sciences* **74**, 2381–2393 (2017).
26. Akhmanova, A. & Steinmetz, M. O. Microtubule +TIPs at a glance. *J Cell Sci* **123**, 3415–3419 (2010).
27. Slep, K. C. *et al.* Structural determinants for EB1-mediated recruitment of APC and spectraplakins to the microtubule plus end. *J Cell Biol* **168**, 587–598 (2005).
28. Kumar, P. & Wittmann, T. +TIPs: SxIPping along microtubule ends. *Trends Cell Biol* **22**, 418–428 (2012).
29. Almeida, T. B., Carnell, A. J., Barsukov, I. L. & Berry, N. G. Targeting SxIP-EB1 interaction: An integrated approach to the discovery of small molecule modulators of dynamic binding sites. *Sci Rep* **7**, 15533 (2017).
30. Jiang, K. *et al.* Microtubule Minus-End Stabilization by Polymerization-Driven CAMSAP Deposition. *Dev Cell* **28**, 295–309 (2014).
31. Jiang, K. *et al.* A Proteome-wide Screen for Mammalian SxIP Motif-Containing Microtubule Plus-End Tracking Proteins. *Current Biology* **22**, 1800–1807 (2012).
32. Tamura, N. *et al.* A proteomic study of mitotic phase-specific interactors of EB1 reveals a role for SXIP-mediated protein interactions in anaphase onset. *Biol Open* **4**, 155–169 (2015).
33. Al-Bassam, J. & Chang, F. Regulation of microtubule dynamics by TOG-domain proteins XMAP215/Dis1 and CLASP. *Trends Cell Biol* **21**, 604–614 (2011).
34. Fox, J. C., Howard, A. E., Currie, J. D., Rogers, S. L. & Slep, K. C. The XMAP215 family drives microtubule polymerization using a structurally diverse TOG array. *Mol Biol Cell* **25**, 2375–2392 (2014).
35. Ali, A., Vineethakumari, C., Lacasa, C. & Lüders, J. Microtubule nucleation and γTuRC centrosome localization in interphase cells require ch-TOG. *Nat Commun* **14**, 289 (2023).
36. Rajeev, R., Mukhopadhyay, S., Bhagyanath, S., Devu Priya, M. R. S. & Manna, T. K. TACC3–ch-TOG interaction regulates spindle microtubule assembly by controlling centrosomal recruitment of γ-TuRC. *Biosci Rep* **43**, (2023).
37. Thawani, A. & Petry, S. Molecular insight into how γ-TuRC makes microtubules. *J Cell Sci* **134**, (2021).
38. Thawani, A., Kadzik, R. S. & Petry, S. XMAP215 is a microtubule nucleation factor that functions synergistically with the γ-tubulin ring complex. *Nat Cell Biol* **20**, 575–585 (2018).
39. Widlund, P. O. *et al.* XMAP215 polymerase activity is built by combining multiple tubulin-binding TOG domains and a basic lattice-binding region. *Proceedings of the National Academy of Sciences* **108**, 2741–2746 (2011).
40. Brouhard, G. J. *et al.* XMAP215 Is a Processive Microtubule Polymerase. *Cell* **132**, 79–88 (2008).
41. Reber, S. B. *et al.* XMAP215 activity sets spindle length by controlling the total mass of spindle microtubules. *Nat Cell Biol* **15**, 1116–1122 (2013).

42. Roostalu, J., Cade, N. I. & Surrey, T. Complementary activities of TPX2 and chTOG constitute an efficient importin-regulated microtubule nucleation module. *Nat Cell Biol* **17**, 1422–1434 (2015).
43. Oakley, C. E. & Oakley, B. R. Identification of γ-tubulin, a new member of the tubulin superfamily encoded by mipA gene of Aspergillus nidulans. *Nature* **338**, 662–664 (1989).
44. Knop, M. The spindle pole body component Spc97p interacts with the gamma -tubulin of Saccharomyces cerevisiae and functions in microtubule organization and spindle pole body duplication. *EMBO J* **16**, 1550–1564 (1997).
45. Geissler, S. *et al.* The spindle pole body component Spc98p interacts with the gamma-tubulin-like Tub4p of Saccharomyces cerevisiae at the sites of microtubule attachment. *EMBO J* **15**, 3899–911 (1996).
46. Kollman, J. M., Polka, J. K., Zelter, A., Davis, T. N. & Agard, D. A. Microtubule nucleating γ-TuSC assembles structures with 13-fold microtubule-like symmetry. *Nature* **466**, 879–882 (2010).
47. Böhler, A. *et al.* The gamma-tubulin ring complex: Deciphering the molecular organization and assembly mechanism of a major vertebrate microtubule nucleator. *BioEssays* **43**, 2100114 (2021).
48. Kollman, J. M. *et al.* The Structure of the γ-Tubulin Small Complex: Implications of Its Architecture and Flexibility for Microtubule Nucleation. *Mol Biol Cell* **19**, 207–215 (2008).
49. Kollman, J. M., Polka, J. K., Zelter, A., Davis, T. N. & Agard, D. A. Microtubule nucleating γ-TuSC assembles structures with 13-fold microtubule-like symmetry. *Nature* **466**, 879–882 (2010).
50. Kollman, J. M. *et al.* Ring closure activates yeast γTuRC for species-specific microtubule nucleation. *Nat Struct Mol Biol* **22**, 132–137 (2015).
51. Gunawardane, R. N. *et al.* Characterization and Reconstitution of *Drosophila* γ-Tubulin Ring Complex Subunits. *J Cell Biol* **151**, 1513–1524 (2000).
52. Oegema, K. *et al.* Characterization of Two Related *Drosophila* γ-tubulin Complexes that Differ in Their Ability to Nucleate Microtubules. *J Cell Biol* **144**, 721–733 (1999).
53. Liu, P. *et al.* Insights into the assembly and activation of the microtubule nucleator γ-TuRC. *Nature* **578**, 467–471 (2020).
54. Consolati, T. *et al.* Microtubule Nucleation Properties of Single Human γTuRCs Explained by Their Cryo-EM Structure. *Dev Cell* **53**, 603-617.e8 (2020).
55. Haren, L. *et al.* NEDD1-dependent recruitment of the γ-tubulin ring complex to the centrosome is necessary for centriole duplication and spindle assembly. *J Cell Biol* **172**, 505–515 (2006).
56. Liu, L. & Wiese, C. *Xenopus* NEDD1 is required for microtubule organization in *Xenopus* egg extracts. *J Cell Sci* **121**, 578–589 (2008).
57. Manning, J. A., Shalini, S., Risk, J. M., Day, C. L. & Kumar, S. A Direct Interaction with NEDD1 Regulates γ-Tubulin Recruitment to the Centrosome. *PLoS One* **5**, e9618 (2010).
58. Liu, P., Choi, Y.-K. & Qi, R. Z. NME7 is a functional component of the γ-tubulin ring complex. *Mol Biol Cell* **25**, 2017–2025 (2014).
59. Wieczorek, M. *et al.* Asymmetric Molecular Architecture of the Human γ-Tubulin Ring Complex. *Cell* **180**, 165-175.e16 (2020).
60. Cota, R. R. *et al.* MZT1 regulates microtubule nucleation by linking γTuRC assembly to adapter-mediated targeting and activation. *J Cell Sci* (2016) doi:10.1242/jcs.195321.
61. Lin, T. *et al.* MOZART1 and γ-tubulin complex receptors are both required to turn γ-TuSC into an active microtubule nucleation template. *Journal of Cell Biology* **215**, 823–840 (2016).
62. Würtz, M. *et al.* Modular assembly of the principal microtubule nucleator γ-TuRC. *Nat Commun* **13**, 473 (2022).

63. Huang, T.-L., Wang, H.-J., Chang, Y.-C., Wang, S.-W. & Hsia, K.-C. Promiscuous Binding of Microprotein Mozart1 to γ-Tubulin Complex Mediates Specific Subcellular Targeting to Control Microtubule Array Formation. *Cell Rep* **31**, (2020).
64. Wieczorek, M., Huang, T.-L., Urnavicius, L., Hsia, K.-C. & Kapoor, T. M. MZT Proteins Form Multi-Faceted Structural Modules in the γ-Tubulin Ring Complex. *Cell Rep* **31**, (2020).
65. Würtz, M. *et al.* Reconstitution of the recombinant human γ-tubulin ring complex. *Open Biol* **11**, 200325 (2023).
66. Zupa, E., Liu, P., Würtz, M., Schiebel, E. & Pfeffer, S. The structure of the γ-TuRC: a 25-years-old molecular puzzle. *Curr Opin Struct Biol* **66**, 15–21 (2021).
67. Choi, Y.-K., Liu, P., Sze, S. K., Dai, C. & Qi, R. Z. CDK5RAP2 stimulates microtubule nucleation by the γ-tubulin ring complex. *Journal of Cell Biology* **191**, 1089–1095 (2010).
68. Citron, Y. R. *et al.* The centrosomin CM2 domain is a multi-functional binding domain with distinct cell cycle roles. *PLoS One* **13**, e0190530 (2018).
69. Kim, T.-S. *et al.* Hierarchical recruitment of Plk4 and regulation of centriole biogenesis by two centrosomal scaffolds, Cep192 and Cep152. *Proceedings of the National Academy of Sciences* **110**, (2013).
70. Wang, Z. *et al.* Conserved Motif of CDK5RAP2 Mediates Its Localization to Centrosomes and the Golgi Complex. *Journal of Biological Chemistry* **285**, 22658–22665 (2010).
71. Brilot, A. F. *et al.* CM1-driven assembly and activation of yeast γ-tubulin small complex underlies microtubule nucleation. *Elife* **10**, (2021).
72. Goshima, G. *et al.* Genes Required for Mitotic Spindle Assembly in *Drosophila* S2 Cells. *Science (1979)* **316**, 417–421 (2007).
73. Goodwin, S. S. & Vale, R. D. Patronin Regulates the Microtubule Network by Protecting Microtubule Minus Ends. *Cell* **143**, 263–274 (2010).
74. Nagae, S., Meng, W. & Takeichi, M. Non-centrosomal microtubules regulate <scp>F</scp> -actin organization through the suppression of <scp>GEF</scp> - <scp>H</scp> 1 activity. *Genes to Cells* **18**, 387–396 (2013).
75. Tanaka, N., Meng, W., Nagae, S. & Takeichi, M. Nezha/CAMSAP3 and CAMSAP2 cooperate in epithelial-specific organization of noncentrosomal microtubules. *Proceedings of the National Academy of Sciences* **109**, 20029–20034 (2012).
76. Schoborg, T., Zajac, A. L., Fagerstrom, C. J., Guillen, R. X. & Rusan, N. M. An Asp–CaM complex is required for centrosome–pole cohesion and centrosome inheritance in neural stem cells. *Journal of Cell Biology* **211**, 987–998 (2015).
77. do Carmo Avides, M. & Glover, D. M. Abnormal Spindle Protein, Asp, and the Integrity of Mitotic Centrosomal Microtubule Organizing Centers. *Science (1979)* **283**, 1733–1735 (1999).
78. Morris-Rosendahl, D. J. & Kaindl, A. M. What next-generation sequencing (NGS) technology has enabled us to learn about primary autosomal recessive microcephaly (MCPH). *Mol Cell Probes* **29**, 271–281 (2015).
79. Passemard, S. *et al.* Expanding the clinical and neuroradiologic phenotype of primary microcephaly due to *ASPM* mutations. *Neurology* **73**, 962–969 (2009).
80. Jiang, K. *et al.* Microtubule minus-end regulation at spindle poles by an ASPM–katanin complex. *Nat Cell Biol* **19**, 480–492 (2017).
81. Atherton, J. *et al.* A structural model for microtubule minus-end recognition and protection by CAMSAP proteins. *Nat Struct Mol Biol* **24**, 931–943 (2017).
82. Atherton, J. *et al.* Structural determinants of microtubule minus end preference in CAMSAP CKK domains. *Nat Commun* **10**, 5236 (2019).
83. Jiang, K. *et al.* Structural Basis of Formation of the Microtubule Minus-End-Regulating CAMSAP-Katanin Complex. *Structure* **26**, 375-382.e4 (2018).

84. Gao, L., Xu, F., Jin, Z., Ying, X. & Liu, J. Microtubule-severing protein Katanin p60 ATPase-containing subunit A-like 1 is involved in pole-based spindle organization during mouse oocyte meiosis. *Mol Med Rep* (2019) doi:10.3892/mmr.2019.10605.
85. Ribbeck, K. & Mitchison, T. J. Meiotic Spindle: Sculpted by Severing. *Current Biology* **16**, R923–R925 (2006).
86. Srayko, M., O'Toole, E. T., Hyman, A. A. & Müller-Reichert, T. Katanin Disrupts the Microtubule Lattice and Increases Polymer Number in C. elegans Meiosis. *Current Biology* **16**, 1944–1949 (2006).
87. Jiang, K. *et al.* Structural Basis of Formation of the Microtubule Minus-End-Regulating CAMSAP-Katanin Complex. *Structure* **26**, 375-382.e4 (2018).
88. Sanchez, A. D. & Feldman, J. L. Microtubule-organizing centers: from the centrosome to non-centrosomal sites. *Curr Opin Cell Biol* **44**, 93–101 (2017).
89. Tillery, M. M. L., Blake-Hedges, C., Zheng, Y., Buchwalter, R. A. & Megraw, T. L. Centrosomal and Non-Centrosomal Microtubule-Organizing Centers (MTOCs) in Drosophila melanogaster. *Cells* **7**, 121 (2018).
90. Jana, S. C. Centrosome structure and biogenesis: Variations on a theme? *Semin Cell Dev Biol* **110**, 123–138 (2021).
91. Takeda, Y., Kuroki, K., Chinen, T. & Kitagawa, D. Centrosomal and Non-centrosomal Functions Emerged through Eliminating Centrosomes. *Cell Struct Funct* **45**, 57–64 (2020).
92. Tillery, M. M. L., Blake-Hedges, C., Zheng, Y., Buchwalter, R. A. & Megraw, T. L. Centrosomal and Non-Centrosomal Microtubule-Organizing Centers (MTOCs) in Drosophila melanogaster. *Cells* **7**, (2018).
93. Dumont, J. & Desai, A. Acentrosomal spindle assembly and chromosome segregation during oocyte meiosis. *Trends Cell Biol* **22**, 241–249 (2012).
94. Masoud, K., Herzog, E., Chabouté, M. & Schmit, A. Microtubule nucleation and establishment of the mitotic spindle in vascular plant cells. *The Plant Journal* **75**, 245–257 (2013).
95. Cavazza, T. & Vernos, I. The RanGTP Pathway: From Nucleo-Cytoplasmic Transport to Spindle Assembly and Beyond. *Front Cell Dev Biol* **3**, (2016).
96. Kaláb, P., Šolc, P. & Motlík, J. The Role of RanGTP Gradient in Vertebrate Oocyte Maturation. in 235–267 (2011). doi:10.1007/978-3-642-19065-0_12.
97. Scrofani, J., Sardon, T., Meunier, S. & Vernos, I. Microtubule Nucleation in Mitosis by a RanGTP-Dependent Protein Complex. *Current Biology* **25**, 131–140 (2015).
98. Rüthnick, D. & Schiebel, E. Duplication of the Yeast Spindle Pole Body Once per Cell Cycle. *Mol Cell Biol* **36**, 1324–1331 (2016).
99. Klena, N. *et al.* Architecture of the centriole cartwheel-containing region revealed by cryo-electron tomography. *EMBO J* **39**, (2020).
100. Azimzadeh, J. & Bornens, M. Structure and duplication of the centrosome. *J Cell Sci* **120**, 2139–2142 (2007).
101. van Breugel, M. *et al.* Structures of SAS-6 Suggest Its Organization in Centrioles. *Science (1979)* **331**, 1196–1199 (2011).
102. Vasquez-Limeta, A. & Loncarek, J. Human centrosome organization and function in interphase and mitosis. *Semin Cell Dev Biol* **117**, 30–41 (2021).
103. Slevin, L. K. *et al.* The Structure of the Plk4 Cryptic Polo Box Reveals Two Tandem Polo Boxes Required for Centriole Duplication. *Structure* **20**, 1905–1917 (2012).
104. Park, S.-Y. *et al.* Molecular basis for unidirectional scaffold switching of human Plk4 in centriole biogenesis. *Nat Struct Mol Biol* **21**, 696–703 (2014).
105. Sonnen, K. F., Gabryjonczyk, A.-M., Anselm, E., Stierhof, Y.-D. & Nigg, E. A. Human Cep192 and Cep152 cooperate in Plk4 recruitment and centriole duplication. *J Cell Sci* (2013) doi:10.1242/jcs.129502.

106. Park, S.-Y. *et al.* Molecular basis for unidirectional scaffold switching of human Plk4 in centriole biogenesis. *Nat Struct Mol Biol* **21**, 696–703 (2014).
107. Lukinavičius, G. *et al.* Selective Chemical Crosslinking Reveals a Cep57-Cep63-Cep152 Centrosomal Complex. *Current Biology* **23**, 265–270 (2013).
108. Wei, Z. *et al.* Requirement of the Cep57-Cep63 Interaction for Proper Cep152 Recruitment and Centriole Duplication. *Mol Cell Biol* **40**, (2020).
109. Novak, Z. A., Conduit, P. T., Wainman, A. & Raff, J. W. Asterless Licenses Daughter Centrioles to Duplicate for the First Time in Drosophila Embryos. *Current Biology* **24**, 1276–1282 (2014).
110. Yamamoto, S. & Kitagawa, D. Self-organization of Plk4 regulates symmetry breaking in centriole duplication. *Nat Commun* **10**, 1810 (2019).
111. Park, J.-E. *et al.* Phase separation of Polo-like kinase 4 by autoactivation and clustering drives centriole biogenesis. *Nat Commun* **10**, 4959 (2019).
112. Lopes, C. A. M. *et al.* PLK4 trans-Autoactivation Controls Centriole Biogenesis in Space. *Dev Cell* **35**, 222–235 (2015).
113. Guderian, G., Westendorf, J., Uldschmid, A. & Nigg, E. A. Plk4 *trans* -autophosphorylation regulates centriole number by controlling βTrCP-mediated degradation. *J Cell Sci* **123**, 2163–2169 (2010).
114. Holland, A. J. *et al.* The autoregulated instability of Polo-like kinase 4 limits centrosome duplication to once per cell cycle. *Genes Dev* **26**, 2684–2689 (2012).
115. Moyer, T. C. & Holland, A. J. PLK4 promotes centriole duplication by phosphorylating STIL to link the procentriole cartwheel to the microtubule wall. *Elife* **8**, (2019).
116. Ohta, M. *et al.* Direct interaction of Plk4 with STIL ensures formation of a single procentriole per parental centriole. *Nat Commun* **5**, 5267 (2014).
117. Ohta, M. *et al.* Direct interaction of Plk4 with STIL ensures formation of a single procentriole per parental centriole. *Nat Commun* **5**, 5267 (2014).
118. Ohta, M. *et al.* Bimodal Binding of STIL to Plk4 Controls Proper Centriole Copy Number. *Cell Rep* **23**, 3160-3169.e4 (2018).
119. Arquint, C. *et al.* STIL binding to Polo-box 3 of PLK4 regulates centriole duplication. *Elife* **4**, (2015).
120. Guichard, P. *et al.* Cell-free reconstitution reveals centriole cartwheel assembly mechanisms. *Nat Commun* **8**, 14813 (2017).
121. Nazarov, S. *et al.* Novel features of centriole polarity and cartwheel stacking revealed by cryo-tomography. *EMBO J* **39**, (2020).
122. Tang, C.-J. C. *et al.* The human microcephaly protein STIL interacts with CPAP and is required for procentriole formation. *EMBO J* **30**, 4790–4804 (2011).
123. Gupta, H. *et al.* SAS-6 Association with γ-Tubulin Ring Complex Is Required for Centriole Duplication in Human Cells. *Current Biology* **30**, 2395-2403.e4 (2020).
124. Guichard, P., Laporte, M. H. & Hamel, V. The centriolar tubulin code. *Semin Cell Dev Biol* **137**, 16–25 (2023).
125. Pudlowski, R. *et al.* A delta-tubulin/epsilon-tubulin/Ted protein complex is required for centriole architecture. *bioRxiv* 2024.04.19.590208 (2024) doi:10.1101/2024.04.19.590208.
126. Comartin, D. *et al.* CEP120 and SPICE1 Cooperate with CPAP in Centriole Elongation. *Current Biology* **23**, 1360–1366 (2013).
127. Lin, Y.-N. *et al.* CEP120 interacts with CPAP and positively regulates centriole elongation. *Journal of Cell Biology* **202**, 211–219 (2013).
128. Chang, C.-W., Hsu, W.-B., Tsai, J.-J., Tang, C.-J. C. & Tang, T. K. CEP295 interacts with microtubules and is required for centriole elongation. *J Cell Sci* (2016) doi:10.1242/jcs.186338.
129. Gudi, R., Zou, C., Li, J. & Gao, Q. Centrobin–tubulin interaction is required for centriole elongation and stability. *Journal of Cell Biology* **193**, 711–725 (2011).

130. Keller, L. C. *et al.* Molecular Architecture of the Centriole Proteome: The Conserved WD40 Domain Protein POC1 Is Required for Centriole Duplication and Length Control. *Mol Biol Cell* **20**, 1150–1166 (2009).
131. Azimzadeh, J. *et al.* hPOC5 is a centrin-binding protein required for assembly of full-length centrioles. *Journal of Cell Biology* **185**, 101–114 (2009).
132. Schmidt, T. I. *et al.* Control of Centriole Length by CPAP and CP110. *Current Biology* **19**, 1005–1011 (2009).
133. Spektor, A., Tsang, W. Y., Khoo, D. & Dynlacht, B. D. Cep97 and CP110 Suppress a Cilia Assembly Program. *Cell* **130**, 678–690 (2007).
134. Bowler, M. *et al.* High-resolution characterization of centriole distal appendage morphology and dynamics by correlative STORM and electron microscopy. *Nat Commun* **10**, 993 (2019).
135. Huang, N. *et al.* Hierarchical assembly of centriole subdistal appendages via centrosome binding proteins CCDC120 and CCDC68. *Nat Commun* **8**, 15057 (2017).
136. Wu, J. & Akhmanova, A. Microtubule-Organizing Centers. *Annu Rev Cell Dev Biol* **33**, 51–75 (2017).
137. Deretic, J., Odabasi, E. & Firat-Karalar, E. N. The multifaceted roles of microtubule-associated proteins in the primary cilium and ciliopathies. *J Cell Sci* **136**, (2023).
138. Usami, F. M. *et al.* Intercellular and intracellular cilia orientation is coordinated by CELSR1 and CAMSAP3 in oviduct multi-ciliated cells. *J Cell Sci* **134**, (2021).
139. Robinson, A. M. *et al.* CAMSAP3 facilitates basal body polarity and the formation of the central pair of microtubules in motile cilia. *Proceedings of the National Academy of Sciences* **117**, 13571–13579 (2020).
140. Vergarajauregui, S. *et al.* AKAP6 orchestrates the nuclear envelope microtubule-organizing center by linking golgi and nucleus via AKAP9. *Elife* **9**, (2020).
141. Imasaki, T. *et al.* CAMSAP2 organizes a γ-tubulin-independent microtubule nucleation centre through phase separation. *Elife* **11**, e77365 (2022).
142. Efimov, A. *et al.* Asymmetric CLASP-Dependent Nucleation of Noncentrosomal Microtubules at the trans-Golgi Network. *Dev Cell* **12**, 917–930 (2007).
143. Fant, X., Srsen, V., Espigat-Georger, A. & Merdes, A. Nuclei of Non-Muscle Cells Bind Centrosome Proteins upon Fusion with Differentiating Myoblasts. *PLoS One* **4**, e8303 (2009).
144. Espigat-Georger, A., Dyachuk, V., Chemin, C., Emorine, L. & Merdes, A. Nuclear alignment in myotubes requires centrosome proteins recruited by nesprin-1. *J Cell Sci* (2016) doi:10.1242/jcs.191767.
145. Wilson, M. H. & Holzbaur, E. L. F. Nesprins anchor kinesin-1 motors to the nucleus to drive nuclear distribution in muscle cells. *Development* **142**, 218–228 (2015).
146. Gimpel, P. *et al.* Nesprin-1α-Dependent Microtubule Nucleation from the Nuclear Envelope via Akap450 Is Necessary for Nuclear Positioning in Muscle Cells. *Current Biology* **27**, 2999-3009.e9 (2017).
147. Wu, S. *et al.* AKAP9 supports spermatogenesis through its effects on microtubule and actin cytoskeletons in the rat testis. *The FASEB Journal* **35**, (2021).
148. Akhmanova, A. & Kapitein, L. C. Mechanisms of microtubule organization in differentiated animal cells. *Nat Rev Mol Cell Biol* **23**, 541–558 (2022).
149. Harris, T. J. C. & Peifer, M. aPKC Controls Microtubule Organization to Balance Adherens Junction Symmetry and Planar Polarity during Development. *Dev Cell* **12**, 727–738 (2007).
150. Wang, S. *et al.* NOCA-1 functions with γ-tubulin and in parallel to Patronin to assemble non-centrosomal microtubule arrays in C. elegans. *Elife* **4**, (2015).
151. Castiglioni, V. G. *et al.* Epidermal PAR-6 and PKC-3 are essential for larval development of C. elegans and organize non-centrosomal microtubules. *Elife* **9**, (2020).
152. Toya, M. *et al.* CAMSAP3 orients the apical-to-basal polarity of microtubule arrays in epithelial cells. *Proceedings of the National Academy of Sciences* **113**, 332–337 (2016).

153. Goldspink, D. A. *et al.* Ninein is essential for apico-basal microtubule formation and CLIP-170 facilitates its redeployment to non-centrosomal microtubule organizing centres. *Open Biol* **7**, 160274 (2017).
154. Noordstra, I. *et al.* Control of apico-basal epithelial polarity by the microtubule minus-end binding protein CAMSAP3 and spectraplakin ACF7. *J Cell Sci* (2016) doi:10.1242/jcs.194878.
155. Gillard, G., Girdler, G. & Röper, K. A release-and-capture mechanism generates an essential non-centrosomal microtubule array during tube budding. *Nat Commun* **12**, 4096 (2021).
156. Meng, W., Mushika, Y., Ichii, T. & Takeichi, M. Anchorage of Microtubule Minus Ends to Adherens Junctions Regulates Epithelial Cell-Cell Contacts. *Cell* **135**, 948–959 (2008).
157. Lechler, T. & Fuchs, E. Desmoplakin: an unexpected regulator of microtubule organization in the epidermis. *J Cell Biol* **176**, 147–154 (2007).
158. Travis, S. M., Mahon, B. P. & Petry, S. How Microtubules Build the Spindle Branch by Branch. *Annu Rev Cell Dev Biol* **38**, 1–23 (2022).
159. Alfaro-Aco, R., Thawani, A. & Petry, S. Structural analysis of the role of TPX2 in branching microtubule nucleation. *Journal of Cell Biology* **216**, 983–997 (2017).
160. Garrido, G. & Vernos, I. Non-centrosomal TPX2-Dependent Regulation of the Aurora A Kinase: Functional Implications for Healthy and Pathological Cell Division. *Front Oncol* **6**, (2016).
161. Kamasaki, T. *et al.* Augmin-dependent microtubule nucleation at microtubule walls in the spindle. *Journal of Cell Biology* **202**, 25–33 (2013).
162. Lawo, S., Hasegan, M., Gupta, G. D. & Pelletier, L. Subdiffraction imaging of centrosomes reveals higher-order organizational features of pericentriolar material. *Nat Cell Biol* **14**, 1148–1158 (2012).
163. Sánchez-Huertas, C. *et al.* Non-centrosomal nucleation mediated by augmin organizes microtubules in post-mitotic neurons and controls axonal microtubule polarity. *Nat Commun* **7**, 12187 (2016).
164. Sánchez-Huertas, C. & Lüders, J. The Augmin Connection in the Geometry of Microtubule Networks. *Current Biology* **25**, R294–R299 (2015).
165. Liu, T. *et al.* Augmin Triggers Microtubule-Dependent Microtubule Nucleation in Interphase Plant Cells. *Current Biology* **24**, 2708–2713 (2014).
166. Garrido, G. & Vernos, I. Non-centrosomal TPX2-Dependent Regulation of the Aurora A Kinase: Functional Implications for Healthy and Pathological Cell Division. *Front Oncol* **6**, (2016).
167. Chen, J. V., Buchwalter, R. A., Kao, L.-R. & Megraw, T. L. A Splice Variant of Centrosomin Converts Mitochondria to Microtubule-Organizing Centers. *Current Biology* **27**, 1928-1940.e6 (2017).
168. Valdez, V. A., Neahring, L., Petry, S. & Dumont, S. Mechanisms underlying spindle assembly and robustness. *Nat Rev Mol Cell Biol* **24**, 523–542 (2023).
169. Noguchi, T., Koizumi, M. & Hayashi, S. Sustained Elongation of Sperm Tail Promoted by Local Remodeling of Giant Mitochondria in Drosophila. *Current Biology* **21**, 805–814 (2011).
170. Roostalu, J. & Surrey, T. Microtubule nucleation: beyond the template. *Nat Rev Mol Cell Biol* **18**, 702–710 (2017).
171. Desai, A. & Mitchison, T. J. MICROTUBULE POLYMERIZATION DYNAMICS. *Annu Rev Cell Dev Biol* **13**, 83–117 (1997).
172. Roll-Mecak, A. The Tubulin Code in Microtubule Dynamics and Information Encoding. *Dev Cell* **54**, 7–20 (2020).
173. Roostalu, J. & Surrey, T. Microtubule nucleation: beyond the template. *Nat Rev Mol Cell Biol* **18**, 702–710 (2017).
174. Howard, J. & Hyman, A. A. Dynamics and mechanics of the microtubule plus end. *Nature* **422**, 753–758 (2003).

175. Nishita, M., Satake, T., Minami, Y. & Suzuki, A. Regulatory mechanisms and cellular functions of non-centrosomal microtubules. *The Journal of Biochemistry* **162**, 1–10 (2017).
176. Gudimchuk, N. B. & McIntosh, J. R. Regulation of microtubule dynamics, mechanics and function through the growing tip. *Nat Rev Mol Cell Biol* **22**, 777–795 (2021).
177. Mandelkow, E. M., Mandelkow, E. & Milligan, R. A. Microtubule dynamics and microtubule caps: a time-resolved cryo-electron microscopy study. *J Cell Biol* **114**, 977–991 (1991).
178. Chrétien, D., Fuller, S. D. & Karsenti, E. Structure of growing microtubule ends: two-dimensional sheets close into tubes at variable rates. *J Cell Biol* **129**, 1311–1328 (1995).
179. Zhou, J. *et al.* Structural insights into the mechanism of GTP initiation of microtubule assembly. *Nat Commun* **14**, 5980 (2023).
180. Wang, H.-W., Long, S., Finley, K. R. & Nogales, E. Assembly of GMPCPP-Bound Tubulin into Helical Ribbons and Tubes and Effect of Colchicine. *Cell Cycle* **4**, 1157–1160 (2005).
181. McIntosh, J. R. *et al.* Microtubules grow by the addition of bent guanosine triphosphate tubulin to the tips of curved protofilaments. *Journal of Cell Biology* **217**, 2691–2708 (2018).
182. Brouhard, G. J. & Rice, L. M. The contribution of αβ-tubulin curvature to microtubule dynamics. *Journal of Cell Biology* **207**, 323–334 (2014).
183. Yajima, H. *et al.* Conformational changes in tubulin in GMPCPP and GDP-taxol microtubules observed by cryoelectron microscopy. *Journal of Cell Biology* **198**, 315–322 (2012).
184. Grafmüller, A. & Voth, G. A. Intrinsic Bending of Microtubule Protofilaments. *Structure* **19**, 409–417 (2011).
185. Igaev, M. & Grubmüller, H. Microtubule assembly governed by tubulin allosteric gain in flexibility and lattice induced fit. *Elife* **7**, (2018).
186. Peng, L. X., Hsu, M. T., Bonomi, M., Agard, D. A. & Jacobson, M. P. The Free Energy Profile of Tubulin Straight-Bent Conformational Changes, with Implications for Microtubule Assembly and Drug Discovery. *PLoS Comput Biol* **10**, e1003464 (2014).
187. Fedorov, V. A. *et al.* Mechanical properties of tubulin intra- and inter-dimer interfaces and their implications for microtubule dynamic instability. *PLoS Comput Biol* **15**, e1007327 (2019).
188. Tong, D. & Voth, G. A. Microtubule Simulations Provide Insight into the Molecular Mechanism Underlying Dynamic Instability. *Biophys J* **118**, 2938–2951 (2020).
189. Chumová, J. *et al.* γ-Tubulin has a conserved intrinsic property of self-polymerization into double stranded filaments and fibrillar networks. *Biochimica et Biophysica Acta (BBA) - Molecular Cell Research* **1865**, 734–748 (2018).
190. Lindström, L. & Alvarado-Kristensson, M. Characterization of gamma-tubulin filaments in mammalian cells. *Biochimica et Biophysica Acta (BBA) - Molecular Cell Research* **1865**, 158–171 (2018).
191. Rosselló, C. A., Lindström, L., Glindre, J., Eklund, G. & Alvarado-Kristensson, M. Gamma-tubulin coordinates nuclear envelope assembly around chromatin. *Heliyon* **2**, e00166 (2016).
192. Melki, R., Vainberg, I., Chow, R. & Cowan, N. Chaperonin-mediated folding of vertebrate actin-related protein and gamma-tubulin. *J Cell Biol* **122**, 1301–1310 (1993).
193. Lin, T. *et al.* Cell-cycle dependent phosphorylation of yeast pericentrin regulates γ-TuSC-mediated microtubule nucleation. *Elife* **3**, (2014).
194. Thawani, A. *et al.* The transition state and regulation of γ-TuRC-mediated microtubule nucleation revealed by single molecule microscopy. *Elife* **9**, (2020).
195. Rale, M. J., Romer, B., Mahon, B. P., Travis, S. M. & Petry, S. The conserved centrosomin motif, γTuNA, forms a dimer that directly activates microtubule nucleation by the γ-tubulin ring complex (γTuRC). *Elife* **11**, (2022).
196. Chang, C.-W., Hsu, W.-B., Tsai, J.-J., Tang, C.-J. C. & Tang, T. K. CEP295 interacts with microtubules and is required for centriole elongation. *J Cell Sci* (2016) doi:10.1242/jcs.186338.

197. Watanabe, K., Takao, D., Ito, K. K., Takahashi, M. & Kitagawa, D. The Cep57-pericentrin module organizes PCM expansion and centriole engagement. *Nat Commun* **10**, 931 (2019).
198. Wei, Z. *et al.* Requirement of the Cep57-Cep63 Interaction for Proper Cep152 Recruitment and Centriole Duplication. *Mol Cell Biol* **40**, (2020).
199. Atorino, E. S., Hata, S., Funaya, C., Neuner, A. & Schiebel, E. CEP44 ensures the formation of bona fide centriole wall, a requirement for the centriole-to-centrosome conversion. *Nat Commun* **11**, 903 (2020).
200. Zheng, X. *et al.* Conserved TCP domain of Sas-4/CPAP is essential for pericentriolar material tethering during centrosome biogenesis. *Proceedings of the National Academy of Sciences* **111**, (2014).
201. Mennella, V. *et al.* Subdiffraction-resolution fluorescence microscopy reveals a domain of the centrosome critical for pericentriolar material organization. *Nat Cell Biol* **14**, 1159–1168 (2012).
202. Joukov, V., Walter, J. C. & De Nicolo, A. The Cep192-Organized Aurora A-Plk1 Cascade Is Essential for Centrosome Cycle and Bipolar Spindle Assembly. *Mol Cell* **55**, 578–591 (2014).
203. Cabral, G., Laos, T., Dumont, J. & Dammermann, A. Differential Requirements for Centrioles in Mitotic Centrosome Growth and Maintenance. *Dev Cell* **50**, 355-366.e6 (2019).
204. Alvarez-Rodrigo, I. *et al.* Evidence that a positive feedback loop drives centrosome maturation in fly embryos. *Elife* **8**, (2019).
205. Vasquez-Limeta, A. & Loncarek, J. Human centrosome organization and function in interphase and mitosis. *Semin Cell Dev Biol* **117**, 30–41 (2021).
206. Zimmerman, W. C., Sillibourne, J., Rosa, J. & Doxsey, S. J. Mitosis-specific Anchoring of γ Tubulin Complexes by Pericentrin Controls Spindle Organization and Mitotic Entry. *Mol Biol Cell* **15**, 3642–3657 (2004).
207. Kim, S. & Rhee, K. Importance of the CEP215-Pericentrin Interaction for Centrosome Maturation during Mitosis. *PLoS One* **9**, e87016 (2014).
208. O'Rourke, B. P. *et al.* Cep192 Controls the Balance of Centrosome and Non-Centrosomal Microtubules during Interphase. *PLoS One* **9**, e101001 (2014).
209. Chinen, T. *et al.* Centriole and PCM cooperatively recruit CEP192 to spindle poles to promote bipolar spindle assembly. *Journal of Cell Biology* **220**, (2021).
210. Haren, L., Stearns, T. & Lüders, J. Plk1-Dependent Recruitment of γ-Tubulin Complexes to Mitotic Centrosomes Involves Multiple PCM Components. *PLoS One* **4**, e5976 (2009).
211. Fong, K.-W., Choi, Y.-K., Rattner, J. B. & Qi, R. Z. CDK5RAP2 Is a Pericentriolar Protein That Functions in Centrosomal Attachment of the γ-Tubulin Ring Complex. *Mol Biol Cell* **19**, 115–125 (2008).
212. Chen, C.-T. *et al.* A Unique Set of Centrosome Proteins Requires Pericentrin for Spindle-Pole Localization and Spindle Orientation. *Current Biology* **24**, 2327–2334 (2014).
213. Delaval, B. & Doxsey, S. J. Pericentrin in cellular function and disease. *Journal of Cell Biology* **188**, 181–190 (2010).
214. Ohta, M. *et al.* Polo-like kinase 1 independently controls microtubule-nucleating capacity and size of the centrosome. *Journal of Cell Biology* **220**, (2021).
215. Sdelci, S. *et al.* Nek9 Phosphorylation of NEDD1/GCP-WD Contributes to Plk1 Control of γ-Tubulin Recruitment to the Mitotic Centrosome. *Current Biology* **22**, 1516–1523 (2012).
216. Ramani, A. *et al.* Plk1/Polo Phosphorylates Sas-4 at the Onset of Mitosis for an Efficient Recruitment of Pericentriolar Material to Centrosomes. *Cell Rep* **25**, 3618-3630.e6 (2018).
217. Clarke, P. R. & Zhang, C. Spatial and temporal coordination of mitosis by Ran GTPase. *Nat Rev Mol Cell Biol* **9**, 464–477 (2008).
218. Gruss, O. J. *et al.* Ran Induces Spindle Assembly by Reversing the Inhibitory Effect of Importin α on TPX2 Activity. *Cell* **104**, 83–93 (2001).

219. Oh, D., Yu, C.-H. & Needleman, D. J. Spatial organization of the Ran pathway by microtubules in mitosis. *Proceedings of the National Academy of Sciences* **113**, 8729–8734 (2016).
220. Bayliss, R., Sardon, T., Vernos, I. & Conti, E. Structural Basis of Aurora-A Activation by TPX2 at the Mitotic Spindle. *Mol Cell* **12**, 851–862 (2003).
221. Kufer, T. A. *et al.* Human TPX2 is required for targeting Aurora-A kinase to the spindle. *J Cell Biol* **158**, 617–623 (2002).
222. Hirota, T. *et al.* Aurora-A and an Interacting Activator, the LIM Protein Ajuba, Are Required for Mitotic Commitment in Human Cells. *Cell* **114**, 585–598 (2003).
223. Hutterer, A. *et al.* Mitotic Activation of the Kinase Aurora-A Requires Its Binding Partner Bora. *Dev Cell* **11**, 147–157 (2006).
224. Park, J.-G. *et al.* Structural basis for CEP192-mediated regulation of centrosomal AURKA. *Sci Adv* **9**, (2023).
225. Reboutier, D., Troadec, M.-B., Cremet, J.-Y., Fukasawa, K. & Prigent, C. Nucleophosmin/B23 activates Aurora A at the centrosome through phosphorylation of serine 89. *Journal of Cell Biology* **197**, 19–26 (2012).
226. Satinover, D. L., Leach, C. A., Stukenberg, P. T. & Brautigan, D. L. Activation of Aurora-A kinase by protein phosphatase inhibitor-2, a bifunctional signaling protein. *Proceedings of the National Academy of Sciences* **101**, 8625–8630 (2004).
227. Zhao, Z., Lim, J. P., Ng, Y.-W., Lim, L. & Manser, E. The GIT-Associated Kinase PAK Targets to the Centrosome and Regulates Aurora-A. *Mol Cell* **20**, 237–249 (2005).
228. Littlepage, L. E. *et al.* Identification of phosphorylated residues that affect the activity of the mitotic kinase Aurora-A. *Proceedings of the National Academy of Sciences* **99**, 15440–15445 (2002).
229. Bruinsma, W., Macůrek, L., Freire, R., Lindqvist, A. & Medema, R. H. Bora and Aurora-A continue to activate Plk1 in mitosis. *J Cell Sci* (2013) doi:10.1242/jcs.137216.
230. Seki, A., Coppinger, J. A., Jang, C.-Y., Yates, J. R. & Fang, G. Bora and the Kinase Aurora A Cooperatively Activate the Kinase Plk1 and Control Mitotic Entry. *Science (1979)* **320**, 1655–1658 (2008).
231. Joukov, V., Walter, J. C. & De Nicolo, A. The Cep192-Organized Aurora A-Plk1 Cascade Is Essential for Centrosome Cycle and Bipolar Spindle Assembly. *Mol Cell* **55**, 578–591 (2014).
232. Timón Pérez, K., Scrofani, J. & Vernos, I. NEDD1-S411 phosphorylation plays a critical function in the coordination of microtubule nucleation during mitosis. *Biol Open* **11**, (2022).
233. Pinyol, R., Scrofani, J. & Vernos, I. The Role of NEDD1 Phosphorylation by Aurora A in Chromosomal Microtubule Nucleation and Spindle Function. *Current Biology* **23**, 143–149 (2013).
234. Reber, S. B. *et al.* XMAP215 activity sets spindle length by controlling the total mass of spindle microtubules. *Nat Cell Biol* **15**, 1116–1122 (2013).
235. Würtz, M. *et al.* Reconstitution of the recombinant human γ-tubulin ring complex. *Open Biol* **11**, (2021).
236. Rai, D. *et al.* CAMSAP-driven microtubule release from γ-TuRC and its regulation by nucleation-promoting factors. *bioRxiv* 2022.08.03.502613 (2022) doi:10.1101/2022.08.03.502613.
237. Tovey, C. A. *et al.* Autoinhibition of Cnn binding to γ-TuRCs prevents ectopic microtubule nucleation and cell division defects. *Journal of Cell Biology* **220**, (2021).
238. Chinen, T. *et al.* The γ-tubulin-specific inhibitor gatastatin reveals temporal requirements of microtubule nucleation during the cell cycle. *Nat Commun* **6**, 8722 (2015).
239. Collins, C. A. & Vallee, R. B. Temperature-dependent reversible assembly of taxol-treated microtubules. *Journal of Cell Biology* **105**, 2847–2854 (1987).

240. Vermeulen, B. J. *et al.* γ-TuRC asymmetry induces local protofilament mismatch at the RanGTP-stimulated microtubule minus end. *EMBO J* (2024) doi:10.1038/s44318-024-00087-4.
241. Groen, A. C. *et al.* XRHAMM Functions in Ran-Dependent Microtubule Nucleation and Pole Formation during Anastral Spindle Assembly. *Current Biology* **14**, 1801–1811 (2004).
242. Li, G. & Moore, J. K. Microtubule dynamics at low temperature: evidence that tubulin recycling limits assembly. *Mol Biol Cell* **31**, 1154–1166 (2020).
243. SCHIFF, P. B., FANT, J. & HORWITZ, S. B. Promotion of microtubule assembly in vitro by taxol. *Nature* **277**, 665–667 (1979).
244. Wieczorek, M. *et al.* Biochemical reconstitutions reveal principles of human γ-TuRC assembly and function. *Journal of Cell Biology* **220**, e202009146 (2021).
245. Session, A. M. *et al.* Genome evolution in the allotetraploid frog Xenopus laevis. *Nature* **538**, 336–343 (2016).
246. Peshkin, L. *et al.* The protein repertoire in early vertebrate embryogenesis. *bioRxiv* 571174 (2019) doi:10.1101/571174.
247. Paul, D. M. *et al.* In situ cryo-electron tomography reveals filamentous actin within the microtubule lumen. *Journal of Cell Biology* **219**, (2020).
248. Ventura Santos, C., Rogers, S. L. & Carter, A. P. <scp>CryoET</scp> shows cofilactin filaments inside the microtubule lumen. *EMBO Rep* **24**, (2023).
249. Liu, P., Würtz, M., Zupa, E., Pfeffer, S. & Schiebel, E. Microtubule nucleation: The waltz between γ-tubulin ring complex and associated proteins. *Curr Opin Cell Biol* **68**, 124–131 (2021).
250. Martin, C.-A. *et al.* Mutations in PLK4, encoding a master regulator of centriole biogenesis, cause microcephaly, growth failure and retinopathy. *Nat Genet* **46**, 1283–1292 (2014).
251. Vérollet, C. *et al. Drosophila melanogaster* γ-TuRC is dispensable for targeting γ-tubulin to the centrosome and microtubule nucleation. *J Cell Biol* **172**, 517–528 (2006).
252. Thawani, A. & Petry, S. Molecular insight into how γ-TuRC makes microtubules. *J Cell Sci* **134**, jcs245464 (2021).
253. Thawani, A. *et al.* The transition state and regulation of γ-TuRC-mediated microtubule nucleation revealed by single molecule microscopy. *Elife* **9**, e54253 (2020).
254. Berman, A. Y. *et al.* A nucleotide binding–independent role for γ-tubulin in microtubule capping and cell division. *Journal of Cell Biology* **222**, (2023).
255. Rai, D. *et al.* CAMSAPs and nucleation-promoting factors control microtubule release from γ-TuRC. *Nat Cell Biol* **26**, 404–420 (2024).
256. Zimmermann, F. *et al.* Assembly of the asymmetric human γ-tubulin ring complex by RUVBL1-RUVBL2 AAA ATPase. *Sci Adv* **6**, (2020).
257. Prota, A. E. *et al.* Structural insight into the stabilization of microtubules by taxanes. *Elife* **12**, (2023).
258. Aher, A., Urnavicius, L., Xue, A., Neselu, K. & Kapoor, T. M. Structure of the γ-tubulin ring complex-capped microtubule. *Nat Struct Mol Biol* (2024) doi:10.1038/s41594-024-01264-z.
259. Brito, C., Serna, M., Guerra, P., Llorca, O. & Surrey, T. Transition of human γ-tubulin ring complex into a closed conformation during microtubule nucleation. *Science (1979)* **383**, 870–876 (2024).
260. Anders, K. R. & Botstein, D. Dominant-Lethal α-Tubulin Mutants Defective in Microtubule Depolymerization in Yeast. *Mol Biol Cell* **12**, 3973–3986 (2001).
261. Roostalu, J. *et al.* The speed of GTP hydrolysis determines GTP cap size and controls microtubule stability. *Elife* **9**, (2020).
262. LaFrance, B. J. *et al.* Structural transitions in the GTP cap visualized by cryo-electron microscopy of catalytically inactive microtubules. *Proceedings of the National Academy of Sciences* **119**, (2022).

263. Dendooven, T. *et al.* Structure of the native γ-tubulin ring complex capping spindle microtubules. *Nat Struct Mol Biol* (2024) doi:10.1038/s41594-024-01281-y.
264. Würtz, M. *et al.* Modular assembly of the principal microtubule nucleator γ-TuRC. *Nat Commun* **13**, 473 (2022).
265. Gombos, L. *et al.* GTP regulates the microtubule nucleation activity of γ-tubulin. *Nat Cell Biol* **15**, 1317–1327 (2013).
266. Kristensson, M. A. The Game of Tubulins. *Cells* **10**, 745 (2021).
267. Rai, A. *et al.* Taxanes convert regions of perturbed microtubule growth into rescue sites. *Nat Mater* **19**, 355–365 (2020).
268. Petry, S., Groen, A. C., Ishihara, K., Mitchison, T. J. & Vale, R. D. Branching Microtubule Nucleation in Xenopus Egg Extracts Mediated by Augmin and TPX2. *Cell* **152**, 768–777 (2013).
269. Gabel, C. A. *et al.* Molecular architecture of the augmin complex. *Nat Commun* **13**, 5449 (2022).
270. Shurygina, M. F. *et al.* Genotype Phenotype Correlation and Variability in Microcephaly Associated With Chorioretinopathy or Familial Exudative Vitreoretinopathy. *Investigative Opthalmology & Visual Science* **61**, 2 (2020).
271. Puffenberger, E. G. *et al.* Genetic Mapping and Exome Sequencing Identify Variants Associated with Five Novel Diseases. *PLoS One* **7**, e28936 (2012).
272. Chen, J. *et al.* The novel compound heterozygous rare variants may impact positively selected regions of TUBGCP6, a microcephaly associated gene. *Front Ecol Evol* **10**, (2022).
273. Ochoa, D. *et al.* The functional landscape of the human phosphoproteome. *Nat Biotechnol* **38**, 365–373 (2020).
274. Karasu, O. R., Neuner, A., Atorino, E. S., Pereira, G. & Schiebel, E. The central scaffold protein CEP350 coordinates centriole length, stability, and maturation. *Journal of Cell Biology* **221**, (2022).
275. Kowarz, E., Löscher, D. & Marschalek, R. Optimized Sleeping Beauty transposons rapidly generate stable transgenic cell lines. *Biotechnol J* **10**, 647–653 (2015).
276. Mátés, L. *et al.* Molecular evolution of a novel hyperactive Sleeping Beauty transposase enables robust stable gene transfer in vertebrates. *Nat Genet* **41**, 753–761 (2009).
277. Zupa, E. *et al.* The cryo-EM structure of a γ-TuSC elucidates architecture and regulation of minimal microtubule nucleation systems. *Nat Commun* **11**, 5705 (2020).
278. Cook, A. D., Manka, S. W., Wang, S., Moores, C. A. & Atherton, J. A microtubule RELION-based pipeline for cryo-EM image processing. *J Struct Biol* **209**, 107402 (2020).
279. Zivanov, J. *et al.* New tools for automated high-resolution cryo-EM structure determination in RELION-3. *Elife* **7**, (2018).
280. Pintilie, G. D., Zhang, J., Goddard, T. D., Chiu, W. & Gossard, D. C. Quantitative analysis of cryo-EM density map segmentation by watershed and scale-space filtering, and fitting of structures by alignment to regions. *J Struct Biol* **170**, 427–438 (2010).

8. Abreviations

ASPM	abnormal spindle like microcephaly associated protein
CAMSAP1-3	calmodulin-regulated spectrin-associated protein 1-3
CD	circular dichroism
CDK5RAP2	CDK5 regulatory subunit-associated protein 2, other name CEP215
CEP152	Centrosomal protein of 152 kDa
CEP192	Centrosomal protein of 192 kDa
CEP215	Centrosomal protein of 215 kDa, other name CDK5RAP2
CM1	centrosomin motiv 1
Cnn	centrosomin
cryo EM	cryo Electron Microscopy
CSF	Cztostatic factor
Cy3	Sulfo-Cyanine3 used for labbeling
DMP	dimethyl phthalate
DTT	Dithiothreitol
DTX	docetaxel
EB	end binding protein
EDTA	Ethylenediaminetetraacetic acid
GCP2-6	γ-tubulin complex proteins 2-6
GDP	Guanosine diphosphate
GFP	green fluorescent protein
GTP	Guanosine triphosphate
HEPES	2-(4-(2-hydroxyethyl)-1-piperazinyl)-ethanesulfonic acid
chTOG	Colonic and hepatic tumour overexpressed gene (protein)
p60	subunit p60 of katanin
LB	Lysogeny broth medium
LSS	low speed supernatant of the X. leavis CSF egg's extract
MAPs	microtubule associated proteins
MT	microtubule
MTOC	microtubule organizing centers
MZT1/2	Mitotic-spindle organizing protein 1/2
NEDD1	Neural precursor cell expressed, developmentally down-regulated 1

NME7	Nucleoside diphosphate kinase homolog 7
NS EM	Negative stain electron microscopy
PAGE	polyacrylamide gel electrophoresis
PLK1	Serine/threonine-protein kinase 1
PLK4	Serine/threonine-protein kinase 4
pt	α-β- tubulin dimers protofilament of microtubules
Ran (Q69L)	RAs-related Nuclear protein wirh Q69L modification activating MT nucleation
RanGTP	RAs-related Nuclear protein in GTP form
SAFs	Spindle assembly factors
SAS6	Spindle assembly abnormal protein 6 homolog
SDS	Sodium dodecyl-sulfate
TBS	Tris-buffered saline
+/-TIPs	plus and minus MT ends tracking proteins
TPX2	Targeting protein for Xklp2
TUBGCP2-6	genes name for GCP2 to 6
XMAP215	*Xenopus* Microtubule-associated protein 215
γTuC	γ tubulin complex
γTuRC	γ tubulin ring complex
γTuSC	γ tubulin small complex

9. Publications

1. Insights into the assembly and activation of the microtubule nucleator γ-TuRC. **(2019)** Liu P., Zupa E., Neuner A., **Böhler A**., Loerke J., Flemming D., Ruppert T., Rudack T., Peter C., Spahn C., Gruss O.J., Pfeffer S., Schiebel E., Nature, doi : 10.1038/s41586-019-1896-6

2. The cryo-EM structure of a γ-TuSC elucidates architecture and regulation of minimal microtubule nucleation systems. **(2020)** Zupa E., Zheng A., Neuner A., Würtz M., Liu P., **Böhler A.**, Schiebel E., Pfeffer S. Nature Communication, doi: 10.1038/s41467-020-19456-8

3. Reconstruction of the recombinant human γ-tubulin ring complex. **(2021**) Würtz M., **Böhler A.** *, Neuner A., Zupa E., Rohland L., Liu P., Vermeulen B.J.A., Pfeffer S., Schiebel E., Open Biology, doi: 10.1098/rsob.200325

4. The gamma-tubulin ring complex: Deciphering the molecular organization and assembly mechanism of a major vertebrate microtubule nucleator. **(2021) Böhler A.** *, Vermeulen B.J.A., Würtz M., Zupa E., Pfeffer S., Schiebel E., Bioessays, doi: 10.1002/bies.202100114

5. Modular assembly of the principal microtubule nucleator γ-TuRC. **(2022)** Würtz M., Zupa E., Atorino E.S., Neuner A., **Böhler A.**, Rahadian A.S., Vermeulen B.J.A., Tonon G., Eustermann S., Schiebel E., Pfeffer S., Nature Communication, doi: 10.1038/s41467-022-28079-0

6. The augmin complex architecture reveals structural insights into microtubule branching. **(2022**) Zupa E., Würtz M., Neuner A., Hoffmann T., Rettel M., **Böhler A.**, Vermeulen B.J.A., Eustermann S., Schiebel E., Pfeffer S., Nature Communication, doi: 10.1038/s41467-022-33228-6

7. γTuRC asymmetry induces local protofilament mismatch at the RanGTP-stimulated microtule minus end. **(2024)** Vermeulen B.J., **Böhler A**. *, Gao Q., Neuner A., Župa E., Chu Z., Würtz M., Jäkle U., Gruss O. J., Pfeffer S., Schiebel E., EMBO Journal, doi: 10.1038/s44318-024-00087-4.

Marked * is as a first autor.

10. Acknowledgments

First of all I would like to thank Prof. Dr. Elmar Schiebel for the opportunity to learn, grown and be successful under his leadership. PhD work is time, where I have grown not only in my scientific perspective but shaped my personality as well.

Dr. Stefan Pfeffer, thank you for your input, expertise in cryo EM leading in successful teamwork and supervising me as my TAC member.

I would like to thank my colleagues for perfect collaboration and team management on projects, Dr. Peng Liu, Dr. Martin Würtz, Dr. Erik Župa, Bram Vermeulen, Dr. Enrico Atorino, Anjun Zheng, Qi Gao.

I would like to acknowledge Dr. Annett Neuner. Annett's kindness, motivation and always positive attitude helped to overcome the thought times. Her NS EM expertise made further development of experiments and directives. Annett, your friendship made this thesis possible.

I would like to thank Ursula Jäckle for her laboratory expertise and sharing it with me.

I appretiate Dr. Onur Karasu for his friendship, his "can help" attitude and discussions.

I am grateful to Dr. Janina Luitz for perfect collaboration, friendship and all what she thought me about *Drosophila melanogaster.*

I appreciate Günter Stieg and Dr. Kopp for their input in my knowledge of protein biochemistry.

That way I would like to acknowledge also the collaborators, Prof. Dr. Sylvia Erhardt for *Drosophila melanogaster* γTuRC identification and Prof. Dr. Oliver Gruss – for your support, suggestions, inputs and *Xenopus leavis* egg's extract and LSS.

Not the last, I am grateful to my family, who support me. Mum, dad, Nati – I am who I am thanks to you.

11. Erklärung

Hiermit erkläre ich, Anna Böhler, geboren am 18.05.1991 in Kremennaja (Kremina), Ukraine, dass ich die vorliegende Dissertation mit dem Titel „Structure of the microtubule nucleation sites“ selbständig und unter ausschließlicher Verwendung der angeführten Hilfsmittel angefertigt habe. Die Dissertation wurde in der jetzigen oder ähnlichen Form noch bei keiner anderen Hochschule zur Erlangung eines akademischen Grades eingereicht.

Heidelberg, den _____

_____

Anna Böhler